

---

## MASTER IN SCIENTIFIC COMPUTING

---

# Master Thesis



---

### Approximation of Koopman Operators

### by Randomly Chosen Basis Functions

---

**Author:**

Moussa Atwi

**Supervisors:**

PD. Dr. Marcus Weber

**ID:**

464241

PD. Dr. Michael Karow

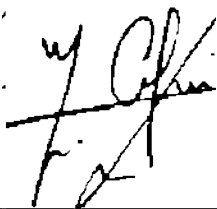
**Marcus Weber**  
Zuse Institut Berlin, Takustraße 7, 14195 Berlin  
Research Group Leader "Computational Molecular Design"  
Department of Modeling and Simulation of Complex Processes

**Michael Karow**  
Technical University of Berlin, Straße des 17. Juni 135, 10623 Berlin  
Institute of Mathematics



# Declaration

I hereby declare under oath that this Master's Thesis has been composed solely by myself and that it has not been previously submitted, in whole or in part, for a degree or professional qualification at any other institution. Except where explicitly indicated otherwise by reference or acknowledgment, the work presented herein is entirely the result of my own independent research.



---

Author's Signature

Berlin, 04/05/2023

---

Place, Date



# Acknowledgement

I would like to express my sincere gratitude and appreciation to my advisor, Doctor Marcus Weber for not only introducing such an interesting topic which is lying in the intersection of Koopman theory and neural networks, but also for his enthusiasm as well. I am indebted for his support and guidance through scheduled meetings, prompt response and continuous encouragement.

I am also deeply grateful to my committee member, Doctor Michael Karow, for his time, valuable insights and helpful feedback.

Furthermore, I would also like to thank everyone at Zuse Institute Berlin who made this whole experience very pleasant by providing such a great work atmosphere. Likewise, I extend my sincere thanks to the referees for their helpful suggestions.

Last, but for certain not least, I would like to thank my family for their love, support and belief in me, and above all my best friends. Google, ChatGPT and YouTube for providing access to a wealth of information and resources that were instrumental in my research process.



# Abstract

The behavior of dynamical systems can often be investigated by analyzing the eigenvalues and corresponding eigenfunctions of linear operators. In this context, the Koopman operator, which governs the evolution of scalar observables on the state space of autonomous dynamical systems, has emerged as a powerful tool for the analysis and decomposition of nonlinear systems. However, the Koopman operator is an infinite-dimensional operator, making its direct computation infeasible. To overcome this challenge, a data-driven method called Extended Dynamic Mode Decomposition (EDMD) has been developed. EDMD can effectively approximate the finite-dimensional Koopman operator, and its leading eigenvalues, eigenfunctions, and modes. Therefore, this thesis provides an overview of EDMD and its application in approximating the Koopman operator for the analysis of nonlinear dynamical systems. To apply the EDMD method, a dataset of snapshot pairs and a dictionary of scalar observables, which serves as a basis set of functions, are required. The method is capable of reducing the complexity of both deterministic and non-deterministic dynamical systems. The results of illustrative examples demonstrate the ability of EDMD to identify the Koopman eigenfunctions, which generate an invariant subspace where the dynamics behave linearly. The invariant subspace generated by Koopman eigenfunctions offers intrinsic coordinates for the system, leading to the restriction of the Koopman operator to a finite-dimensional linear operator. This discovery underlines the significance of Koopman eigenfunctions and their capacity to enhance the analysis and control of dynamical systems. The thesis also aims to investigate the effectiveness of EDMD with various basis functions, including monomials up to and including order 10, random Gaussians, and randomly initialized neural networks. Our key contribution is to demonstrate that the use of random Gaussians results in superior approximations compared to monomials. We showcase the effectiveness of this powerful method through multiple examples, including the one-dimensional Ornstein-Uhlenbeck process and the two-dimensional overdamped Langevin equation, which are characterized by stochastic differential equations with double-well, triple-well, and quadruple-well potentials.

**Keywords** Dynamical systems · Koopman operator · Spectral analysis · Koopman eigenfunctions · Model reduction · Data-driven methods · Extended dynamic mode decomposition (EDMD) · Embeddings · Random Gaussians · Randomized neural networks.



---

# Contents

<b>Declaration</b>	iii
<b>Acknowledgement</b>	v
<b>Abstract</b>	vii
<b>Introduction</b>	xi
<b>Glossary</b>	xv
<b>1 Data-Driven Dynamical systems</b>	1
1.1 Dynamical Systems . . . . .	2
1.2 Classification of Dynamical Systems . . . . .	2
1.3 Modern Objectives and Challenges in Dynamical Systems . . . . .	3
<b>2 Koopman Operator Theory</b>	7
2.1 An Overview of Koopman Operator . . . . .	8
2.1.1 Koopman Operator for Deterministic Dynamical Systems . . . . .	9
2.1.2 Koopman Operator for Stochastic Dynamical Systems . . . . .	11
2.2 Koopman Spectral Analysis . . . . .	13
2.2.1 Spectral Decomposition of Koopman Operators . . . . .	13
2.2.2 Koopman Mode Decomposition . . . . .	17
2.3 Koopman Invariant Subspaces and Intrinsic Coordinates . . . . .	20
2.3.1 Koopman-Invariant Subspaces Containing the State . . . . .	21
2.3.2 Applications of Koopman Embedding . . . . .	21
2.3.2.1 Continuous-Time Representation for Koopman Embedding . . . . .	21

2.3.2.2	Discrete-Time Representation for Koopman Embedding . . . . .	25
2.4	Numerical Approximation Methods . . . . .	27
2.4.1	Laurent and Taylor Series for Eigenfunctions Expansion. . . . .	28
2.4.2	Galerkin Approximation of the Koopman Generator . . . . .	29
<b>3</b>	<b>Data Driven Methods</b>	<b>31</b>
3.0.1	Extended Dynamical Mode Decomposition (EDMD) . . . . .	32
3.0.1.1	Approximating the Koopman Operator and its Eigenfunctions .	32
3.0.1.2	Computing the Koopman Modes . . . . .	34
3.0.1.3	Convergence of the EDMD Algorithm to a Galerkin Method .	35
3.0.1.4	EDMD with Stochastic Data . . . . .	36
3.0.1.5	Dynamic Mode Decomposition (DMD) . . . . .	37
3.0.2	Numerical Examples: EDMD with Monomial Basis Functions . . . . .	40
<b>4</b>	<b>Numerical Results</b>	<b>47</b>
4.1	Random Dynamic Mode Decomposition (RDMD) . . . . .	48
4.1.1	EDMD with Random Gaussian Functions . . . . .	48
4.1.2	EDMD with Randomized Neural Networks . . . . .	54
<b>5</b>	<b>Conclusion and Outlook</b>	<b>57</b>
5.1	Summary . . . . .	58
5.2	Discussion . . . . .	58
5.3	Contributions . . . . .	58
5.4	Perspectives . . . . .	59
5.5	Data Availability . . . . .	60
<b>Bibliography</b>		<b>66</b>

# Introduction

Dynamical systems are frequently utilized to represent real-world phenomena, as they provide a means of describing the world around us, particularly with regard to how things change and develop over time based on a set of rules. The Koopman theory is a mathematical framework that allows for the analysis of nonlinear dynamical systems, with the goal of gaining insights into the underlying processes and making well-informed decisions on how to regulate the system. It was introduced in 1931 by American mathematician Bernard O. Koopman [2] as a way to study the evolution of measurement or observable functions, defined as  $g(x)$ , within the state space of a given system. He showed that the *Koopman operator*, which is a linear operator that acts on functions of state space, can be used to lift the nonlinear dynamics of the system to a linear dynamics in an infinite-dimensional function space. This allows one to use linear algebra and operator theory to study the nonlinear dynamics of the system, such as the spectral decomposition of Koopman operator that completely characterizes the behavior of a nonlinear system.

One of the methods to approximate the Koopman operator from data is EDMD method, which uses measurements of the system's state and observables to construct an approximation of the operator and therefore the leading eigenfunctions, eigenvalues and eigenmodes, which play a crucial role in understanding the long-term behavior of the nonlinear system. Eigenvalues of the operator can indicate the slow and fast dynamics of the system. And eigenfunctions are crucial to the understanding the underlying structure of the dynamics. Furthermore, eigenvalues and eigenfunctions contain information about timescales and *metastable* sets. In addition, by using a full-state observable,  $g(x) = x$  it's possible to represent the entire system dynamics with the eigenmodes, and analyze how different regions of the state space are behaving.

An important concept in Koopman theory is that of invariant spaces, where the Koopman analysis method does not track the evolution of all measurement functions in a state space, instead it approximates the evolution on a subset of the state space which is defined as the "Koopman-invariant subspace", subspace spanned by a finite set of measurement functions on which the Koopman operator acts, that are left unchanged by the operator. A finite-dimensional matrix representation of the operator can be obtained by restricting it to this subspace. The challenge is identifying a set of eigenfunctions that span this subspace, as they provide coordinates along which the dynamics behave linearly. In practice, an approximately invariant subspace is often used, which is defined by a set of functions that are well approximated by a finite sum of eigenfunctions. In order to be able to compute Koopman eigenfunctions numerically, the infinite-dimensional operator is projected onto a finite-dimensional space that is often chosen to be an approximately invariant subspace, depending on the choice of the dictionary of observables.

Consider a continuous-time and autonomous dynamical system described by the following ordinary differential equation:

$$\frac{d}{dt}\mathbf{x}(t) = \dot{\mathbf{x}}(t) = \mathbf{f}(\mathbf{x}(t)), \quad (0.1)$$

where  $\mathbf{x}(t) \in \mathcal{M}$  is a d-dimensional state of the system at time  $t$ , possibly living on a smooth

manifold  $\mathcal{M} \subseteq \mathbb{R}^d$  and  $\mathbf{f} : \mathcal{M} \rightarrow \mathcal{M}$  is a vector field describing the dynamics.

An important goal of modern dynamical systems is to find a new set of coordinates, denoted by  $\mathbf{z}$ , where the dynamics in the original equation (0.1) are linearized, such that the dynamics can be expressed as

$$\dot{\mathbf{z}} = \mathbf{L}\mathbf{z}. \quad (0.2)$$

In these new coordinates, the evolution of the system is fully characterized by the eigendecomposition of the discrete and continuous-time matrices  $\mathbf{L}$ . These new coordinates are represented by eigenfunctions of the Koopman operator, denoted by  $\mathcal{K}$ , which advances a measurement function  $g(\mathbf{x})$  related to the state forward through time according to the dynamics

$$\mathcal{K}g(\mathbf{x}_k) := g(\mathbf{F}(\mathbf{x}_k)) = g(\mathbf{x}_{k+1}), \quad (0.3)$$

where the autonomous, discrete-time dynamical system defined as

$$x_{k+1} = \mathbf{F}(x_k), \quad (0.4)$$

where  $x_k = x(t_k) = x(k\Delta t)$  for all  $k \geq 0$  with time step  $\Delta t$  and  $\mathbf{F} : \mathcal{M} \rightarrow \mathcal{M}$  is the flow map.

An eigenfunction  $\varphi$  of the Koopman operator with an associated eigenvalue  $\lambda$  is expressed as

$$\mathcal{K}\varphi(\mathbf{x}_k) = \lambda\varphi(\mathbf{x}_k) = \varphi(\mathbf{x}_{k+1}). \quad (0.5)$$

when applied to the measurement function  $g(\mathbf{x}_k)$ . Linear dynamical systems are desirable because significant effort has been invested in understanding the Koopman operator and approximating its spectral decomposition using measurement data.

## Outline of This Thesis

This thesis is divided into four chapters, which are as follows:

**Data-Driven Dynamical systems.** Chapter 1 of this thesis focuses on the analysis of dynamical systems, which are models of reality that can be used to predict and understand the behavior of complex systems. The chapter is divided into three sections, each of which addresses a different aspect of dynamical systems analysis. In the first section, we provide a brief definition of dynamical systems and discuss the two main components of a dynamical system: the state space and the evolution function. The second section covers the classification of dynamical systems, which is necessary for simplifying the analysis of complex systems. We explore different characteristics that can be used to classify dynamical systems, such as being deterministic or stochastic, autonomous or non-autonomous, and reversible or irreversible. In the third section, we discuss the objectives and challenges of modern dynamical systems analysis, including long-term prediction, estimation and control, and understanding system behavior. We also highlight the two main challenges in the analysis of modern dynamical systems: nonlinearity and unknown dynamics. To overcome these challenges, data-driven approaches such as machine learning and numerical simulations are becoming increasingly important in the field. We discuss two major strategies that are shaping modern data-driven dynamical systems: operator-based approaches and data-driven techniques such as DMD and EDMD. This chapter lays the foundation for the rest of the thesis, as it provides the necessary background and context for the analysis of the dynamical systems that will be explored in subsequent chapters.

**Koopman Operator Theory.** In Chapter 2, we introduce the Koopman operator, which is a mathematical tool used to analyze dynamical systems. The chapter is divided into four sections and several subsections. In the first section, an overview of the Koopman operator is presented for discrete and continuous-time dynamical systems. The Koopman operator is defined as an operator that acts on observables, which are functions that map the state space of the dynamical system to the complex plane. The section also discusses the generator of the Koopman operator and how it can be used for stochastic dynamical systems.

The second section of the chapter focuses on Koopman spectral analysis, where the eigenfunctions of the Koopman operator and its generator are defined for both discrete and continuous-time dynamical systems. The section also discusses how a collection of Koopman eigenfunctions can be utilized to create additional eigenfunctions. The third section of the chapter discusses Koopman invariant subspaces and intrinsic coordinates, which are used to represent the dynamical system in a higher-dimensional space. Finally, the fourth section of the chapter presents the Galerkin approximation of the Koopman generator and numerical approximation methods, to solve Koopman eigenfunction PDE and to estimate eigenfunctions analytically, such as the Laurent and Taylor series for eigenfunction expansion.

**Data Driven Methods.** Chapter 3 of this thesis focuses on data-driven methods for approximating the Koopman operator and its eigenfunctions. The chapter starts by introducing the extended dynamical mode decomposition (EDMD) algorithm, which is designed to calculate finite-dimensional approximations of the Koopman operator for highly nonlinear systems. EDMD relies on a dataset of snapshot pairs and a dictionary of observables to approximate the Koopman operator and its corresponding eigenfunctions, eigenvalues, and modes. The chapter also covers the convergence of the EDMD algorithm to a Galerkin method and presents examples of EDMD applied to stochastic differential equations.

The chapter then introduces the dynamic mode decomposition (DMD) algorithm and explains its relation to EDMD. Finally, the chapter presents several examples of EDMD with stochastic dynamical systems combined with monomials up to and including order 10. These examples include a 1D Ornstein-Uhlenbeck process, a 2D double-well problem, a 2D triple-well problem, and a 2D quadruple-well problem. Overall, the chapter presents a comprehensive overview of data-driven methods for approximating the Koopman operator and its eigenfunctions, with a focus on the EDMD algorithm and its applications to stochastic dynamical systems.

**Numerical Results.** Finally, In chapter 4, our focus is on the concept of Random Dynamic Mode Decomposition (RDMD) to combine EDMD with random basis functions to approximate the dominant Koopman eigenvalues and eigenfunctions. Specifically, we use random Gaussians with randomly chosen centers from a uniform distribution, as well as the untrained, randomly initialized neural networks (RINNs) for one- and two-dimensional (linear and nonlinear) systems. Towards the end of the chapter, we also introduce the use of trained RINNs in combination with EDMD to improve the accuracy of the approximation. The chapter begins by introducing the same examples as discussed in chapter 3, including a one-dimensional Ornstein-Uhlenbeck process, a one-dimensional triple-well problem, a two-dimensional double-well problem, a two-dimensional triple-well problem, and a quadruple-well problem. The primary goal of RDMD is to identify metastable regions that indicate system stability and provide insights into the long-term behavior of the dynamic system.



# Glossary

**Adjoint** – When dealing with a linear map of finite dimensions (i.e., a matrix  $\mathbf{K}$ ), its adjoint  $\mathbf{K}^*$  can be obtained by taking the complex conjugate transpose of the matrix. When the linear operator  $\mathcal{K}$  operates in infinite-dimensional spaces, the adjoint  $\mathcal{K}^*$  is defined such that  $\langle \mathcal{K}f, g \rangle = \langle f, \mathcal{K}^*g \rangle$ , where  $\langle \cdot, \cdot \rangle$  denotes an inner product.

**Control theory** – The methodology used to modify a dynamical system using sensing and actuation techniques in order to meet desired engineering specifications.

**Data matrix** – A matrix consisting of column vectors, where each vector represents a snapshot of the system state at a particular point in time. These snapshots can be sequential or obtained from a collection of experiments or initial conditions.

**DMD eigenvalue** – Eigenvalues of the best-fit DMD operator  $\mathbf{A}$  (as defined in dynamic mode decomposition) correspond to an oscillation frequency and a growth or decay term.

**DMD mode** – An eigenvector of the best-fit DMD operator  $\mathbf{A}$  (as defined in dynamic mode decomposition), also known as a dynamic mode. These modes exhibit spatial coherence and oscillate at a consistent frequency and growth or decay rate over time.

**Dynamic mode decomposition (DMD)** – The primary eigendecomposition of an best-fit linear operator  $\mathbf{K} = \mathbf{Y}\mathbf{X}^\dagger$ , which advances the data matrix  $\mathbf{X}$  into a subsequent data matrix  $\mathbf{Y}$ . The DMD modes are the eigenvectors of  $\mathbf{K}$ , and their time dynamics are determined by the corresponding eigenvalues.

**Dynamical system** – A mathematical representation of a system’s dynamic evolution. Usually, a dynamical system is formulated on a state-space, expressed through ordinary differential equations. The equations may be linear or nonlinear and may account for actuation inputs and sensor measurements of the state as outputs.

**Extended Dynamic Mode Decomposition (EDMD)** – It is a generalization of DMD, that approximates the Koopman operator and therefore the Koopman eigenvalue, eigenfunction, and mode tuples. The EDMD procedure requires two prerequisites: A data set of snapshot pairs and a dictionary of observables. Define a vector-valued function  $\Psi : \mathcal{M} \rightarrow \mathbb{C}^{1 \times p}$  as

$$\Psi(x) = [\psi_1(x), \psi_2(x), \dots, \psi_p(x)], \quad (0.6)$$

then instead of assuming a linear relationship between the data matrices  $\mathbf{X}$  and  $\mathbf{Y}$ , EDMD aims at finding a linear relationship between the two transformed data matrices  $\Psi_X$  and  $\Psi_Y \in \mathbb{C}^{p \times M}$

$$\mathbf{K} \triangleq \mathbf{G}^\dagger \mathbf{A} = \Psi_X^\dagger \Psi_Y. \quad (0.7)$$

**Galerkin projection** – A technique that reduces governing partial differential equations to ordinary differential equations. The method utilizes orthogonal basis modes to approximate the solution and focuses on the dynamics of the coefficients of the modes.

**Hilbert space** – A generalized vector space that comes with an inner product. When referred to in this text, a Hilbert space typically refers to an infinite-dimensional function space. They are also complete metric spaces, which provide a robust mathematical foundation for calculus on functions.

**Koopman eigenfunction** – An eigenfunction of the Koopman operator. These functions correspond to measurements on the state-space of a dynamical system, forming intrinsic coordinates. In other words, these intrinsic measurements exhibit linear time evolution despite the underlying system being nonlinear.

**Koopman operator** – An infinite-dimensional linear operator that advances measurement functions from an infinite-dimensional Hilbert space through a dynamical system.

**Least squares regression** – A regression technique where a best-fit line or vector is found by minimizing the sum of squares of the error between the model and the data.

**Linear system** – A system that exhibits superposition, meaning that the output resulting from the combination of any two inputs is equal to the sum of the outputs produced by each input separately. Specifically, linear time-invariant dynamical systems are represented by linear operators, which take the form of matrices, and satisfy the properties of additivity and homogeneity.

**Machine learning** – A collection of statistical methods and algorithms that can identify and extract significant patterns from data. The analysis can be supervised or unsupervised, and the aim is to group, classify, or make predictions based on the available information.

**Observable function** – A function that quantifies or describes a specific aspect or property of the state of a system. Observable functions are usually defined as elements of a Hilbert space.

**Perron-Frobenius operator** – The adjoint of the Koopman operator, the Perron-Frobenius operator is an operator that moves probability density functions through a dynamical system in an infinite-dimensional space.

**Proper orthogonal decomposition (POD)** – A technique for breaking down data from a dynamic system into a series of orthogonal modes using methods such as singular value decomposition. In the case where the data represents the velocity measurements of a system, such as a fluid, the modes are ranked based on the amount of energy they contain in the data.

**Reduced-order model (ROM)** – A mathematical model that approximates the behavior of a high-dimensional system using a low-dimensional representation. ROMs are typically used to reduce the computational cost of simulating complex systems while maintaining an acceptable level of accuracy.

**Singular value decomposition (SVD)** - Given a matrix  $\mathbf{K} \in \mathbb{C}^{n \times m}$ , the SVD is given by  $\mathbf{K} = U\Sigma V^*$ , where  $U \in \mathbb{C}^{n \times n}$ ,  $\Sigma \in \mathbb{C}^{n \times m}$ , and  $V \in \mathbb{C}^{m \times m}$ . The matrices  $U$  and  $V$  are unitary, so that  $UU^* = U^*U = I$  and  $VV^* = V^*V = I$ . The matrix  $\Sigma$  has entries along the diagonal corresponding to the singular values that are ordered from largest to smallest. This produces a hierarchical matrix decomposition that splits a matrix into a sum of rank-1 matrices given by the outer product of a column vector (left singular vector) with a row vector (conjugate transpose of right singular vector). These rank-1 matrices are ordered by the singular value so that the first  $r$  rank-1 matrices form the best rank- $r$  matrix approximation of the original matrix in a least-squares sense.

**Snapshot** – A single measurement of a high-dimensional system at a specific time. Multiple snapshots collected at different times can be organized as column vectors in a data matrix.

**State space** – the collection of all feasible states that a system can be in. This space can often be represented as a vector space like  $\mathbb{R}^n$ , but it can also be a smooth manifold, denoted by  $\mathcal{M}$ .

**Stochastic gradient descent** – A technique used in optimization problems where the gradient is approximated with a single data point instead of using all available data. This method is also known as incremental gradient descent. In each step of the algorithm, a randomly selected data point is used to compute the gradient direction.

**System identification** – The process by which a model is constructed for a system from measurement data, possibly after perturbing the system.

**Unitary matrix** – A matrix that has the property of its complex conjugate transpose being equal to its inverse. The eigenvalues of a unitary matrix lie on the complex unit circle, and it can be thought of as a coordinate transformation that maintains the Euclidean distance between any two vectors.

Chapter 1

# Data-Driven Dynamical systems

In this chapter, we present a modern perspective on dynamical systems, focusing on current objectives and open challenges. Through a mathematical introduction to notation, we provide a summary of key motivations and challenges in the field of dynamical systems, with a particular emphasis on classification.

## Contents

---

1.1	Dynamical Systems	2
1.2	Classification of Dynamical Systems	2
1.3	Modern Objectives and Challenges in Dynamical Systems	3

---

## 1.1 Dynamical Systems

Dynamical system is our model of reality and can be found in a variety of fields, including mathematics, physics, biology, chemistry, and engineering. It is how we describe the world around us, especially how things change and evolve in time according to a set of rules or laws! Those things are states that represent the current configuration of the system. For instance, dynamical systems can be used to model the Brownian motion of particles suspended in a fluid, the growth and population of a species of bacteria, the behavior of a fluid, such as the flow of water through a pipe or the movement of air over an aircraft wing, the behavior of a machine learning model, such as a neural network or a support vector machine. At any given time, a dynamical system is typically composed of two parts that together form a complete description of the dynamical system and can be used to understand and predict the behavior of the system over time; the state space and the evolution function.

- **State space:** The state space is the set of all possible states of a dynamical system. It can be finite, consisting of just a few points or finite-dimensional, consisting of infinite number of points forming a smooth manifold or infinite-dimensional. The number of variables the modeler feels is needed to completely describe the system is the dimension of its state space.
- **Evolution function:** The evolution function, also known as the dynamics or flow function, is a rule that describes how the state changes over time, i.e., given the current state, what is the state of the system will be in the next instant of time.

## 1.2 Classification of Dynamical Systems

For investigating the dynamical systems, it is necessary to specify some characteristics that provide a subdivision into classes of dynamical systems. Specific methods are available for some of these classes, thus such a classification can help to simplify the analysis. Dynamical systems can be either discrete or continuous, linear or nonlinear, and may also exhibit other characteristics such as being deterministic or stochastic, autonomous or nonautonomous, and reversible or irreversible.

- **Deterministic vs. stochastic model:** In a deterministic system the present state can be determined uniquely from the past states (no randomness is allowed), evolution equations fully determine the future behavior of the system. Stochastic models possess some inherent randomness, the evolution equations include some random elements or uncertainties and the behavior cannot be entirely predicted. Chaotic model is a deterministic model with a behavior that cannot be entirely predicted. They are predictable in the very short term, but appears random for longer periods.
- **Autonomous vs. non-autonomous:** An autonomous or time-independent dynamical system is a system where the evolution of the system is determined by its own internal dynamics that do not depend on time or any external inputs. A non-autonomous or time-variant dynamical system is a system where the evolution of the system depends on controls or external inputs which can be time varying.
- **Reversible vs. irreversible:** A reversible dynamical system is one in which the evolution of the system can be "undone" by reversing the direction of time. This means that the final state of the system will be the same as the initial state, regarding the direction of evolution. On the other hand, if the evolution of a system is irreversible, then reversing the direction of time will not cause the system to return to its original state.

**Example 1.2.1.** Consider a deterministic, continuous-time, and autonomous dynamical system described by the following ordinary differential equation:

$$\dot{x}(t) = \mathbf{f}(x(t)), \quad (1.1)$$

where  $x(t) \in \mathcal{M}$  is a  $d$ -dimensional state of the system at time  $t$ , possibly living on a smooth manifold  $\mathcal{M} \subseteq \mathbb{R}^d$  and  $\mathbf{f} : \mathcal{M} \rightarrow \mathcal{M}$  is a vector field describing the dynamics.

In practice, we typically have access to measurement data of our system, discretely sampled in time. This data is governed by the deterministic, autonomous, discrete-time dynamical system or difference equation

$$x_{k+1} = \mathbf{F}(x_k), \quad (1.2)$$

where  $x_k = x(t_k) = x(k\Delta t)$  for all  $k \geq 0$  with time step  $\Delta t$  and  $\mathbf{F} : \mathcal{M} \rightarrow \mathcal{M}$  is the flow map.

Discrete-time dynamics are more general than the continuous-time formulation, encompassing discontinuous and hybrid systems as well. For every continuous differential equation, we can define a discrete-time dynamical system corresponding to (1.1), where we may essentially write the discrete-time propagator  $\mathbf{F}^{\Delta t}(x) \equiv \mathbf{F}(x, \Delta t)$  or  $\Phi^{\Delta t}(x) \equiv \Phi(x, \Delta t)$  representing the flow map through  $\Delta t$  of (1.1) in terms of continuous-time differential equation as follows

$$\mathbf{F}^{\Delta t}(x_k) = x_{k+1} = x_k + \int_{k\Delta t}^{(k+1)\Delta t} \mathbf{f}(x(\tau)) d\tau. \quad (1.3)$$

We can also express (1.3) as follows: for an arbitrary time  $t$ , the flow map  $\mathbf{F}^t$  or  $\Phi^t$  is defined as

$$\Phi^t(x(t_0)) = x(t_0 + t) = x(t_0) + \int_{t_0}^{t_0+t} \mathbf{f}(x(\tau)) d\tau. \quad (1.4)$$

Therefore, if  $x(t)$  is a solution of (1.1) with initial condition  $x(t_0) = x_0$ , then  $\{\Phi(x_0, .)\}_{t \geq 0}$  is a solution of (1.1) with initial condition  $x(t_0) = x_0$ , i.e.,  $\Phi^t(x_0) = x(t)$ .

## 1.3 Modern Objectives and Challenges in Dynamical Systems

A major goal of modern dynamical systems is to find a new vector of coordinates  $\mathbf{z}$  where the dynamics (1.1) are simplified, or ideally, linearized:

$$\dot{\mathbf{z}} = \mathbf{L}\mathbf{z}. \quad (1.5)$$

Also, in the discrete-time case (1.2) the goal is still to find a linearizing coordinate transform so that

$$\mathbf{z}_{k+1} = \mathbf{K}\mathbf{z}_k. \quad (1.6)$$

In these new linearizing coordinates, the dynamics and the evolution of the system are entirely characterized by the eigendecomposition of the discrete and continuous-time matrices  $\mathbf{K}$  and  $\mathbf{L}$  respectively. These coordinates are represented by eigenfunctions of the Koopman operator,  $\mathcal{K}$ , which moves a measurement function  $g(x)$  related to the state forward through time according to the dynamics:

$$\mathcal{K}g(x_k) := g(\mathbf{F}(x_k)) = g(x_{k+1}). \quad (1.7)$$

For an eigenfunction  $\varphi$  of  $\mathcal{K}$ , corresponding to an eigenvalue  $\lambda$ , this becomes

$$\mathcal{K}\varphi(x_k) = \lambda\varphi(x_k) = \varphi(x_{k+1}). \quad (1.8)$$

Thus, it is highly desirable to work with linear dynamical systems because a lot of effort has been put into understanding the Koopman operator and using measurement data to approximate its spectral decomposition. Additionally, there are many techniques available for analyzing, predicting, simulating, estimating, and controlling these systems. [3, 5].

Dynamical systems are often used to model real-world phenomena, and by analyzing these systems we can gain insights into the underlying processes and make well-informed decisions on how to manipulate or regulate the system. This section addresses three primary objectives of modern dynamical systems analysis:

- **Long-term prediction:** One of the main goals is to make predictions about the future state of a system over a long period of time.
- **Estimation and control:** It is often necessary to estimate the full state of a system from limited measurements or observations, and to manipulate or optimize the behavior of a system to achieve a desired outcome.
- **Understanding and interpreting system behavior:** Dynamical systems analysis seeks to identify and understand the structures and patterns of a system while minimizing complexity and analyzing trajectories and solutions to the governing equations of motion to gain physical insight into its behavior.

Real-world systems often exhibit complex, nonlinear behavior at multiple scales in both space and time. There is often uncertainty in the equations that govern their motion, as well as in the values of their parameters and in the measurements we take of them. Some systems are more sensitive to this uncertainty than others, and stochastic approaches may be necessary to analyze them. This section focuses on addressing two main challenges in the analysis of modern dynamical systems:

- **Nonlinearity:** Nonlinear systems are more difficult to analyze, control and predict than linear systems because their behavior cannot be described by a set of linear equations. This means that traditional linear analysis techniques, such as eigenvalue analysis, may not be applicable. In addition, nonlinear systems can exhibit complex behavior, such as bifurcations, chaos, and attractors, which can make them difficult to understand and predict.
- **Unknown dynamics:** Unknown dynamics can also pose a challenge in the study of dynamical systems. In many cases, the governing equations or laws that describe the behavior of a system are not known or are difficult to obtain. This can make it difficult to analyze and predict the behavior of the system, especially if the system is nonlinear. Even in systems where we do know the governing equations, we struggle to find patterns in high-dimensional systems to uncover intrinsic coordinates and coarse-grained variables along which the dominant behavior evolves.

It is also worth mentioning that **high-dimensionality** a third major challenge associated with many modern dynamical systems, and it refers to the fact that the presence of large number of variables or the presence of hidden variables make it harder to uncover or analyze and understand the behavior of the underlying dynamics of the system.

Determining unknown dynamics from data and finding intrinsic coordinates that allow for linear representation of nonlinear systems are two key goals in modern dynamical systems research, which can be achieved through data-driven approaches such as machine learning and numerical simulations to discover governing equations, model and understand the system. There are various methods for addressing these difficulties. Specifically, there are two major strategies that are shaping modern data-driven dynamical systems:

- **Operator-based approaches:** To tackle the problem of nonlinearity, operator-based techniques for dynamical systems are gaining popularity. As we will demonstrate, it is possible to express nonlinear dynamical systems using infinite-dimensional linear operators, such as the **Koopman** operator that enhances *measurement* or *observable* functions, and the **Perron-Frobenius** operator that enhances probability densities through the dynamics. These two operators are adjoint to each other and it should therefore theoretically not matter which one is used to study the system's behavior.
- **Data-driven techniques:** One of the key approaches that defines modern data-driven dynamical systems is the use of advanced data-driven dimension reduction or data-analysis techniques such as the dynamic mode decomposition (DMD) and extended dynamic mode decomposition (EDMD) which use different types of basis functions like Gaussian, Monomials, or neural networks. These methods use a combination of mathematical techniques and machine learning algorithms to extract meaningful information from large datasets and provide accurate representations of the dynamics of systems which can be used for prediction, control, and optimization.



Chapter **2**

# Koopman Operator Theory

This chapter presents an introduction to Koopman Operator Theory, a mathematical framework for analyzing and modeling dynamical systems. We begin with an overview of the Koopman Operator, including its applications to both deterministic and stochastic dynamical systems. Next, we discuss Koopman Spectral Analysis, which provides a powerful tool for understanding the dynamics of a system through spectral decomposition. We also explore the Koopman Mode Decomposition and Koopman-invariant subspaces, which enable the identification of key features and patterns in the system's behavior. Finally, we explore numerical approximation methods for Koopman Operators, including Laurent and Taylor series expansions and Galerkin Approximation of the Koopman Generator.

## Contents

<b>2.1 An Overview of Koopman Operator</b> . . . . .	<b>8</b>
2.1.1 Koopman Operator for Deterministic Dynamical Systems . . . . .	9
2.1.2 Koopman Operator for Stochastic Dynamical Systems . . . . .	11
<b>2.2 Koopman Spectral Analysis</b> . . . . .	<b>13</b>
2.2.1 Spectral Decomposition of Koopman Operators . . . . .	13
2.2.2 Koopman Mode Decomposition . . . . .	17
<b>2.3 Koopman Invariant Subspaces and Intrinsic Coordinates</b> . . . . .	<b>20</b>
2.3.1 Koopman-Invariant Subspaces Containing the State . . . . .	21
2.3.2 Applications of Koopman Embedding . . . . .	21
2.3.2.1 Continuous-Time Representation for Koopman Embedding . .	21
2.3.2.2 Discrete-Time Representation for Koopman Embedding . . .	25
<b>2.4 Numerical Approximation Methods</b> . . . . .	<b>27</b>
2.4.1 Laurent and Taylor Series for Eigenfunctions Expansion. . . . .	28
2.4.2 Galerkin Approximation of the Koopman Generator . . . . .	29

## 2.1 An Overview of Koopman Operator

The Koopman operator is a linear operator that acts on functions of state space in a nonlinear dynamical system. It can be used to transform the nonlinear dynamics of the system into a linear dynamics in an infinite-dimensional function space. This allows for the use of linear algebra and operator theory to analyze the system's behavior. The spectral decomposition of the Koopman operator completely characterizes the behavior of a nonlinear system, with eigenvalues indicating the slow and fast dynamics and eigenfunctions providing information about the underlying structure of the dynamics.

One method to approximate the Koopman operator is the EDMD method, which constructs an approximation of the operator and identifies the leading eigenfunctions and eigenvalues. Invariant spaces are important in Koopman theory, as the operator analysis method does not track the evolution of all measurement functions in a state space, but instead approximates the evolution on a subset of the state space defined as the "Koopman-invariant subspace". In practice, an approximately invariant subspace is often used, defined by a set of functions that are well-approximated by a finite sum of eigenfunctions. By using a full-state observable, it's possible to represent the entire system dynamics with the eigenmodes and analyze how different regions of the state space are behaving.

We begin by establishing some conventions and introducing the concept of the Koopman operator in the context of both discrete-time and continuous-time systems, as adopted from [6]. We Consider a *measure space*  $(\mathcal{M}, \mathcal{B}, \rho)$ , comprised of a *state space*  $\mathcal{M} \subseteq \mathbb{R}^d$ , a  $\sigma$ -algebra, and a (probability) measure, respectively. The transformation of the state, often in the course of time, is described by a dynamical system  $\mathbf{F} : \mathcal{M} \rightarrow \mathcal{M}$ , where  $\mathbf{F}$  is a  $\rho$ -measurable map. Our focus is on the behavior of observables within the state space, as the Koopman operator explains the evolution of these observables. To this end, we characterize an observable as a function  $g : \mathcal{M} \rightarrow \mathbb{C}$ , where  $g$  is an element of some infinite-dimensional function space  $\mathcal{G}$ . Consequently, rather than analyzing the trajectory where the state  $x \in \mathcal{M}$  evolves as  $\{x, \mathbf{F}(x), \mathbf{F}^2(x), \dots\}$ , we now track the trace where the observable  $g \in \mathcal{G}$  evolves as  $\{g(x), g(\mathbf{F}(x)), g(\mathbf{F}^2(x)), \dots\}$ .

For the discrete dynamical system  $x_{k+1} = \mathbf{F}(x_k)$ , we characterize the (discrete) Koopman operator,  $\mathcal{K} : \mathcal{G} \longleftrightarrow \mathcal{G}$ , as

$$(\mathcal{K}g)(x) = g(\mathbf{F}(x)), \quad (2.1)$$

which is basically a composition,  $\mathcal{K}g = g \circ \mathbf{F}$ , of the observable  $g$  and the map  $\mathbf{F}$ . Note that, when  $\mathcal{M}$  is a finite set,  $\mathcal{K}$  is a finite dimensional operator and can be expressed by a matrix. Nonetheless, when  $\mathcal{M}$  is finite-dimensional or infinite-dimensional,  $\mathcal{K}$  is generally infinite-dimensional. Often, we have access to a specific collection of observables  $\{g_1, \dots, g_m\} \subset \mathcal{G}$ . We can extend the Koopman operator to a larger space in an intuitive and straightforward manner: If the vector valued observables,  $\mathbf{g} = \{g_1, \dots, g_m\}^\top \in \mathcal{G}^m$ , the space of  $\mathbb{C}^m$ -valued observables on  $\mathcal{M}$ , then  $\mathcal{K}_m : \mathcal{G}^m \rightarrow \mathcal{G}^m$  is defined as

$$(\mathcal{K}_m \mathbf{g})(x) := \begin{bmatrix} \mathcal{K}g_1(x) \\ \vdots \\ \mathcal{K}g_m(x) \end{bmatrix}. \quad (2.2)$$

Note that, for simplicity, we often refer to  $\mathcal{K}_m$  as  $\mathcal{K}$ .

The Koopman operator can be extended to accommodate continuous-time dynamical systems of the form  $\dot{x} = \mathbf{f}(x)$ , where  $\mathbf{f}$  is a vector field describing the dynamics. In this case, there is not just the Koopman operator  $\mathcal{K}$ , but a set or semi-group of operators  $\{\mathcal{K}^t\}_{t \geq 0}$  generated by  $\mathcal{L}$ . We refer to the semi-group  $\{\mathcal{K}^t\}$  as the *Koopman semigroup*.

We explicitly specify the influence of the semigroup on the observable  $g \in \mathcal{G}$  as

$$(\mathcal{K}^t g)(x) = g(\Phi^t(x)). \quad (2.3)$$

Here,  $\Phi^t(x) \equiv \Phi(x, t)$  serves as the flow map that maps a given initial state  $x_0 \in \mathcal{M}$  to the solution at time  $t$  of the initial value problem (IVP) having initial condition  $x(0) = x_0 \in \mathcal{M}$ ; i.e., for a fixed  $x_0 \in \mathcal{M}$ , the trajectory  $\{\Phi(x_0, .)\}_{t \geq 0}$  is a solution of the IVP

$$\dot{x} = \mathbf{f}(x), \quad x(0) = x_0. \quad (2.4)$$

That is,  $\Phi^t(x(0)) = x(t)$ .

The generator of the Koopman semigroup is characterized by

$$\mathcal{L}g := \lim_{t \rightarrow 0} \frac{\mathcal{K}^t g - g}{t}, \quad (2.5)$$

in which the limit is taken in the strong sense.

Regarding the selection of the function space  $\mathcal{G}$ , in most cases,  $\mathcal{G}$  is not determined beforehand, but is roughly outlined by a set of properties it should possess, e.g., a vector space, complete or Banach space, such as integrable functions  $L^1(\mathcal{M}) := L^1(\mathcal{M}, \mathcal{B}, \rho)$  and essentially bounded measurable functions  $L^\infty(\mathcal{M})$ . Hilbert spaces, such as  $L^2(\mathcal{M}, \rho)$  is a popular choice in modern applied mathematics. The selection of the space can have consequences on the characteristics of the operator and its approximations. In any event,  $\mathcal{G}$  is of significantly higher dimension than  $\mathcal{M}$ , that is, countably or uncountably infinite.

Throughout this section we will refer to [8, 13, 17], and we aim to connect the Koopman operator and the data-driven technique EDMD, that takes advantage of a data set of successive "snapshot" pairs and a dictionary of observables which spans a subspace of the space of observables. We will define Koopman operator along with the properties relevant to EDMD for different types of dynamical systems, such as **deterministic** and **non-deterministic**, and then explain how the algorithm can be utilized to approximate the Koopman tuples.

In what follows, let  $\mathcal{M} \subseteq \mathbb{R}^d$ , be the finite-dimensional state space. We consider complex-valued *measurement* or *observable* functions  $g : \mathcal{M} \rightarrow \mathbb{C}$ . These observables are elements of an infinite-dimensional Hilbert space  $\mathcal{G} = L^2(\mathcal{M}, \rho)$ , given by the Lebesgue square-integrable functions on  $\mathcal{M}$  with respect to a positive, single-valued analytic function  $\rho$  where  $\|\rho\|_{\mathcal{M}} = \int_{\mathcal{M}} \rho(x) dx = 1$ , but it does not have to be an invariant measure for the system. This requirement is necessary in order for us to use inner products in the Galerkin-like method that will be discussed later.

### 2.1.1 Koopman Operator for Deterministic Dynamical Systems

The Koopman operator, enhances *measurement* or *observable* functions of the state and allows for the analysis of nonlinear dynamics through the lifting of nonlinear system to a higher-dimensional linear system. To understand the fundamental characteristics of the Koopman operator, we will first examine an autonomous ordinary differential equation on  $\mathcal{M}$  of the form

$$\dot{x} = \mathbf{f}(x), \quad (2.6)$$

where  $\mathbf{f} : \mathcal{M} \rightarrow \mathcal{M}$ . The family of Koopman operators  $\mathcal{K}^t : L^2(\mathcal{M}) \rightarrow L^2(\mathcal{M})$  or the *Koopman semigroup* of operators  $\{\mathcal{K}^t\}$  parameterized by  $t$ , is given by

$$(\mathcal{K}^t g)(x) = g(\mathbf{F}^t(x)), \quad (2.7)$$

where  $\mathbf{F}^t : \mathcal{M} \rightarrow \mathcal{M}$  is the flow map operator, see [Example 1.2.1](#) and [\(2.3\)](#), and  $\mathcal{G}$  is a set of *observables*  $g : \mathcal{M} \rightarrow \mathbb{C}$ . The infinite-dimensional Koopman operator is linear, a property which is derived from the linearity of the composition or addition operation in function spaces  $\mathcal{G}$ , i.e.,

$$\mathcal{K}^t(\alpha_1 g_1(x) + \alpha_2 g_2(x)) = \mathcal{K}^t(\alpha_1 g_1 + \alpha_2 g_2)(x) \quad (2.8a)$$

$$= (\alpha_1 g_1 + \alpha_2 g_2)(\mathbf{F}^t(x)) \quad (2.8b)$$

$$= \alpha_1 g_1(\mathbf{F}^t(x)) + \alpha_2 g_2(\mathbf{F}^t(x)) \quad (2.8c)$$

$$= \alpha_1 \mathcal{K}^t g_1(x) + \alpha_2 \mathcal{K}^t g_2(x). \quad (2.8d)$$

The Koopman framework achieves linearity in  $\mathcal{K}^t$ , despite the nonlinearity of  $\mathbf{F}^t$ , by replacing the finite-dimensional state space  $\mathcal{M}$  with an infinite-dimensional function space  $\mathcal{G}$ .

- **When time  $t$  is discrete**,  $t \in \mathbb{N}$  and the system's behavior does not change over time (dynamics are autonomous), then  $\mathbf{F}^t$  that describes the system's evolution is a repeated composition of a single  $\mathbf{F} \equiv \mathbf{F}^1$  given by  $\mathbf{F}^t(x) = \mathbf{F}(\mathbf{F}(\dots(\mathbf{F}(x))))$ , so that the  $\mathcal{K}^t g$  is also created by repeatedly applying  $\mathcal{K} \equiv \mathcal{K}^1$ . The generator  $\mathcal{K}$  of the (countable) composition semigroup is then called *the* Koopman operator, which leads to a dynamical system

$$g_{k+1} = \mathcal{K} g_k, \quad (2.9)$$

analogous to  $x_{k+1} = \mathbf{F}(x_k)$ , except that [\(2.9\)](#) is linear and infinite-dimensional.

In simpler terms, for a discrete-time system with timestep  $\Delta t$ , [\(2.7\)](#) becomes:

$$\mathcal{K}^{\Delta t} g(x_k) = g(\mathbf{F}^{\Delta t}(x_k)) = g(x_{k+1}), \quad (2.10)$$

where the Koopman operator defines an infinite-dimensional dynamical system that can be described linearly, and forwards the observation of the state  $g_k = g(x_k)$  to the next time step.

- **When time  $t$  is continuous** the flow map family satisfies the semigroup property, i.e., for  $t, s \geq 0$  it holds that

$$\mathbf{F}^{t+s}(x) = \mathbf{F}^t(\mathbf{F}^s(x)), \quad (2.11)$$

which can be enriched to  $t, s \in \mathbb{R}$  if the flow map is invertible. Also, the Koopman operator family  $\mathcal{K}^t$  satisfies these properties that follow from the semigroup properties of the flow map

$$(\mathcal{K}^t \mathcal{K}^s g)(x) = (\mathcal{K}^t g)(\mathbf{F}^s(x)) = g(\mathbf{F}^t(\mathbf{F}^s(x))) = g(\mathbf{F}^{t+s}(x)) = (\mathcal{K}^{t+s} g)(x). \quad (2.12)$$

For sufficiently smooth dynamical systems, it is also possible to define the continuous-time analogue of the Koopman dynamical system in [\(2.10\)](#):

$$\dot{g} = \mathcal{L} g, \quad (2.13)$$

where  $\mathcal{L}$  is the infinitesimal generator of the Koopman operator semigroup  $\mathcal{K}^t$ , defined as:

$$\mathcal{L} g := \lim_{t \rightarrow 0} \frac{\mathcal{K}^t g - g}{t} = \lim_{t \rightarrow 0} \frac{g \circ \mathbf{F}^t - g}{t}, \quad (2.14)$$

and with respect to [\(2.6\)](#) given by

$$\mathcal{L} g = \frac{d}{dt} g = \nabla g \cdot \mathbf{f} = \sum_{i=1}^d \frac{\partial g}{\partial x_i} \mathbf{f}_i \quad (2.15)$$

which results from the chain rule applied to  $g(x(t))$ :

$$\frac{d}{dt}g(x(t)) = \nabla g \cdot \dot{x}(t) = \nabla g \cdot \mathbf{f}(x(t)), \quad (2.16)$$

and equating with

$$\frac{d}{dt}g(x(t)) = \lim_{\tau \rightarrow 0} \frac{g(x(t + \tau)) - g(x(t))}{\tau} = \mathcal{L}(g(x(t))), \quad (2.17)$$

as the generator  $\mathcal{L}$  is the Lie derivative of  $g$  along the vector field  $\mathbf{f}(x)$  when the dynamics is given by (1.1), and hence also called the Lie operator. If  $g$  is continuously differentiable, then  $u(t, x) = \mathcal{K}^t g(x)$  satisfies the first-order partial differential equation

$$\frac{\partial u}{\partial t} = \mathcal{L}u, \quad (2.18)$$

which is known as *Liouville* equation, and consequently  $\mathcal{K}^t = \exp(t\mathcal{L})$ , where the adjoint of the Lie operator is called the *Liouville operator*  $\mathcal{L}^*$ , especially in Hamiltonian dynamics, while the adjoint of the Koopman operator is the *Perron–Frobenius operator*. Thus, the generator of the *Perron–Frobenius operator*, is given by

$$\mathcal{L}^*g = - \sum_{i=1}^d \frac{\partial(\mathbf{f}_i g)}{\partial x_i}. \quad (2.19)$$

The linear dynamical systems in (2.9) and (2.13) are analogous to the dynamical systems in (1.1) and (1.2), respectively.

### 2.1.2 Koopman Operator for Stochastic Dynamical Systems

Similarly, the definition of the Koopman operator can be generalized to the following s-dimensional Ornstein-Uhlenbeck process, given by an Itô stochastic differential equations<sup>1</sup> of the form

$$dX_t = b(X_t)dt + \sigma(X_t)dW_t, \quad (2.20)$$

where  $\{X_t\}_{t \geq 0}$  is a time-homogeneous<sup>2</sup> stochastic process defined on the bounded state space  $\mathcal{M} \subset \mathbb{R}^d$  and  $b : \mathbb{R}^d \rightarrow \mathbb{R}^d$  denotes the drift term,  $\sigma : \mathbb{R}^d \rightarrow \mathbb{R}^{d \times s}$  the diffusion term, and  $W_t$  an s-dimensional Wiener process (Brownian motion). This leads to the stochastic Koopman operator that is defined by

$$(\mathcal{K}^t g)(x) = \mathbb{E}[g(\mathbf{F}^t(x)) | X_t = x], \quad (2.21)$$

where  $\mathbb{E}[\cdot]$  denotes the expectation value. It can be proven, using Itô's lemma, that when a function  $g$  that is twice continuously differentiable is given, the infinitesimal generator of the Koopman operator in a stochastic context can be identified by

$$\mathcal{L}g = b \cdot \nabla_x g + \frac{1}{2}a : \nabla_x^2 g = \sum_{i=1}^d b_i \frac{\partial g}{\partial x_i} + \frac{1}{2} \sum_{i=1}^d \sum_{j=1}^d a_{ij} \frac{\partial^2 g}{\partial x_i \partial x_j}, \quad (2.22)$$

---

<sup>1</sup>A general time-homogeneous Itô SDE is given by  $dX_t = -\alpha(X_t)X_t dt + \sigma(X_t)dW_t$ , where  $\alpha : \mathbb{R}^d \rightarrow \mathbb{R}^d$  and  $\sigma : \mathbb{R}^d \rightarrow \mathbb{R}^{d \times s}$  are coefficient functions, and  $\{W_t\}_{t \geq 0}$  is a s-dimensional standard Wiener process.

<sup>2</sup>We call a stochastic process  $\{X_t\}_{t \geq 0}$  time-homogeneous, or autonomous, if it holds for every  $t \geq s \geq 0$  that the distribution of  $X_t$  conditional to  $X_s = x$  only depends on  $x$  and  $(t - s)$ . It is the stochastic analogue of the flow of an autonomous (time-independent) ordinary differential equation.

$a = \sigma\sigma^\top$  and  $\nabla_x^2$  denotes the Hessian, see [15] for more details about the properties of the generator associated with non-deterministic dynamical systems. If  $g$  is twice continuously differentiable, then  $u(t, x) = \mathcal{K}^t g(x)$  satisfies the second-order partial differential equation  $\frac{\partial u}{\partial t} = \mathcal{L}u$ , which is called *Kolmogorov backward* equation. Due to this relationship, the Koopman operator is also known as the backward operator. In this case the adjoint operator of  $\mathcal{L}$  which is the infinitesimal generator of the *Perron–Frobenius operator* is

$$\mathcal{L}^*g = -\sum_{i=1}^d \frac{\partial(b_i g)}{\partial x_i} + \frac{1}{2} \sum_{i=1}^d \sum_{j=1}^d \frac{\partial^2(a_{ij}g)}{\partial x_i \partial x_j}, \quad (2.23)$$

so that  $\frac{\partial u}{\partial t} = \mathcal{L}^*u$  becomes the *Fokker–Planck equation* or *Kolmogorov forward equation*, therefore the *Perron–Frobenius operator* is also referred to as forward operator [1].

A significant category of stochastic differential equations are those that are reversible with respect to a measure  $\rho$ . This measure  $\rho$ , in this scenario, must be a stationary measure. Reversible systems can just be described by the diffusion  $\sigma$  and a scalar potential  $V : \mathbb{R}^d \rightarrow \mathbb{R}$ , from which the drift is obtained by

$$b = -\frac{1}{2}a\nabla V + \frac{1}{2}\nabla \cdot a, \quad (2.24)$$

where the divergence in  $\frac{1}{2}\nabla \cdot a$  is applied to each column of  $a$ . In this reversible context, both the Koopman operator and the Perron–Frobenius operator are self-adjoint. The Koopman generator of a reversible SDE becomes self-adjoint and is typically an unbounded operator on a suitable dense subspace of  $L^2(\mathcal{M}, \rho)$ .

**Example 2.1.1.** *The one-dimensional Ornstein–Uhlenbeck process, given by an Itô SDE of the form*

$$dX_t = -\nabla V(X_t)dt + \sqrt{2\beta^{-1}}dW_t, \quad (2.25)$$

*is reversible for any given potential  $V$ , with the stationary measure  $\rho(x) \sim \exp(-\beta V(x))$ . In particular, for a potential  $V(x) = \frac{1}{2}\alpha x^2$  we obtain*

$$\rho(x) = \frac{1}{\sqrt{2\pi\alpha^{-1}\beta^{-1}}} \exp\left(-\frac{x^2}{2\alpha^{-1}\beta^{-1}}\right) \sim \exp(-\beta V(x)). \quad (2.26)$$

*The parameter  $\alpha$  is the friction coefficient, and  $\beta$  is the diffusion coefficient or inverse temperature. The infinitesimal generator  $\mathcal{L}$  of the Koopman semigroup becomes self-adjoint on  $L^2(\mathcal{M}, \rho)$ , where we obtain*

$$\mathcal{L}g = -\alpha\nabla g + \beta^{-1}\Delta g \quad \text{and} \quad \mathcal{L}^*g = \alpha\nabla g + \Delta V g + \beta^{-1}\Delta g, \quad (2.27)$$

*and*

$$\langle \mathcal{L}g, f \rangle_\mu = \langle g, \mathcal{L}^*f \rangle_\mu = \langle g, \mathcal{L}f \rangle_\mu, \quad (2.28)$$

*where  $\langle f, g \rangle_\mu = \int_{\mathcal{M}} f(x)g(x)d\rho(x)$ .*

**Example 2.1.2.** *The general Smoluchowski equations of a  $d$ -dimensional system of the form*

$$dX_t = -D\nabla V(X_t)dt + \sqrt{2dD}dW_t \quad (2.29)$$

*with dimensionless potential  $V(x)$  are reversible. The stationary density is then given by  $\rho(x) \propto \exp(-V(x))$  [10]. In particular, for a potential  $V(x) = \frac{1}{2}\alpha x^2$  it becomes*

$$\rho(x) = \frac{1}{\sqrt{2\pi\alpha^{-1}}} \exp(-V(x)) \sim \exp(-V(x)). \quad (2.30)$$

## 2.2 Koopman Spectral Analysis

The linearity of the Koopman operator in the space of observables  $\mathcal{G}$ , that is a Hilbert vector space, making it attractive, however its infinite dimensionality creates challenges in terms of representation and computation. By understanding the spectral properties of the operator, we can gain insight into the dynamics of the system. Rather than tracking the evolution of all observables within  $\mathcal{G}$ , the approach of applied Koopman analysis is to identify significant measurement functions that evolve linearly with the dynamics. *Eigenfunctions* of the Koopman operator provide a simplified representation of the system's behavior and they are special observables that behave linearly in time. Through the decomposition of the operator into its *eigenfunctions* and *eigenvalues*, we can gain a deeper understanding of the global behavior of the system.

Another crucial component of analyzing the Koopman operator is the set of *Koopman modes* for the full-state observable function  $g(x) = x$ . These modes, along with the eigenvalues and eigenfunctions, enable us to rebuild and predict the state of the system.

### 2.2.1 Spectral Decomposition of Koopman Operators

Let  $\{\varphi_1, \dots, \varphi_p\}$  be a set of Koopman eigenfunctions, where  $p = 1, 2, \dots$ , or  $\infty$ , not necessarily forming a complete basis set for  $\mathcal{G}$ .

- **In a discrete-time case:** A Koopman eigenfunction  $\varphi(x)$  associated to the eigenvalue  $\lambda$  fulfills

$$\varphi(x_{k+1}) = \mathcal{K}\varphi(x_k) = \lambda\varphi(x_k). \quad (2.31)$$

In simpler terms, for a discrete-time system with timestep  $\Delta t$ , (2.31) becomes:

$$\varphi(x_{k+1}) = \mathcal{K}^{\Delta t}\varphi(x_k) = \lambda\varphi(x_k). \quad (2.32)$$

- **In a continuous-time case:** The eigenvalues, are eigenvalues of the Lie operator or generator  $\mathcal{L}$  of the Koopman semigroup  $\mathcal{K}^t$ . Then we say, a Koopman eigenfunction or a Lie operator eigenfunction  $\varphi(x)$  associated to a continuous-time eigenvalue  $\mu$  fulfills

$$\frac{d}{dt}\varphi(x) = \mathcal{L}\varphi(x) = \mu\varphi(x), \quad (2.33)$$

which is equivalent to

$$(\mathcal{K}^t\varphi)(x) = \exp(\mu t)\varphi(x), \quad (2.34)$$

so that  $\exp(\mu t)$  are the eigenvalues for the Koopman semigroup  $\mathcal{K}^t$ .

That means, in the context of autonomous dynamical systems, the Koopman operator and the Lie operator have the same eigenfunctions, but with different eigenvalues. Indeed, consider the continuous-time definition in (2.14) applied to an eigenfunction  $\varphi$  leads,

$$(\mathcal{K}^t\varphi)(x) = \exp(\mu t)\varphi(x) \implies \mathcal{L}\varphi(x) := \lim_{t \rightarrow 0} \frac{\mathcal{K}^t\varphi(x) - \varphi(x)}{t} \quad (2.35a)$$

$$= \lim_{t \rightarrow 0} \frac{\exp(\mu t)\varphi(x) - \varphi(x)}{t} \quad (2.35b)$$

$$= \mu\varphi(x). \quad (2.35c)$$

Similarly, for a given  $\lambda \neq 0$ , and using  $\lambda^t = \exp(t \log(\lambda))$ , we can show that if  $\lambda^t$  are eigenvalues of the Koopman semigroup, we obtain

$$(\mathcal{K}^t \varphi)(x) = \lambda^t \varphi(x) \implies \mathcal{L}\varphi(x) := \lim_{t \rightarrow 0} \frac{\mathcal{K}^t \varphi(x) - \varphi(x)}{t} \quad (2.36a)$$

$$= \lim_{t \rightarrow 0} \frac{\lambda^t - 1}{t} \varphi(x) \quad (2.36b)$$

$$= \log(\lambda) \varphi(x). \quad (2.36c)$$

Conversely, the induced linear dynamics by  $\mathcal{L}$  in (2.13) applied to an eigenfunction of  $\mathcal{L}$  leads to

$$\mathcal{L}\varphi = \mu\varphi \implies \dot{\varphi} = \mathcal{L}\varphi = \mu\varphi. \quad (2.37)$$

Therefore, in the context of autonomous systems, we usually do not differentiate between Lie and Koopman eigenfunctions. Generally, eigenvalues and eigenfunctions are complex-valued scalars and measurements, respectively, even when the state space  $\mathcal{M}$  and dynamics  $\mathbf{F}(x)$  are real-valued.

**Remark 2.2.1.** *By applying the chain rule to the derivative of the Koopman eigenfunction  $\varphi(x)$  with respect to time, we obtain the equation:*

$$\dot{\varphi}(x) = \nabla \varphi(x) \cdot \dot{x} = \nabla \varphi(x) \cdot \mathbf{f}(x). \quad (2.38)$$

*When this equation is combined with (2.33), the eigenfunction of the operator  $\mathcal{L}$ , we arrive at the partial differential equation:*

$$\nabla \varphi(x) \cdot \mathbf{f}(x) = \mu \varphi(x). \quad (2.39)$$

*This PDE can be used to approximate eigenfunctions, either by solving for the Laurent series [3, 5] or by using data-driven regression methods as explored in sections [2.4.1, 3.0.1]. However, this formulation relies on the assumption that the dynamics are both continuous and differentiable.*

**Remark 2.2.2.** *In (2.35) and (2.36), we demonstrate that an eigenfunction  $\varphi$  of  $\mathcal{L}$  with eigenvalue  $\mu$  is then an eigenfunction of  $\mathcal{K}^t$  with eigenvalue  $\lambda^t = \exp(\mu t)$ . Moreover, the relationship between eigenvalues in continuous time and those in discrete time is straightforward. If the discrete-time eigenvalues are given by  $\mu$ , then the corresponding continuous-time eigenvalues are given by  $\exp(\mu t)$ . That means,  $\mu$  are also eigenvalues of the generator  $\mathcal{L}$  and  $\lambda^t = \exp(\mu t)$  are also eigenvalues of Koopman semigroup  $\{\mathcal{K}^t\}$ .*

In various systems, a collection of Koopman eigenfunctions can be utilized to create additional eigenfunctions. This is supported by the algebraic structure of eigenfunctions under the product, which will be further discussed in the underlined property.

**Proposition 2.2.3.** *Considering  $\mathcal{G}$  as a subset of all  $\mathbb{C}$ -valued functions on  $\mathcal{M}$  that forms a vector space which is closed under pointwise products of functions, then the set of eigenfunctions is an Abelian semigroup under pointwise products of functions. Specifically, if  $\varphi_1, \varphi_2 \in \mathcal{G}$  are eigenfunctions of  $\mathcal{K}$  with eigenvalues  $\gamma_1, \gamma_2$ , then  $\varphi_1 \varphi_2$  is an eigenfunction of  $\mathcal{K}$  with eigenvalue  $\gamma_1 \gamma_2$ . Moreover, if  $p \in \mathbb{R}^+$  and  $\varphi$  is an eigenfunction with eigenvalue  $\gamma$ , then  $\varphi^p$  is an eigenfunction with eigenvalue  $\gamma^p$ , where  $\varphi^p(x) := (\varphi(x))^p$ . If  $\varphi$  is an eigenfunction that does not vanish and  $r \in \mathbb{R}$ , then  $\varphi^r$  is an eigenfunction with eigenvalue  $\gamma^r$ . Additionally, the eigenfunctions that do not vanish anywhere form an Abelian group.*

*Proof.* To avoid confusion, we will separate our proof into discrete-time and continuous-time.

- **In discrete-time:** Assume  $\mathcal{K}\varphi_1 = \mu_1\varphi_1$  and  $\mathcal{K}\varphi_2 = \mu_2\varphi_2$  and put  $\psi(x) = \varphi_1(x)\varphi_2(x)$ .

$$(\mathcal{K}\psi)(x) = \psi(\mathbf{F}(x)) \quad (2.40a)$$

$$= \varphi_1(\mathbf{F}(x))\varphi_2(\mathbf{F}(x)) \quad (2.40b)$$

$$= (\mathcal{K}\varphi_1)(x)(\mathcal{K}\varphi_2)(x) \quad (2.40c)$$

$$= \mu_1\mu_2\varphi_1(x)\varphi_2(x) \quad (2.40d)$$

$$= \mu_1\mu_2\psi(x). \quad (2.40e)$$

- **In continuous-time:** Assume  $\mathcal{K}^t\varphi_1 = \lambda_1^t\varphi_1 = \exp(\mu_1 t)\varphi_1$  and  $\mathcal{K}^t\varphi_2 = \lambda_2^t\varphi_2 = \exp(\mu_2 t)\varphi_2$ .

$$(\mathcal{K}^t\psi)(x) = \psi(\mathbf{F}^t(x)) \quad (2.41a)$$

$$= \varphi_1(\mathbf{F}^t(x))\varphi_2(\mathbf{F}^t(x)) \quad (2.41b)$$

$$= (\mathcal{K}^t\varphi_1)(x)(\mathcal{K}^t\varphi_2)(x) \quad (2.41c)$$

$$= \exp(\mu_1 t)\varphi_1(x)\exp(\mu_2 t)\varphi_2(x) \quad (2.41d)$$

$$= \exp(\mu_1 t)\exp(\mu_2 t)\varphi_1(x)\varphi_2(x), \quad (2.41e)$$

which is equivalent to assuming  $\frac{d}{dt}\varphi_1 = \mathcal{L}\varphi_1 = \mu_1\varphi_1$  and  $\frac{d}{dt}\varphi_2 = \mathcal{L}\varphi_2 = \mu_2\varphi_2$ .

$$(\mathcal{L}\psi)(x) = \frac{d}{dt}\psi(x) \quad (2.41f)$$

$$= \frac{d}{dt}(\varphi_1(x)\varphi_2(x)) \quad (2.41g)$$

$$= \dot{\varphi}_1(x)\varphi_2(x) + \varphi_1(x)\dot{\varphi}_2(x) \quad (2.41h)$$

$$= \mu_1\varphi_1(x)\varphi_2(x) + \varphi_1(x)\mu_2\varphi_2(x) \quad (2.41i)$$

$$= (\mu_1 + \mu_2)\psi(x), \quad (2.41j)$$

that is clearly obtained from (**Remark 2.2.2**), as

$$\exp(\mu_1 t)\exp(\mu_2 t)\varphi_1(x)\varphi_2(x) = \exp((\mu_1 + \mu_2)t)\varphi_1(x)\varphi_2(x). \quad (2.41k)$$

Thus, the set of eigenfunctions is closed under pointwise products. Additionally, both in discrete and continuous cases, a constant function are eigenfunctions at eigenvalues 1 and 0 respectively. Hence the constant function that is equal to 1 everywhere is an eigenfunction and as a sort of "identity" within the set of eigenfunctions. Combining this with the above closure property and standard properties of pointwise products of functions shows that the set of eigenfunctions is an Abelian semigroup without the requirement of inverses.

- **In discrete-time:** Let  $\mathcal{K}\varphi = \mu\varphi$  and fix  $p \in \mathbb{R}^+$ . Then due to the linearity of  $\varphi$

$$(\mathcal{K}\varphi^p)(x) = \varphi^p(\mathbf{F}(x)) \quad (2.42a)$$

$$= (\varphi(\mathbf{F}(x)))^p \quad (2.42b)$$

$$= (\mu\varphi(x))^p \quad (2.42c)$$

$$= \mu^p\varphi^p(x). \quad (2.42d)$$

- **In continuous-time:** Let  $\mathcal{K}^t\varphi = \exp(\mu t)\varphi$  and fix  $p \in \mathbb{R}^+$ . Then due to the linearity of  $\varphi$

$$(\mathcal{K}^t\varphi^p)(x) = \varphi^p(\mathbf{F}^t(x)) \quad (2.43a)$$

$$= (\varphi(\mathbf{F}^t(x)))^p \quad (2.43b)$$

$$= (\exp(\mu t)\varphi(x))^p \quad (2.43c)$$

$$= \exp(p\mu t)\varphi^p(x). \quad (2.43d)$$

which is equivalent to taking  $\mathcal{L}\varphi = \frac{d}{dt}\varphi = \mu\varphi$  and fix  $p \in \mathbb{R}^+$ . Then

$$(\mathcal{L}\varphi^p)(x) = \frac{d}{dt}\varphi^p(x) \quad (2.43e)$$

$$= p\varphi^{p-1}\frac{d}{dt}\varphi(x) \quad (2.43f)$$

$$= p\varphi^{p-1}\mu\varphi(x) \quad (2.43g)$$

$$= p\mu\varphi^p(x). \quad (2.43h)$$

If  $\varphi$  does not vanish anywhere, then its inverse function  $\varphi^{-1}(x) := \frac{1}{\varphi(x)}$  is well-defined. This means that the previous chain of identities remains valid for  $r \in \mathbb{R}$  instead of just  $p \in \mathbb{R}^+$ . As a result, the Abelian semigroup of eigenfunctions also includes all of its inverses. Therefore, the set of eigenfunctions that do not vanish anywhere is an Abelian group.  $\square$

**Example 2.2.4.** Given a linear system  $\dot{x} = \mu x$ , with  $x, \mu \in \mathbb{C}$  and  $|\mu| \neq 1$ . Then,  $\mathbf{F}^t(x) = \exp(\mu t)x$  and  $\varphi(x) = x$  is a Koopman eigenfunction or a Lie operator eigenfunction with eigenvalue  $\mu$ . Indeed,

$$(\mathcal{K}^t\varphi)(x) = \varphi(\mathbf{F}^t(x)) \quad (2.44a)$$

$$= \varphi(\exp(\mu t)x) \quad (2.44b)$$

$$= \exp(\mu t)x \quad (2.44c)$$

$$= \exp(\mu t)\varphi(x). \quad (2.44d)$$

Moreover, by proposition 2.2.3,  $\varphi_r(x) := (\varphi(x))^r = x^r$  is also an eigenfunction of  $\mathcal{L}$  with eigenvalue  $\mu^r$  for any  $r \in \mathbb{R}$ . In addition to that, observables that can be formed as linear combinations of eigenfunctions, i.e.,  $g \in \text{span}\{\varphi_r\}_{r=1}^p$  have a particularly simple evolution under the Koopman operator. Let  $g(x) = \sum_r c_r \varphi_r(x)$ , where  $c_r = \frac{1}{r!} \frac{d^r g(0)}{dx^r}$ . Then,

$$(\mathcal{K}^t g)(x) = \mathcal{K}^t \sum_r c_r \varphi_r(x) \quad (2.45a)$$

$$= \sum_r c_r (\mathcal{K}^t \varphi_r)(x) \quad (2.45b)$$

$$= \sum_r \exp(r\mu t) \varphi_r(x) c_r. \quad (2.45c)$$

This implies that the subspace  $\text{span}\{\varphi_r\}_{r=1}^p$  is invariant under the action of  $\mathcal{K}^t$ .

**Example 2.2.5.** Consider a continuous-time nonlinear dynamical system

$$\frac{d}{dt} \begin{bmatrix} x_1 \\ x_2 \end{bmatrix} = \begin{bmatrix} \gamma x_1 \\ \delta(x_2 - x_1^2) \end{bmatrix}. \quad (2.46a)$$

In addition to the simple eigenfunction  $\varphi_1(x) = 1$  with a generator eigenvalue of  $\mu_1 = 0$ , we also have  $\varphi_2(x) = x_1$  and  $\varphi_3(x) = \frac{2\gamma-\delta}{\delta}x_2 + x_1^2$  with generator eigenvalues  $\mu_2 = \gamma$  and  $\mu_3 = \delta$ , respectively. This can be verified by:

$$\mathcal{L}\varphi_2 = \frac{d}{dt}\varphi_2 = \dot{x}_1 = \gamma\varphi_2 \quad (2.46b)$$

$$\mathcal{L}\varphi_3 = \frac{d}{dt}\varphi_3 = \frac{2\gamma-\delta}{\delta}\dot{x}_2 + 2x_1\dot{x}_1 = \delta\varphi_3 \quad (2.46c)$$

Moreover, the product of two eigenfunctions is an eigenfunction with its corresponding generator eigenvalue obtained through multiplication, such as:

$$\mu_4 = 4\delta, \quad \varphi_4(x) = (\varphi_3(x))^4 \quad (2.46d)$$

$$\mu_5 = 2\gamma + \delta, \quad \varphi_5(x) = (\varphi_2(x))^2 \varphi_3(x) \quad (2.46e)$$

## 2.2.2 Koopman Mode Decomposition

Assuming that  $g \in \mathcal{G}$  is an observable in the closed, linear span of a set of linearly independent eigenfunction  $\{\varphi_i\}_{i=1}^p$ , recall  $p$  could be finite or infinite, the following equation holds:

$$g(x) = \sum_{i=1}^p v_i \varphi_i(x), \quad (2.47)$$

for the constants  $v_i \in \mathbb{C}$ . The behavior of  $g$  is straightforward:

$$(\mathcal{K}g)(x) = g(\mathbf{F}(x)) \quad (2.48a)$$

$$= \sum_{i=1}^p v_i (\mathcal{K}\varphi_i)(x) \quad (2.48b)$$

$$= \sum_{i=1}^p \mu_i v_i \varphi_i(x), \quad (2.48c)$$

likewise,

$$(\mathcal{K}^t g)(x) = \sum_{i=1}^p \exp(\mu_i t) v_i \varphi_i(x). \quad (2.48d)$$

So far, we have discussed scalar measurements of a system and examined special eigen-measurements (i.e., Koopman eigenfunctions) that evolve linearly in time. However, it is common to take multiple measurements of a system, which can be arranged in a vector  $\mathbf{g}$ .

$$\mathbf{g}(x) = \begin{bmatrix} g_1(x) \\ \vdots \\ g_m(x) \end{bmatrix}, \quad (2.49)$$

where each  $g_k$  is in the closed linear span of the eigenfunctions  $\varphi_i(x)$ :

$$g_k = \sum_{i=1}^p v_{ki} \varphi_i(x). \quad (2.50a)$$

Therefore, the vector of observables,  $\mathbf{g}$ , can be expressed in a similar way:

$$\mathbf{g}(x) = \begin{bmatrix} g_1(x) \\ \vdots \\ g_m(x) \end{bmatrix} = \sum_{i=1}^p \varphi_i(x) \begin{bmatrix} v_{1i} \\ \vdots \\ v_{mi} \end{bmatrix} \quad (2.50b)$$

$$= \sum_{i=1}^p \varphi_i(x) \mathbf{v}_i. \quad (2.50c)$$

And, similarly, the extension of (2.48d) to vector-valued observables  $\mathbf{g}$ , is then

$$(\mathcal{K}^t \mathbf{g})(x) = \sum_{i=1}^p \exp(\mu_i t) \varphi_i(x) [v_{1i}, \dots, v_{mi}]^\top \quad (2.50d)$$

$$= \sum_{i=1}^p \exp(\mu_i t) \varphi_i(x) \mathbf{v}_i, \quad (2.50e)$$

where

$$\mathbf{v}_i := [v_{1i}, \dots, v_{mi}]^\top \in \mathbb{C}^m. \quad (2.50f)$$

Motivated by (2.50e), we have the following definition.

**Definition 2.2.6.** Consider an eigenfunction  $\varphi_i$ , corresponding to the eigenvalue  $\mu_i$ , for the Koopman operator. Given a vector-valued observable  $\mathbf{g} : \mathcal{M} \rightarrow \mathbb{C}^m$ , the  $i$ -th Koopman mode, associated with  $\varphi_i$ , denoted by  $\mathbf{v}_i$ , can be defined as the vector of coefficients obtained by projecting  $\mathbf{g}$  onto  $\text{span}\{\varphi_i\}$ .

**Remark 2.2.7.** For dynamical systems that conserve energy, such as those governed by Hamiltonian dynamics, the Koopman operator preserves the space  $\mathcal{G}(\mathcal{M}) = L^2(\mathcal{M}, \rho)$ , of functions that are square-integrable with respect to the conserved measure. In other words, when  $\mathbf{F}$  preserves a measure  $\rho$ , the Koopman operator is unitary on the space  $\mathcal{G}(\mathcal{M}) = L^2(\mathcal{M}, \rho)$ . Therefore, for this specific scenario, the eigenvalues of the linked Koopman operator  $\mathcal{K}$  are all located on the unit circle, meaning its spectrum is restricted to the unit circle in the complex plane. Additionally, the Koopman eigenfunctions form an orthonormal basis for conservative systems and the Koopman modes  $\mathbf{v}_i$  can be computed directly through projection:

$$\mathbf{v}_i = \begin{bmatrix} \langle \varphi_i, g_1 \rangle \\ \langle \varphi_i, g_2 \rangle \\ \vdots \\ \langle \varphi_i, g_m \rangle \end{bmatrix} \quad (2.51)$$

where  $\langle \cdot, \cdot \rangle$  represents the standard inner product of functions in  $\mathcal{G}(\mathcal{M})$ . Therefore, the representation of  $\mathbf{g}(x)$  in (2.50c) can be interpreted as a change of basis into eigenfunction coordinates.

By analyzing the decomposition in (2.50c), the behavior of  $\mathbf{g}$  can be described as follows:

$$\mathbf{g}(x(t)) = \mathbf{g}(\mathbf{F}^t(x_0)) = (\mathcal{K}^t \mathbf{g})(x_0) = \mathcal{K}^t \sum_{i=1}^p \varphi_i(x_0) \mathbf{v}_i \quad (2.52a)$$

$$= \sum_{i=1}^p \mathcal{K}^t \varphi_i(x_0) \mathbf{v}_i \quad (2.52b)$$

$$= \sum_{i=1}^p \exp(\mu_i t) \varphi_i(x_0) \mathbf{v}_i, \quad (2.52c)$$

The set of  $p$  "tuples",  $\{(\mu_i, \varphi_i, \mathbf{v}_i)\}_{i=1}^p$ , is referred as *Koopman mode decomposition*, which was first proposed by Mezić in 2005 [11].

**Remark 2.2.8.** The connection between the dynamical system  $\mathbf{F}^t$  and the Koopman semigroup  $\mathcal{K}^t$ , that have a same fundamental behavior, is given by the identity operator or the full-state observable  $\mathbf{g}(x) = x$  and the corresponding Koopman mode decomposition require to reconstruct the full state. As a result

$$x = \mathbf{g}(x) = \sum_{i=1}^p \varphi_i(x) \mathbf{v}_i. \quad (2.53a)$$

Since,

$$(\mathcal{K}^t \mathbf{g})(x) = (\mathbf{g}(\mathbf{F}^t(x))) = \mathbf{F}^t(x) \quad (2.53b)$$

and, using  $\mathbf{v}_i$  we can compute  $\mathbf{F}^t(x)$  with the aid of the Koopman operator. Indeed,

$$\mathbf{F}^t(x) = (\mathcal{K}^t \mathbf{g})(x) = \sum_{i=1}^p \mathbf{v}_i (\mathcal{K}^t \varphi_i)(x) = \sum_{i=1}^p \mathbf{v}_i \exp(\mu_i t) \varphi_i(x). \quad (2.53c)$$

The benefits of this representation of  $\mathbf{F}^t(x)$  are particularly clear because the behavior associated with each eigenfunction is determined by the eigenvalue connected to it.

Figure 2.1 provides a pictorial summary or a visual representation of the preceding discussion, where  $\mathcal{F} \equiv \mathcal{G}$  and  $n \in \mathbb{Z}$  is discrete time.

The top row illustrates the direct progression of states,  $x \in \mathcal{M}$ , governed by  $\mathbf{F}$ . The bottom row shows the progression of observables,  $\psi \in \mathcal{F}$ , governed by the Koopman operator,  $\mathcal{K}$ . Although  $\mathbf{F}$  and  $\mathcal{K}$  operate on different spaces, they both represent the same dynamics. In this case, both systems are autonomous, so the discrete time,  $n \in \mathbb{Z}$ , is not explicitly shown. For instance, once given a state  $x$ , to compute  $(\mathcal{K}\psi)(x)$  one could either take the observable  $\psi$ , apply  $\mathcal{K}$ , and evaluate it at  $x$  (the bottom route), or use  $\mathbf{F}$  to compute  $\mathbf{F}(x)$  and then evaluate  $\psi$  at this updated position (the top route). Similarly, to compute  $\mathbf{F}(x)$ , one could either apply  $\mathbf{F}$  to  $x$  (the top route) or apply  $\mathcal{K}$  to the full-state observable  $\mathbf{g}(x) = x$  and evaluate  $(\mathcal{K}\mathbf{g})(x)$  (the bottom route) as shown in (2.53c). Therefore, these two routes are equivalent, and one can either choose to work with a finite-dimensional, nonlinear system (the top route) or an infinite-dimensional, linear system (the bottom route) depending on which route is simpler or more useful for a given problem, if one can compute the Koopman eigenvalues, eigenfunctions, and modes.

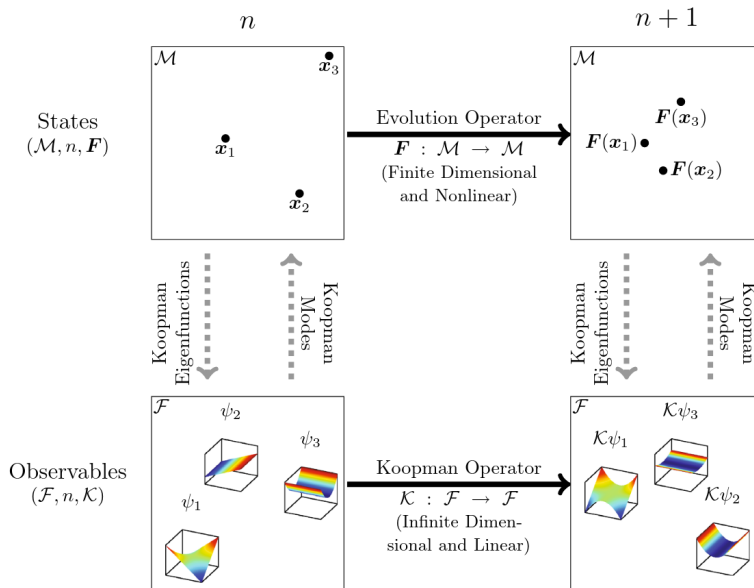


Figure 2.1: Relation between the Koopman operator and the underlying dynamical system. Adapted from [17].

**Example 2.2.9.** The Ornstein-Uhlenbeck process, previously mentioned in Example (2.1.1), is defined by the stochastic differential equation

$$dX_t = -\alpha X_t dt + \sqrt{2\beta^{-1}} dW_t, \quad (2.54)$$

where  $\alpha$  and  $\beta$  represent the friction coefficient and inverse temperature, respectively. Using recurrence relations for the Hermite polynomials,

$$H_{\ell+1}(x) = xH_\ell(x) - H'_\ell(x), \quad (2.55)$$

it can be shown that the eigenvalues  $\lambda_\ell$  and eigenfunctions  $\varphi_\ell$  of  $\mathcal{K}^t$  associated with this process are given by

$$\lambda_\ell = \exp(\mu_\ell t) = \exp(-\alpha(\ell-1)t), \quad \varphi_\ell(x) = \frac{1}{\sqrt{(\ell-1)!}} H_{\ell-1}(\sqrt{\alpha\beta}x), \quad \ell = 1, 2, \dots, \quad (2.56)$$

where  $H_\ell$  is the  $\ell$ th probabilists' Hermite polynomial, as described in [12].

## 2.3 Koopman Invariant Subspaces and Intrinsic Coordinates

In Koopman analysis, the evolution of a finite set of measurement functions on an invariant subspace is estimated rather than tracking the evolution of all measurement functions in the entire Hilbert space. The observable function  $\psi$  can be expressed using a chosen basis in the Hilbert space. A *Koopman-invariant subspace* is defined as the collection of functions  $\{\psi_1, \psi_2, \dots, \psi_p\}$  that maintain their span after being acted upon by the Koopman operator  $\mathcal{K}$ . Any function  $\psi$  in this subspace can be expressed as a linear combination of  $\psi_i$ ,

$$\psi = \sum_{i=1}^m \alpha_i \psi_i, \quad (2.57a)$$

and after acting with  $\mathcal{K}$ , remains in the subspace,

$$\mathcal{K}\psi = \sum_{i=1}^m \beta_i \psi_i. \quad (2.57b)$$

The Koopman operator can be transformed into a finite-dimensional matrix  $\mathbf{K}$  by restricting it to an invariant subspace spanned by a finite set of functions  $\{\psi_j\}_{j=1}^m$ . This representation  $\mathbf{K}$  acts on a vector space  $\mathbb{C}^m$  with coordinates given by the values of the functions  $\psi_j(x)$  and forms a finite-dimensional linear system as in equations (2.9) and (2.13). Any finite set of Koopman eigenfunctions  $\varphi$ , such that  $\mathcal{K}\varphi = \mu\varphi$  generates an invariant subspace. Finding these eigenfunctions is a crucial task, as they provide intrinsic coordinates where the dynamics behave linearly. In practice, an *approximately* (nearly) invariant subspace is recognized, represented by a set of functions  $\{\psi_j\}_{j=1}^m$  that are well approximated by a finite sum of eigenfunctions:

$$\psi_j \approx \sum_{k=1}^m v_{jk} \varphi_k. \quad (2.58)$$

The Koopman operator is then restricted to this subspace, resulting in a finite-dimensional linear operator  $\mathbf{K}$ . The eigenfunctions of the Koopman operator generate invariant subspaces. However, inverting the eigenfunctions may not restore the original state  $x$ .

To control a system, we aim to find Koopman-invariant subspaces that contain the original state variables  $x_1, x_2, \dots, x_N$ . The Koopman operator in this subspace is finite-dimensional, linear, and it governs the evolution of both the original state dynamics and other observables in the subspace. These subspaces can be discovered using data-driven methods as explained in the following section (3.0.1). However, it is not always possible to include the state in the subspace for most nonlinear systems, as it is impossible to identify a finite-dimensional Koopman-invariant subspace containing the original state variables for systems with multiple fixed points, periodic orbits, or more complex attractors such as chaotic sets. This is due to the fact that all finite-dimensional linear systems only have a single fixed point and cannot be topologically equivalent to a system with multiple fixed points. Nevertheless, it is still possible to identify Koopman-invariant subspaces spanned by Koopman eigenfunctions  $\varphi$ , which can provide valuable intrinsic coordinates [16]. For the original state variables  $x_1, x_2, \dots, x_N$  to be part of the Koopman-invariant subspace, the nonlinear right-hand side function  $\mathbf{f}$  must also belong to that subspace.

$$\frac{d}{dt}x = \mathbf{f}(x), \quad \text{indicates} \quad \frac{d}{dt} \begin{bmatrix} x_1 \\ x_2 \\ \vdots \\ x_N \end{bmatrix} = \begin{bmatrix} f_1(x_1, \dots, x_N) \\ f_2(x_1, \dots, x_N) \\ \vdots \\ f_N(x_1, \dots, x_N) \end{bmatrix}. \quad (2.59a)$$

The first  $N$  observables  $\psi_1, \psi_2, \dots, \psi_N$  are defined as  $\psi_1 = x_1, \psi_2 = x_2, \dots, \psi_N = x_N$ , where  $x$  are the state variables. The remaining  $m - N$  observables are nonlinear functions necessary to express  $\mathbf{f}$ . If each term  $f_k$  in  $\mathbf{f}$  can be represented as a combination of the observables in the subspace,

$$f_k(x_1, x_2, \dots, x_N) = c_{k,1}\psi_1 + c_{k,2}\psi_2 + \dots + c_{k,m}\psi_m, \quad (2.59b)$$

then the first  $N$  rows of the Koopman-induced dynamic system can be written as:

$$\frac{d}{dt} \begin{bmatrix} \psi_1 \\ \psi_2 \\ \vdots \\ \psi_N \\ \psi_{N+1} \\ \vdots \\ \psi_m \end{bmatrix} = \begin{bmatrix} c_{1,1} & c_{1,2} & \cdots & c_{1,N} & c_{1,N+1} & \cdots & c_{1,m} \\ c_{2,1} & c_{2,2} & \cdots & c_{2,N} & c_{2,N+1} & \cdots & c_{2,m} \\ \vdots & \vdots & \ddots & \vdots & \vdots & \ddots & \vdots \\ c_{N,1} & c_{N,2} & \cdots & c_{N,N} & c_{N,N+1} & \cdots & c_{N,m} \\ ? & ? & \cdots & ? & ? & \cdots & ? \\ \vdots & \vdots & \ddots & \vdots & \vdots & \ddots & \vdots \\ ? & ? & \cdots & ? & ? & \cdots & ? \end{bmatrix} \begin{bmatrix} \psi_1 \\ \psi_2 \\ \vdots \\ \psi_N \\ \psi_{N+1} \\ \vdots \\ \psi_m \end{bmatrix}. \quad (2.59c)$$

In practice, to determine the remaining  $m - N$  rows in the Koopman-induced system, we need to compute for  $k > N$  the derivative  $\dot{\psi}_k$  of each observable and represent it in terms of other observables in the subspace. This information can be obtained either analytically by knowing the dynamics of  $\mathbf{f}$  or through a data-driven approach, such as least-squares regression as in extended DMD [17]. The choice of an appropriate observable subspace is crucial, and it depends on the knowledge of the dynamics  $\mathbf{f}$ .

### 2.3.1 Koopman-Invariant Subspaces Containing the State

This work introduces a group of nonlinear dynamical systems in which it is feasible to discover a Koopman-invariant subspace that contains the original state variables as observable functions. Such systems can only have one isolated fixed point as there is no linear system with finite dimensions that can describe multiple fixed points or more complex attractors. Linear representations of the basins of attraction (e.g., metastable region) of some fixed points can be obtained using eigen-function coordinates, as discussed in [9, 17], making it possible to revert back to the state, but these are still not global representations. Finding eigenfunctions and restoring the state remains an unsolved issue for most systems. The examples below exhibit polynomial nonlinearities that result in polynomial slow or fast manifolds.

### 2.3.2 Applications of Koopman Embedding

#### 2.3.2.1 Continuous-Time Representation for Koopman Embedding

**Example 2.3.1.** *The given continuous-time dynamical system has a slow manifold described by a polynomial function,  $p(x)$ .*

$$\frac{d}{dt} \begin{bmatrix} x_1 \\ x_2 \end{bmatrix} = \begin{bmatrix} \mu x_1 \\ \lambda(x_2 - p(x_1)) \end{bmatrix}, \quad (2.60a)$$

*If  $\lambda \ll |\mu| < 0$ , then  $x_2 = p(x_1)$  acts as an asymptotically attracting slow manifold. This system has a single stationary point at the origin  $x_1 = x_2 = 0$ . It will be demonstrated that a finite-dimensional linear system can always be obtained by the closure of the Koopman operator applied to an observable subspace spanned by  $x_1, x_2$  and the active polynomial terms in  $p(x_1)$ .*

For simplicity, let's start by considering  $p(x) = 5x^n - 2x^{n-3}$ . Thus, we augment the state  $x$  with the nonlinear measurements  $x^n$  and  $x^{n-3}$ , so that:

$$\psi = [\psi_1, \psi_2, \psi_3, \psi_4]^\top = [x_1, x_2, x_1^{n-3}, x_1^n]^\top. \quad (2.60b)$$

Now, the first two terms have a linear relationship with the entries of  $\psi$

$$\frac{d}{dt}\psi_1 = \dot{x}_1 = \mu x_1 = \mu\psi_1 \quad \text{and} \quad \frac{d}{dt}\psi_2 = \dot{x}_2 = \lambda(\psi_2 + 2\psi_3 - \psi_4). \quad (2.60c)$$

Thus, to find  $\frac{d}{dt}\psi_3$  and  $\frac{d}{dt}\psi_4$ , we apply the chain rule:

$$\frac{d}{dt}\psi_3 = \frac{d}{dt}x_1^{n-3} = (n-3)x_1^{n-4}\dot{x}_1 = \mu(n-3)\psi_3 \quad \text{and} \quad \frac{d}{dt}\psi_4 = nx_1^{n-1}\dot{x}_1 = \mu n\psi_4. \quad (2.60d)$$

This results in a simplified, or ideally, a linearized system

$$\frac{d}{dt} \begin{bmatrix} \psi_1 \\ \psi_2 \\ \psi_3 \\ \psi_4 \end{bmatrix} = \begin{bmatrix} \mu & 0 & 0 & 0 \\ 0 & \lambda & 2\lambda & -5\lambda \\ 0 & 0 & (n-3)\mu & 0 \\ 0 & 0 & 0 & n\mu \end{bmatrix} \begin{bmatrix} \psi_1 \\ \psi_2 \\ \psi_3 \\ \psi_4 \end{bmatrix} \quad (2.60e)$$

For more general polynomial functions, represented by

$$p(x_1) = \sum_{j=1}^m c_j x_1^{n_j}, \quad (2.60f)$$

the approach is similar

$$\psi = [\psi_1, \psi_2, \psi_3, \psi_4, \dots, \psi_{m+2}]^\top = [x_1, x_2, x_1^{n_1}, x_1^{n_2}, \dots, x_1^{n_m}]^\top. \quad (2.60g)$$

indicates

$$\frac{d}{dt} \begin{bmatrix} \psi_1 \\ \psi_2 \\ \psi_3 \\ \psi_4 \\ \vdots \\ \psi_{m+2} \end{bmatrix} = \begin{bmatrix} \mu & 0 & 0 & 0 & \cdots & 0 \\ 0 & \lambda & -c_1\lambda & -c_2\lambda & \cdots & -c_m\lambda \\ 0 & 0 & \mu n_1 & 0 & \cdots & 0 \\ 0 & 0 & 0 & \mu n_2 & \cdots & 0 \\ \vdots & \vdots & \vdots & \vdots & \ddots & \vdots \\ 0 & 0 & 0 & 0 & \cdots & \mu n_m \end{bmatrix} \begin{bmatrix} \psi_1 \\ \psi_2 \\ \psi_3 \\ \psi_4 \\ \vdots \\ \psi_{m+2} \end{bmatrix}. \quad (2.60h)$$

This representation is finite-dimensional and linear, and it effectively enhances the original state  $x$ , even though the underlying dynamics are nonlinear.

**Example 2.3.2.** When  $\lambda \ll |\mu| < 0$ , two examples of systems with slow manifolds are considered. The first system, with quadratic attracting manifold  $x_2 = x_1^2$ , is given by:

$$\frac{d}{dt} \begin{bmatrix} x_1 \\ x_2 \end{bmatrix} = \begin{bmatrix} \mu x_1 \\ \lambda(x_2 - x_1^2) \end{bmatrix}. \quad (2.61a)$$

To define a three-dimensional Koopman invariant subspace, the state  $x$  is augmented with the nonlinear measurement  $x_1^2$ . Then, in these coordinates, by selecting appropriate observables,

$$\psi = [\psi_1, \psi_2, \psi_3]^\top = [x_1, x_2, x_1^2]^\top. \quad (2.61b)$$

a linear dynamics is obtained, with  $\mathbf{L}$  a finite-dimensional approximation of  $\mathcal{L}$ ,

$$\dot{\psi} = \frac{d}{dt} \begin{bmatrix} \psi_1 \\ \psi_2 \\ \psi_3 \end{bmatrix} = \begin{bmatrix} \mu & 0 & 0 \\ 0 & \lambda & -\lambda \\ 0 & 0 & 2\mu \end{bmatrix} \begin{bmatrix} \psi_1 \\ \psi_2 \\ \psi_3 \end{bmatrix} = \mathbf{L}\psi \quad (2.61c)$$

and the second system, with quartic attracting manifold  $x_2 = -2x_1^8 + 3x_1^4$ , is given by:

$$\frac{d}{dt} \begin{bmatrix} x_1 \\ x_2 \end{bmatrix} = \begin{bmatrix} \mu x_1 \\ \lambda(x_2 + 2x_1^8 - 3x_1^4) \end{bmatrix}, \quad (2.61d)$$

then for

$$\psi = [\psi_1, \psi_2, \psi_3, \psi_4]^\top = [x_1, x_2, x_1^4, x_1^8]^\top. \quad (2.61e)$$

we obtain,

$$\frac{d}{dt} \begin{bmatrix} \psi_1 \\ \psi_2 \\ \psi_3 \\ \psi_4 \end{bmatrix} = \begin{bmatrix} \mu & 0 & 0 & 0 \\ 0 & \lambda & -3\lambda & 2\lambda \\ 0 & 0 & 4\mu & 0 \\ 0 & 0 & 0 & 8\mu \end{bmatrix} \begin{bmatrix} \psi_1 \\ \psi_2 \\ \psi_3 \\ \psi_4 \end{bmatrix}. \quad (2.61f)$$

The embedding of a nonlinear dynamical system into a higher-dimensional observable space is depicted in Figure 2.2. The system with quadratic attracting manifold from (2.61c) is used to understand this concept.

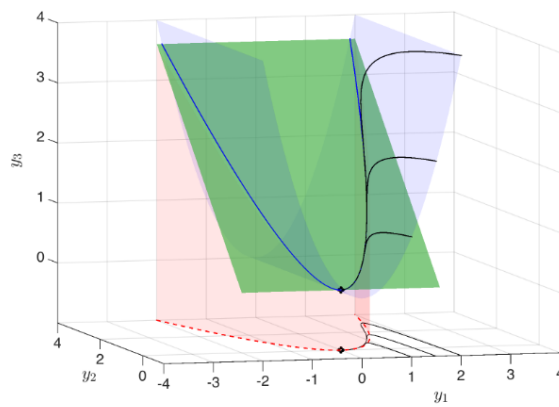


Figure 2.2: Visualization of 3D linear Koopman system from equation (2.61c) along with projection of dynamics onto the  $x_1 - x_2$  plane, with  $\psi \equiv y$ . The attracting slow manifold is depicted in red, the constraint  $\psi_3 = \psi_1^2$  is shown in blue, and the slow unstable subspace of (2.61c) is visualized in green. The black trajectories of the linear Koopman system in  $\psi$  project onto trajectories of the full nonlinear system in  $x$  in the  $\psi_1 - \psi_2$  plane. Here,  $\mu = -0.05$  and  $\lambda = 1$ . Reproduced from [4].

The full 3D Koopman observable vector space is shown. Trajectories that begin on the invariant manifold  $\psi_3 = \psi_1^2$ , represented by the blue surface, are constrained to stay on it. The slow subspace, spanned by the eigenvectors of the slow eigenvalues  $\mu$  and  $2\mu$ , is shown as the green surface. The original asymptotically attracting manifold of the original system,  $\psi_2 = \psi_1^2$ , is shown as the red surface. The blue and red parabolic surfaces intersect at a  $45^\circ$  angle in the  $\psi_2 - \psi_3$  direction. The green surface approaches this angle as the ratio of fast to slow dynamics increases. In full 3D Koopman observable space, dynamics are given by a stable node, with trajectories rapidly attracting onto the green subspace and then slowly approaching the fixed point.

**Example 2.3.3. Intrinsic coordinates defined by eigenfunctions of the Koopman operator.** In this example, we explore the use of left eigenvectors of the Koopman operator as a means of defining intrinsic coordinates. The Koopman eigenobservables, or eigenfunctions, can be obtained through the left eigenvectors of the Koopman operator. The Koopman eigenfunctions of equation (2.61c) that correspond to the eigenvalues  $\mu$  and  $\lambda$  are:

$$\varphi_\mu = x_1 \quad \text{and} \quad \varphi_\lambda = x_2 - bx_1^2 \quad \text{with} \quad b = \frac{\lambda}{\lambda - 2\mu}. \quad (2.62)$$

This constant  $b$  shows that when the ratio of  $\frac{\lambda}{\mu}$  is finite, the dynamics follow parabolic trajectories that are close to the asymptotically attracting slow manifold  $x_2 = x_1^2$ . The various surfaces in

figure 2.2 further demonstrate this concept for different ratios of  $\frac{\lambda}{\mu}$ . The eigen-observables defined by the left eigenvectors of the Koopman operator on an invariant subspace form a set of intrinsic coordinates. This is seen in the equation

$$\varphi_\alpha(x) = \xi_\alpha^\top \psi(x), \quad \text{where} \quad \xi_\alpha^\top \mathbf{K} = \alpha \xi_\alpha^\top. \quad (2.63)$$

These eigen-observables establish invariant subspaces that remain invariant under the Koopman operator even with coordinate transformations. This makes them useful to regard as intrinsic coordinates on the Koopman-invariant subspace [16].

**Example 2.3.4.** The system from equation (2.61c) can be considered in a coordinate system that is rotated by 45°:

$$\eta, \xi = x \pm \psi \quad \text{and} \quad x, \psi = \frac{\eta \pm \xi}{2}, \quad (2.64a)$$

implies

$$\dot{\eta} = \mu \frac{\eta + \xi}{2} + \lambda \frac{\eta - \xi}{2} - \lambda \frac{(\eta + \xi)^2}{4} \quad \text{and} \quad \dot{\xi} = \mu \frac{\eta + \xi}{2} - \lambda \frac{\eta - \xi}{2} + \lambda \frac{(\eta + \xi)^2}{4}. \quad (2.64b)$$

The eigenfunctions from the original system, expressed in the new coordinate system, are:

$$\varphi_\mu(\eta, \xi) = \frac{\eta + \xi}{2} \quad \text{and} \quad \varphi_\lambda(\eta, \xi) = \frac{\eta - \xi}{2} - \frac{\lambda}{\lambda - 2\mu} \frac{(\eta + \xi)^2}{4}. \quad (2.64c)$$

It is evident that these remain eigenfunctions.

$$\frac{d}{dt} \varphi_\mu = \frac{\dot{\eta} + \dot{\xi}}{2} = \mu \frac{\eta + \xi}{2} = \mu \varphi_\mu \quad (2.64d)$$

$$\frac{d}{dt} \varphi_\lambda = \frac{\dot{\eta} - \dot{\xi}}{2} - \frac{\lambda}{\lambda - 2\mu} \frac{2(\eta + \xi)(\dot{\eta} + \dot{\xi})}{4} \quad (2.64e)$$

$$= \lambda \frac{\eta - \xi}{2} - \lambda \frac{(\eta + \xi)^2}{4} - \frac{\lambda \mu}{\lambda - 2\mu} \frac{(\eta + \xi)^2}{2} \quad (2.64f)$$

$$= \lambda \left[ \frac{\eta - \xi}{2} - \frac{\lambda}{\lambda - 2\mu} \frac{(\eta + \xi)^2}{4} \right] = \lambda \varphi_\lambda. \quad (2.64g)$$

In fact, from (2.64c) we obtain

$$\frac{(\eta + \xi)^2}{4} = \frac{\lambda - 2\mu}{\lambda} \left[ \frac{\eta}{2} - \frac{\xi}{2} - \varphi_\lambda \right]. \quad (2.64h)$$

By inserting (2.64h) into (2.64b), the Koopman subspace system can be written in the new coordinate system.

$$\frac{d}{dt} \begin{bmatrix} \eta \\ \xi \\ \varphi_\lambda \end{bmatrix} = \begin{bmatrix} \frac{3\mu}{2} & -\frac{\mu}{2} & (\lambda - 2\mu) \\ -\frac{\mu}{2} & \frac{3\mu}{2} & -(\lambda - 2\mu) \\ 0 & 0 & \lambda \end{bmatrix} \begin{bmatrix} \eta \\ \xi \\ \varphi_\lambda \end{bmatrix} \quad (2.64i)$$

and

$$\frac{d}{dt} \begin{bmatrix} \eta \\ \xi \\ \varphi_\lambda \\ \varphi_\mu \end{bmatrix} = \begin{bmatrix} \mu & -\mu & (\lambda - 2\mu) & \mu \\ -\mu & \mu & -(\lambda - 2\mu) & \mu \\ 0 & 0 & \lambda & 0 \\ 0 & 0 & 0 & \mu \end{bmatrix} \begin{bmatrix} \eta \\ \xi \\ \varphi_\lambda \\ \varphi_\mu \end{bmatrix}. \quad (2.64j)$$

### 2.3.2.2 Discrete-Time Representation for Koopman Embedding

**Example 2.3.5.** A formulation for discrete-time systems has a related form:

$$\begin{bmatrix} x_1 \\ x_2 \end{bmatrix}_{k+1} = \begin{bmatrix} \mu & 0 \\ 0 & \lambda \end{bmatrix} \begin{bmatrix} x_1 \\ x_2 \end{bmatrix}_k + \begin{bmatrix} 0 \\ (1-\lambda)p([x_1]_k) \end{bmatrix}. \quad (2.65a)$$

When  $|\lambda| \ll |\mu|$  and  $|\lambda| < 1$ , this system will converge asymptotically to a slow manifold given by  $x_2 = p(x_1)$ . This can be explained similarly to equations (2.60d) and (2.60h), with the difference that  $\mu^n$  is used instead of  $n\mu$ , since:

$$[x_1^n]_{k+1} = ([x_1]_{k+1})^n = (\mu [x_1]_k)^n = \mu^n [x_1^n]_k. \quad (2.65b)$$

For simplicity, let's start by considering  $p(x) = 5x^n - 2x^{n-3}$ . Then, we have

$$\psi = [\psi_1, \psi_2, \psi_3, \psi_4]^\top = [x_1, x_2, x_1^{n-3}, x_1^n]^\top, \quad (2.65c)$$

where,

$$[\psi_1]_{k+1} = \mu[\psi_1]_k \quad (2.65d)$$

$$[\psi_2]_{k+1} = \lambda[\psi_2]_k + (1-\lambda)(-2[\psi_3]_k + 5[\psi_4]_k) \quad (2.65e)$$

$$[\psi_3]_{k+1} = \mu^{n-3}[\psi_3]_k \quad (2.65f)$$

$$[\psi_4]_{k+1} = \mu^n[\psi_4]_k \quad (2.65g)$$

i.e.,

$$\begin{bmatrix} \psi_1 \\ \psi_2 \\ \psi_3 \\ \psi_4 \end{bmatrix}_{k+1} = \begin{bmatrix} \mu & 0 & 0 & 0 \\ 0 & \lambda & -2(1-\lambda) & 5(1-\lambda) \\ 0 & 0 & \mu^{n-3} & 0 \\ 0 & 0 & 0 & \mu^n \end{bmatrix} \begin{bmatrix} \psi_1 \\ \psi_2 \\ \psi_3 \\ \psi_4 \end{bmatrix}_k. \quad (2.65h)$$

Thus, for discrete-time systems with a general polynomial functions, represented by

$$p(x_1) = \sum_{j=1}^m c_j x_1^{n_j}, \quad (2.65i)$$

the update is given by:

$$\psi = [\psi_1, \psi_2, \psi_3, \psi_4, \dots, \psi_{m+2}]^\top = [x_1, x_2, x_1^{n_1}, x_1^{n_2}, \dots, x_1^{n_m}]^\top. \quad (2.65j)$$

indicates

$$\begin{bmatrix} \psi_1 \\ \psi_2 \\ \psi_3 \\ \psi_4 \\ \vdots \\ \psi_{m+2} \end{bmatrix}_{k+1} = \begin{bmatrix} \mu & 0 & 0 & 0 & \cdots & 0 \\ 0 & \lambda & c_1(1-\lambda) & c_2(1-\lambda) & \cdots & c_m(1-\lambda) \\ 0 & 0 & \mu^{n_1} & 0 & \cdots & 0 \\ 0 & 0 & 0 & \mu^{n_2} & \cdots & 0 \\ \vdots & \vdots & \vdots & \vdots & \ddots & \vdots \\ 0 & 0 & 0 & 0 & \cdots & \mu^{n_m} \end{bmatrix} \begin{bmatrix} \psi_1 \\ \psi_2 \\ \psi_3 \\ \psi_4 \\ \vdots \\ \psi_{m+2} \end{bmatrix}_k. \quad (2.65k)$$

**Example 2.3.6.** Consider the map, where the polynomial slow manifold is inspired from [14]:

$$\begin{bmatrix} x_1 \\ x_2 \end{bmatrix} \mapsto \begin{bmatrix} \lambda x_1 \\ \mu x_2 + (\lambda^2 - \mu) x_1^2 \end{bmatrix}. \quad (2.66a)$$

For the case where  $0 < \mu \ll \lambda < 1$  are real parameters and the polynomial stable manifold is given by  $x_1 = 0$  and  $x_2 = x_1^2$ , the following observable variables are proposed as intrinsic coordinates (eigenfunctions) for the nonlinear dynamics with corresponding eigenvalues  $\lambda$  and  $\mu$ :

$$\begin{bmatrix} \psi_1 \\ \psi_2 \end{bmatrix} = \begin{bmatrix} x_1 \\ x_2 - x_1^2 \end{bmatrix} \implies \begin{bmatrix} \psi_1 \\ \psi_2 \end{bmatrix}_{k+1} = \begin{bmatrix} \lambda & 0 \\ 0 & \mu \end{bmatrix} \begin{bmatrix} \psi_1 \\ \psi_2 \end{bmatrix}_k. \quad (2.66b)$$

Furthermore,  $\psi_1^n$  and  $\psi_2^n$  are eigenfunctions with the associated eigenvalues  $\lambda^n, \mu^n$  and  $\psi_1\psi_2$  is an eigenfunction with the eigenvalue  $\lambda\mu$ .

$$[\psi_1]_{k+1} = [x_1]_{k+1} = \lambda[x_1]_k = \lambda[\psi_1]_k \quad (2.66c)$$

$$[\psi_2]_{k+1} = [x_2 - x_1^2]_{k+1} \quad (2.66d)$$

$$= [x_2]_{k+1} - [x_1^2]_{k+1} \quad (2.66e)$$

$$= \mu[x_2]_k + (\lambda^2 - \mu)[x_1^2]_k - \lambda^2[x_1^2]_k \quad (2.66f)$$

$$= \mu[x_2]_k - \mu[x_1^2]_k = \mu[\psi_2]_k. \quad (2.66g)$$

$$[\psi_1^n]_{k+1} = ([\psi_1]_{k+1})^n = \lambda^n[\psi_1]_k \quad (2.66h)$$

$$[\psi_2^n]_{k+1} = ([\psi_2]_{k+1})^n = \mu^n[\psi_2]_k \quad (2.66i)$$

$$[\psi_1\psi_2]_{k+1} = [x_1x_2 - x_1^3]_{k+1} \quad (2.66j)$$

$$= [x_1]_{k+1}[x_2]_{k+1} - [x_1^3]_{k+1} \quad (2.66k)$$

$$= \lambda[x_1]_k(\mu[x_2]_k + (\lambda^2 - \mu)[x_1^2]_k) - \lambda^3[x_1^3]_k \quad (2.66l)$$

$$= \lambda\mu[x_1x_2]_k - \lambda\mu[x_1^3]_k \quad (2.66m)$$

$$= \lambda\mu([\psi_1]_{k+1})([\psi_2]_{k+1}) = \lambda\mu[\psi_1\psi_2]_k. \quad (2.66n)$$

In our approach, if the correct intrinsic variables are unknown, they can be discovered by reformulating the system in the form:

$$\begin{bmatrix} \psi_1 \\ \psi_2 \\ \psi_3 \end{bmatrix} = \begin{bmatrix} x_1 \\ x_2 \\ x_1^2 \end{bmatrix}, \quad (2.67)$$

indicates

$$\begin{bmatrix} \psi_1 \\ \psi_2 \\ \psi_3 \end{bmatrix}_{k+1} = \begin{bmatrix} \lambda & 0 & 0 \\ 0 & \mu & (\lambda^2 - \mu) \\ 0 & 0 & \lambda^2 \end{bmatrix} \begin{bmatrix} \psi_1 \\ \psi_2 \\ \psi_3 \end{bmatrix}_k. \quad (2.68)$$

The left eigenvectors (coefficients of the eigenfunctions) in this observable function coordinate system are:

$$\begin{aligned} \xi_1 &= \begin{bmatrix} 1 \\ 0 \\ 0 \end{bmatrix} \implies \varphi_1(x) = x_1, \\ \xi_2 &= \begin{bmatrix} 0 \\ 0 \\ 1 \end{bmatrix} \implies \varphi_2(x) = x_1^2, \\ \xi_3 &= \begin{bmatrix} 0 \\ 1 \\ -1 \end{bmatrix} \implies \varphi_3(x) = x_2 - x_1^2 \end{aligned} \quad (2.69)$$

corresponding to the eigenvalues  $\gamma_1 = \lambda$ ,  $\gamma_2 = \lambda^2$  and  $\gamma_3 = \mu$ . These eigenvectors diagonalize the system and define the intrinsic coordinates. For instance, from (2.63), we verify that

$$\varphi_1(x) = \xi_1^\top \psi = \begin{bmatrix} 1 \\ 0 \\ 0 \end{bmatrix}^\top \begin{bmatrix} x_1 \\ x_2 \\ x_1^2 \end{bmatrix} = x_1 \quad (2.70a)$$

and

$$\xi_1^\top \mathbf{K} = \begin{bmatrix} 1 \\ 0 \\ 0 \end{bmatrix}^\top \begin{bmatrix} \lambda & 0 & 0 \\ 0 & \mu & (\lambda^2 - \mu) \\ 0 & 0 & \lambda^2 \end{bmatrix} = \lambda \xi_1^\top. \quad (2.70b)$$

Similarly, for  $\xi_2$  and  $\xi_3$ .

**Remark 2.3.7.** If we take the full state observable  $\psi(x) = x = [x_1, x_2]$ , then for the linear map

$$\begin{bmatrix} x_1 \\ x_2 \end{bmatrix} \mapsto \begin{bmatrix} \lambda x_1 \\ \mu x_2 \end{bmatrix} \quad (2.71)$$

the Koopman eigenfunctions  $\varphi_\lambda(x) = x_1$  and  $\varphi_\mu(x) = x_2$  lie in the span of the observable. However, for the nonlinear dynamics (2.66a), the eigenfunction  $\varphi_\mu = x_2 - x_1^2$  is no longer lies in the span of the observables. Similary, if we take  $\psi(x) = [x_1, x_2, x_1^2 \text{ or } x_1^3]$  the eigenfunction  $\varphi_1 \varphi_3 = x_1 x_2 - x_1^3$  with eigenvalue  $\mu\lambda$  does not lie in the span of the observables, thus we cannot figure out the left eigenvector. However, for the eigenfunction  $\varphi_1 \varphi_2 = x_1^3$  with eigenvalue  $\lambda^3$ , we can find the associated left eigenvector by taking another observables , where the system is reformulated in the form

$$\begin{bmatrix} \psi_1 \\ \psi_2 \\ \psi_3 \\ \psi_4 \end{bmatrix} = \begin{bmatrix} x_1 \\ x_2 \\ x_1^2 \\ x_1^3 \end{bmatrix} \implies \begin{bmatrix} \psi_1 \\ \psi_2 \\ \psi_3 \\ \psi_4 \end{bmatrix}_{k+1} = \begin{bmatrix} \lambda & 0 & 0 & 0 \\ 0 & \mu & (\lambda^2 - \mu) & 0 \\ 0 & 0 & \lambda^2 & 0 \\ 0 & 0 & 0 & \lambda^3 \end{bmatrix} \begin{bmatrix} \psi_1 \\ \psi_2 \\ \psi_3 \\ \psi_4 \end{bmatrix}_k. \quad (2.72)$$

Therefore, the left eigenvectors in this observable function coordinate system are:

$$\xi_\lambda = \begin{bmatrix} 1 \\ 0 \\ 0 \\ 0 \end{bmatrix} \implies \varphi_\lambda(x) = x_1, \quad \xi_{\lambda^2} = \begin{bmatrix} 0 \\ 0 \\ 1 \\ 0 \end{bmatrix} \implies \varphi_{\lambda^2}(x) = x_1^2, \quad (2.73)$$

$$\xi_{\lambda^3} = \begin{bmatrix} 0 \\ 0 \\ 0 \\ 1 \end{bmatrix} \implies \varphi_{\lambda^3}(x) = x_1^3, \quad \xi_\mu = \begin{bmatrix} 0 \\ 1 \\ -1 \\ 0 \end{bmatrix} \implies \varphi_\mu(x) = x_2 - x_1^2. \quad (2.74)$$

## 2.4 Numerical Approximation Methods

The Koopman operator is an infinite-dimensional operator that can be challenging to handle numerically. To make it more manageable, it is often projected onto finite-dimensional subspaces. Despite this, some cases have been demonstrated in the subsection above (2.3.2), where it is possible to create a linear and finite-dimensional representation of a nonlinear dynamical system. The equation (2.15) establishes that the relationship for the eigenfunctions of  $\mathcal{L}$  is the PDE (2.39)

$$\nabla \varphi(x) \cdot \mathbf{f}(x) = \mu \varphi(x). \quad (2.75)$$

By solving this PDE, we can estimate eigenfunctions either analytically, as shown below in subsection 2.4.1, or through regression on data, as demonstrated in section 3.0.1. This method assumes that the dynamics are continuous and differentiable.

### 2.4.1 Laurent and Taylor Series for Eigenfunctions Expansion.

To solve the partial differential equation

$$\nabla \varphi(x) \cdot \mathbf{f}(x) = \mu \varphi(x). \quad (2.76)$$

associated with the dynamics

$$\frac{d}{dt}x = \dot{x} = \mathbf{f}(x(t)), \quad (2.77)$$

traditional methods such as the recursive solution of Taylor or Laurent series terms can be employed. Here, we show number of several straightforward examples.

**Example 2.4.1.** Consider the simple linear dynamics

$$\dot{x} = x. \quad (2.78)$$

Given the Taylor series representation of  $\varphi(x)$ :

$$\varphi(x) = c_0 + c_1x + c_2x^2 + c_3x^3 + \dots \quad (2.79)$$

The gradient and directional derivatives can be determined as:

$$\nabla \varphi = c_1 + 2c_2x + 3c_3x^2 + 4c_4x^3 + \dots \quad (2.80a)$$

$$\nabla \varphi \cdot f = c_1x + 2c_2x^2 + 3c_3x^3 + 4c_4x^4 + \dots \quad (2.80b)$$

To solve for the terms in the Koopman eigenfunction PDE (2.76), it must be the case that  $c_0 = 0$ . For a positive integer  $\mu$  in (2.76), the coefficients with negative indices follow the recursion

$$\mu c_k = c_k, \quad \text{for all } k \in \mathbb{Z}^+, \quad (2.81)$$

meaning only one of the coefficients can be non-zero. For instance,

$$\varphi(x) = c_k x^k \quad \text{when } \mu \in \mathbb{Z}^+, \quad (2.82)$$

is an eigenfunction with any constant  $c = c_k$ . In particular,

$$\varphi(x) = x, \quad \text{when } \mu = 1. \quad (2.83)$$

**Example 2.4.2.** Consider a quadratic nonlinear dynamical system.

$$\dot{x} = x^2. \quad (2.84)$$

The Koopman eigenfunction PDE (2.76) does not admit a Taylor series solution except for the trivial case of  $\varphi = 0$  when  $\mu = 0$ . As an alternative, we use a Laurent series.

$$\varphi(x) = \dots + c_{-3}x^{-3} + c_{-2}x^{-2} + c_{-1}x^{-1} + c_0 + c_1x + c_2x^2 + c_3x^3 + \dots. \quad (2.85)$$

The gradient and directional derivatives are given by:

$$\nabla \varphi = \dots - 3c_{-3}x^{-4} - 2c_{-2}x^{-3} - c_{-1}x^{-2} + c_1 + 2c_2x + 3c_3x^2 + 4c_4x^3 + \dots \quad (2.86)$$

$$\nabla \varphi \cdot f = \dots - 3c_{-3}x^{-2} - 2c_{-2}x^{-1} - c_{-1} + c_1x^2 + 2c_2x^3 + 3c_3x^4 + 4c_4x^5 + \dots \quad (2.87)$$

When solving for the coefficients in the Laurent series that satisfy (2.76), if  $\mu \neq 0$ , we find that

$$\mu c_0 = -c_{-1}, \quad \mu c_1 = 0, \quad \text{and} \quad \mu c_{k+1} = c_k, \quad \text{for all } k \geq 1. \quad (2.88)$$

This means that all coefficients with positive index are zero ( $c_k = 0$  for all  $k \geq 1$ ). However, for nonpositive indices, the coefficients are given by the recursion

$$\mu c_{-k} = -(k+1)c_{-(k+1)}, \quad \text{for } k \geq 0, \quad \text{or} \quad \mu c_{k+1} = kc_k, \quad \text{for } k \leq -1. \quad (2.89)$$

The resulting Laurent series is

$$\varphi(x) = c_0 + c_{-1}x^{-1} + c_{-2}x^{-2} + c_{-3}x^{-3} \dots \quad (2.90)$$

$$\varphi(x) = c_0 - \mu c_0 x^{-1} + \frac{\mu^2}{2} c_0 x^{-2} - \frac{\mu^3}{6} c_0 x^{-3} + \dots \quad (2.91)$$

$$\varphi(x) = c_0 \left( 1 - \mu x^{-1} + \frac{\mu^2}{2} x^{-2} - \frac{\mu^3}{3!} x^{-3} + \dots \right) = c_0 \exp\left(-\frac{\mu}{x}\right). \quad (2.92)$$

For any  $\mu \in \mathbb{C}$ , the results described hold true. Additionally, other eigenfunctions of the Koopman operator can be found by analyzing the Laurent series. Furthermore, for a more general system, the polynomial nonlinear dynamics

$$x = ax^n. \quad (2.93)$$

For all  $\mu \in \mathbb{C}$ ,

$$\varphi(x) = \exp\left(\frac{\mu}{a(1-n)}x^{1-n}\right) \quad (2.94)$$

is an eigenfunction. Another way to generate Koopman eigenfunctions is by taking powers of the primitive eigenfunctions, which results in the eigenvalues forming a lattice in the complex plane, as discussed in the subsection 2.2.1.

It is not always possible to obtain a finite-dimensional representation of transfer operators. In the following, we focus on projecting these operators onto finite-dimensional subspaces.

## 2.4.2 Galerkin Approximation of the Koopman Generator

The Galerkin discretization of an operator  $\mathcal{K}$  in a Hilbert space, such as  $\mathcal{G} = L^2(\mathcal{M}, \rho)$ , can be explained as follows. Given a finite-dimensional subspace  $\mathbb{V} \subset \mathcal{G}$  with basis  $\{\psi_k\}_{k=1}^n$ , the *Galerkin projection* of  $\mathcal{K}$  onto  $\mathbb{V}$  is a unique linear operator  $\mathbf{K} : \mathbb{V} \rightarrow \mathbb{V}$  that satisfies

$$\langle \psi_j, \mathcal{K}\psi_k \rangle = \langle \psi_j, \mathbf{K}\psi_k \rangle, \quad \text{for all } j, k = 1, \dots, n. \quad (2.95)$$

Assuming that  $\psi_k : \mathbb{R}^d \rightarrow \mathbb{C}$  for all basis functions  $\{\psi_k\}_{k=1}^n$ , we can calculate a finite-dimensional Galerkin approximation of the Koopman generator  $\mathcal{L}$  known as  $\hat{\mathbf{K}}$  using the matrices  $\mathbf{A}, \mathbf{G} \in \mathbb{C}^{n \times n}$  defined as

$$\mathbf{A}_{jk} = \langle \mathcal{L}\psi_j, \psi_k \rangle \rho, \quad (2.96)$$

$$\mathbf{G}_{jk} = \langle \psi_j, \psi_k \rangle \rho. \quad (2.97)$$

The matrix representation  $\hat{\mathbf{K}}$  of the projected operator  $\mathbf{K}$  is then given by

$$\hat{\mathbf{K}}^\top = \mathbf{A}\mathbf{G}^{-1}. \quad (2.98)$$

For

$$\psi = \begin{bmatrix} \psi_1 \\ \vdots \\ \psi_n \end{bmatrix} \in \mathbb{C}^n \quad \text{and} \quad c = \begin{bmatrix} c_1 \\ \vdots \\ c_n \end{bmatrix} \in \mathbb{C}^n, \quad (2.99)$$

and given a function

$$g(x) = \sum_{k=1}^n c_k \psi_k(x) = c^\top \psi(x), \quad (2.100)$$

we get

$$(\hat{\mathbf{K}}g)(x) = (\mathbf{K}c)^\top \psi(x). \quad (2.101)$$

By setting  $\varphi_\ell = \xi_\ell^\top \psi(x)$ , the following equation is derived:

$$(\hat{\mathbf{K}}\varphi_\ell)(x) = \gamma_\ell \varphi_\ell(x) = (\mathbf{K}\xi_\ell)^\top \psi(x) = \gamma_\ell \xi_\ell^\top \psi(x), \quad (2.102)$$

which implies that the coefficients of the eigenfunctions of  $\hat{\mathbf{K}}$  are contained within the eigenvector  $\xi_\ell$  of  $\mathbf{K}$  that has the corresponding eigenvalue  $\gamma_\ell$ . It is important to note that, in general, the projected generator does not yield a rate matrix, as noted in [8].

**Example 2.4.3.** For the Ornstein-Uhlenbeck process defined by the stochastic differential equation

$$dX_t = -\alpha X_t dt + \sqrt{2\beta^{-1}} dW_t, \quad (2.103)$$

previously mentioned in Example 2.2.9, it is feasible to calculate the matrix  $\hat{\mathbf{K}}$  analytically. Let's consider a basis that includes polynomials up to degree  $n-1$ , i.e.,  $\psi(x) = [1, x, \dots, x^{n-1}]^\top$ . The result  $\mathcal{L}\psi_j$  lies within the subspace spanned by  $\{\psi_k\}_{k=1}^n$ , and for  $j \geq 3$ ,

$$(\mathcal{L}\psi_j)(x) = -\alpha(k-1)x^{j-1} + \beta^{-1}(j-1)(j-2)x^{j-3}. \quad (2.104)$$

The matrix  $\hat{\mathbf{K}} \in \mathbb{C}^{n \times n}$  is then given by

$$\hat{\mathbf{K}} = \begin{pmatrix} 1 & x & x^2 & x^3 & x^4 & x^5 & x^6 & \dots \\ 0 & 2\beta^{-1} & & & & & & \\ x & -\alpha & 6\beta^{-1} & & & & & \\ x^2 & & -2\alpha & 12\beta^{-1} & & & & \\ x^3 & & & -3\alpha & 20\beta^{-1} & & & \\ x^4 & & & & -4\alpha & 30\beta^{-1} & & \\ x^5 & & & & & -5\alpha & \ddots & \\ x^6 & & & & & & -6\alpha & \ddots \\ \vdots & & & & & & & \ddots \end{pmatrix}, \quad (2.105)$$

For clarity, the rows and columns in the matrix are labeled based on their relationship to the basis functions. As demonstrated in Example 2.2.9, the eigenvalues are found to be  $\gamma_\ell = -\alpha(\ell-1)$ , where  $\ell = 1, \dots, n$ , and the coefficients of the eigenfunctions  $\varphi_\ell$  are represented by the eigenvectors, as noted in [8].

For more information on Galerkin discretization of transfer operators and their characteristics, see references such as [13, 7]. Since analytical solutions for the necessary integrals are not always possible, data-based techniques like regression and Monte Carlo integration must be used to estimate them. Some of the most frequently used algorithms for computing approximate projected transfer operators are listed in section 3.0.1.

Chapter **3**

# Data Driven Methods

In this chapter, we present an overview of Data-Driven Methods for analyzing dynamical systems. We focus on the Extended Dynamical Mode Decomposition (EDMD) and its uses, including approximating the Koopman Operator and its Eigenfunctions, computing the Koopman Modes, and applying the EDMD algorithm to stochastic data. In addition, we cover Dynamic Mode Decomposition (DMD), which reveals underlying structures and trends in the system's behavior. To demonstrate the effectiveness of EDMD, we provide several numerical examples, where we use monomials up to and including 10 as basis functions. These examples include the one-dimensional Ornstein-Uhlenbeck process, as well as various two-dimensional problems such as the Double-Well, Triple-Well, and Quadruple-Well Problems.

## Contents

---

3.0.1	Extended Dynamical Mode Decomposition (EDMD)	32
3.0.1.1	Approximating the Koopman Operator and its Eigenfunctions	32
3.0.1.2	Computing the Koopman Modes	34
3.0.1.3	Convergence of the EDMD Algorithm to a Galerkin Method	35
3.0.1.4	EDMD with Stochastic Data	36
3.0.1.5	Dynamic Mode Decomposition (DMD)	37
3.0.2	Numerical Examples: EDMD with Monomial Basis Functions	40

---

### 3.0.1 Extended Dynamical Mode Decomposition (EDMD)

In order to tackle the challenge of identifying the nonlinear coordinate transformations that are required to approximate the Koopman operator for highly nonlinear systems, an approach known as extended dynamical mode decomposition (EDMD) has been developed. This algorithm is designed to calculate finite-dimensional approximations of the Koopman operator, as well as its corresponding eigenfunctions, eigenvalues, and modes. The EDMD procedure relies on two primary requirements, which are as follows:

1. A data set of snapshot pairs, denoted by  $\{(x_m, y_m)\}_{m=1}^M$ , which we can organize into a pair of datasets:

$$\mathbf{X} = [x_1 \ x_2, \dots, x_M], \quad \mathbf{Y} = [y_1 \ y_2, \dots, y_M] = [x_2 \ x_3, \dots, x_{M+1}], \quad (3.1)$$

where  $x_i \in \mathcal{M}$  and  $y_i \in \mathcal{M}$  represent *snapshots of the system* with  $y_i = x_{i+1} = \mathbf{F}(x_i)$ .

2. A dictionary of observables, denoted by  $\mathcal{D} = \{\psi_1, \psi_2, \dots, \psi_p\}$ , where  $\psi \in \mathcal{G}$ . We define the span of these observables as  $\mathcal{G}_D$ . To simplify notation, we define a vector-valued function  $\Psi : \mathcal{M} \rightarrow \mathbb{C}^{1 \times p}$  as

$$\Psi(x) = [\psi_1(x), \psi_2(x), \dots, \psi_p(x)]. \quad (3.2)$$

EDMD constructs an augmented state  $\mathbf{z} = \Psi(x) \in \mathbb{C}^{1 \times p}$  by nonlinearly measuring the state  $\mathbf{x}$  using functions  $\psi_k$ . The resulting vector  $\mathbf{z}$  may include  $\mathbf{x}$  and nonlinear measurements, with  $d \ll p$ . Because the augmented vector  $\mathbf{z}$  may be significantly larger than the state  $\mathbf{x}$ , i.e., the number of measurement points  $p$  is typically much larger than the number of measurements or snapshots  $M$  it is typically necessary to employ *kernel methods* to compute this regression. Now, two data matrices  $\Psi_X, \Psi_Y \in \mathbb{C}^{p \times M}$  are then constructed using these measurements

$$\Psi_X = \left[ \begin{array}{ccc|c} & & & \\ \Psi(x_1)^\top & \dots & \Psi(x_M)^\top & \\ & & & \end{array} \right], \quad \Psi_Y = \left[ \begin{array}{ccc|c} & & & \\ \Psi(y_1)^\top & \dots & \Psi(y_M)^\top & \\ & & & \end{array} \right] \quad (3.3)$$

The data set required is generally created from multiple short simulation bursts or experimental data, and the optimal choice of dictionary elements is an open question. It is assumed that the dictionary  $\mathcal{D}$  is rich enough to accurately approximate a few of the leading Koopman eigenfunctions.

#### 3.0.1.1 Approximating the Koopman Operator and its Eigenfunctions

Now, the aim is to find a finite-dimensional approximation  $\mathbf{K} \in \mathbb{C}^{p \times p}$  of the Koopman operator  $\mathcal{K}$  with respect to the basis spanned by  $\{\varphi_i\}_{i=1}^p$ . For a function  $\psi \in \mathcal{G}_D$ , expressed as a linear combination of elements in the dictionary with weights  $\mathbf{a}$ ,

$$\psi(x) = \sum_{k=1}^p a_k \psi_k(x) = \Psi(x) \mathbf{a}. \quad (3.4)$$

It should be noted that the value of  $p$  in equations following (3.4) is finite, unlike in equation (2.53a) where  $p$  could be infinite. Since  $\mathcal{G}_D$  is usually not an invariant subspace of  $\mathcal{K}$ , it follows that

$$(\mathcal{K}\psi)(x) = (\Psi \circ \mathbf{F})(x) \mathbf{a} = \Psi(x) (\mathbf{K} \mathbf{a}) + r(x), \quad (3.5)$$

where  $\mathbf{K}$  is the finite-dimensional approximation of  $\mathcal{K}$ , and  $r \in \mathcal{G}$  is the residual. To determine  $\mathbf{K}$ , we will minimize

$$\begin{aligned} J &= \frac{1}{2} \sum_{m=1}^M |r(x_m)|^2 \\ &= \frac{1}{2} \sum_{m=1}^M |((\Psi \circ \mathbf{F})(x_m) - \Psi(x_m)\mathbf{K})\mathbf{a}|^2 \\ &= \frac{1}{2} \sum_{m=1}^M |(\Psi(y_m) - \Psi(x_m)\mathbf{K})\mathbf{a}|^2 \end{aligned} \quad (3.6)$$

where  $x_m$  is the  $m$ th snapshot in  $\mathbf{X}$ , and  $y_m = \mathbf{F}(x_m)$  is the  $m$ th snapshot in  $\mathbf{Y}$ . In the matrix method, a best-fit linear matrix operator  $M$  is created to map  $\Psi_X$  to  $\Psi_Y$  by minimizing the Frobenius norm:

$$\min \| \Psi_Y - M \Psi_X \|_F, \quad (3.7)$$

where  $M^\top \equiv \mathbf{K}$ . The equation above is a least-squares problem and therefore has either a unique global minimizer or a continuous family (or families) of minimizers, but not multiple isolated local minima. To ensure a unique solution, regularization (via the truncated singular value decomposition) may be necessary. The value of  $\mathbf{K}$  that minimizes equation (3.6) is:

$$\mathbf{K} \triangleq \mathbf{G}^\dagger \mathbf{A} = \Psi_X^\dagger \Psi_Y = (\Psi_X^* \Psi_X)^\dagger (\Psi_X^*) \Psi_Y \quad \text{and} \quad M \triangleq \Psi_Y \Psi_X^\dagger = \mathbf{A} \mathbf{G}^\dagger, \quad (3.8)$$

where  $\dagger$  denotes the Moore–Penrose pseudoinverse and

$$\mathbf{G} = \frac{1}{M} \sum_{m=1}^M \Psi(x_m)^* \Psi(x_m), \quad \mathbf{A} = \frac{1}{M} \sum_{m=1}^M \Psi(x_m)^* \Psi(y_m), \quad (3.9a)$$

with  $\mathbf{K}, \mathbf{G}, \mathbf{A} \in \mathbb{C}^{p \times p}$ . The pseudoinverse may be computed using the SVD that is a unique matrix decomposition that exists for every complex-valued matrix  $\mathbf{X} \in \mathbb{C}^{d \times M}$

$$\mathbf{X} = \mathbf{U} \Sigma \mathbf{V}^* \quad \text{as} \quad \mathbf{X}^\dagger = \mathbf{V} \Sigma^{-1} \mathbf{U}^*. \quad (3.10)$$

The matrices  $\mathbf{U} \in \mathbb{C}^{d \times d}$  and  $\mathbf{V} \in \mathbb{C}^{M \times M}$  are unitary with orthonormal columns, so that  $\mathbf{U}^* \mathbf{U} = I$  and  $\mathbf{V}^* \mathbf{V} = I$ , where  $*$  denotes complex-conjugate transpose<sup>1</sup>, and  $\Sigma \in \mathbb{R}^{d \times M}$  is a matrix with real, nonnegative entries on the diagonal and zeros off the diagonal.

Therefore, the matrix  $\mathbf{K}$  is a finite-dimensional approximation of the true Koopman operator  $\mathcal{K}$ , which maps a snapshot  $\psi \in \mathcal{G}_D$  to a different snapshot  $\hat{\psi} \in \mathcal{G}_D$  by minimizing the residuals at the data points. Consequently, if  $\xi_j$  is the  $j$ th eigenvector of  $\mathbf{K}$  with the eigenvalue  $\mu_j$ , then the EDMD approximation of an eigenfunction of  $\mathcal{K}$  is given by

$$\varphi_j(x) = \Psi(x) \xi_j. \quad (3.11)$$

The eigenfunctions  $\varphi(x)$  are formed from left EDMD eigenvectors  $\xi$  of  $\mathbf{K}$ , the right eigenvectors are the EDMD modes. In discrete-time, a Koopman eigenfunction that satisfies  $\mu \varphi(x_k) = \varphi(x_{k+1})$  evaluated on a trajectory of snapshots  $\{x_1, \dots, x_M\}$  will satisfy:

$$\mu [\varphi(x_1) \varphi(x_2) \dots \varphi(x_M)] = [\varphi(x_2) \varphi(x_3) \dots \varphi(x_{M+1})], \quad (3.12a)$$

which can be solved using the least-squares method for EDMD. The equation can be rewritten using the expanded expression for  $\varphi$  obtained from equation (3.11)

$$\mu \Psi(x_k) \xi = \Psi(y_k) \xi. \quad (3.12b)$$

---

<sup>1</sup>For real-valued matrices, this is the same as the regular transpose  $\mathbf{X}^* = \mathbf{X}^\top$

It can be expressed as a matrix system of equations involving  $\Psi_X$  and  $\Psi_Y$ .

$$\mu \Psi_X \xi = \Psi_Y \xi. \quad (3.12c)$$

If we aim for a "least-squares fit" to equation (3.12c), then it simplifies to the EDMD method:

$$\mu \xi = \Psi_Y \Psi_X^\dagger \xi. \quad (3.12d)$$

If the discrete-time data in  $\mathbf{X}$  and  $\mathbf{Y}$  are generated by a continuous-time process with a sampling interval of  $\Delta t$ , then the eigenvalues of the *continuous-time system* can be approximated as  $\lambda_j = \frac{\ln(\mu_j)}{\Delta t}$ . Both the discrete and continuous-time eigenvalues provide the same information, but one may be more appropriate for a particular problem.

### 3.0.1.2 Computing the Koopman Modes

This section describes the process of computing approximations of the Koopman modes for the full-state observable using EDMD. The Koopman modes represent the weights necessary to express the full state in the *Koopman eigenfunction* basis. The process involves two steps: First, expressing the full-state observable using the elements of  $\mathcal{D}$ , and second, mapping the elements of  $\mathcal{D}$  to the numerically computed eigenfunctions. By combining these two steps, the observables can be expressed as a linear combination of Koopman eigenfunctions, which represent the Koopman modes for the full-state observable. The full-state observable,  $\mathbf{g}(\mathbf{x}) = \mathbf{x}$ , is a vector-valued observable that can be generated by stacking  $d$  scalar-valued observables,  $g_i : \mathcal{M} \rightarrow \mathbb{C}$ , as follows

$$\mathbf{g}(\mathbf{x}) = \begin{bmatrix} g_1(\mathbf{x}) \\ g_2(\mathbf{x}) \\ \vdots \\ g_d(\mathbf{x}) \end{bmatrix} = \begin{bmatrix} e_1^* \mathbf{x} \\ e_2^* \mathbf{x} \\ \vdots \\ e_d^* \mathbf{x} \end{bmatrix}, \quad (3.13)$$

where  $e_i$  is the  $i$ th unit vector in  $\mathbb{R}^d$ . At this time, we assume that all scalar-valued observables  $g_i(\mathbf{x}) \in \mathcal{G}_D$  can be expressed as a linear combination of  $\psi_k(\mathbf{x})$ , multiplied by some appropriate vector of weights,  $\mathbf{b}_i$

$$g_i(\mathbf{x}) = \sum_{k=1}^p \psi_k(\mathbf{x}) b_{k,i} = \Psi(\mathbf{x}) \mathbf{b}_i. \quad (3.14)$$

This allows us to represent the full-state observable,  $\mathbf{g}(\mathbf{x})$ , as a vector-valued observable. However, if some  $g_i(\mathbf{x})$  cannot be represented as a linear combination, we can still approximate the Koopman modes by projecting  $g_i$  onto  $\mathcal{G}_D$  the space spanned by the observable functions. The accuracy of this approximation depends on the choice of the EDMD dictionary,  $\mathcal{D}$ . To avoid this issue, we assume that all  $g_i(\mathbf{x})$  can be expressed as a linear combination, i.e.,  $g_i \in \mathcal{G}_D$  for  $i = 1, \dots, d$ . In either case, the full-state observable can be approximated in this manner.

$$\mathbf{g}(\mathbf{x}) = \mathbf{B}^\top \Psi(\mathbf{x})^\top = (\Psi(\mathbf{x}) \mathbf{B})^\top, \quad \mathbf{B} = [\mathbf{b}_1 \ \mathbf{b}_2, \dots, \mathbf{b}_d], \quad (3.15)$$

where  $\mathbf{B} \in \mathbb{C}^{d \times p}$ .

In the next step, we aim to represent the  $\psi_i$  in terms of all the  $\varphi_i$  which are the numerical approximations of the Koopman eigenfunctions. To make the notation easier, we introduce a vector-valued function  $\Phi : \mathcal{M} \rightarrow \mathbb{C}^{1 \times p}$ , where

$$\Phi(\mathbf{x}) = [\varphi_1(\mathbf{x}) \ \varphi_2(\mathbf{x}), \dots, \varphi_p(\mathbf{x})]. \quad (3.16)$$

Using (3.11) and (3.13), this function can also be written as

$$\Phi(\mathbf{x}) = \Psi(\mathbf{x})\Xi, \quad \Xi = [\xi_1 \ \xi_2, \dots, \xi_p], \quad (3.17)$$

where  $\xi_i \in \mathbb{C}^p$  is the  $i$ th right eigenvector of  $\mathbf{K}$  associated with  $\mu_i$ . The statement means that the values of  $\psi_i$  can be found in terms of  $\varphi_i$  by taking the inverse of the transpose of the matrix  $\Xi$ . The matrix  $\Xi$  is composed of eigenvectors, and its inverse is

$$\Xi^{-1} = \mathbf{W}^* = [ \mathbf{w}_1 \ \mathbf{w}_2, \dots, \mathbf{w}_p ]^*, \quad (3.18)$$

where  $w_i$  represents the  $i$ th left eigenvector of  $\mathbf{K}$  that is associated with the eigenvalue  $\mu_i$  such that  $\mathbf{w}_i^* \mathbf{K} = \mathbf{w}_i^* \mu_i$ . It is also scaled such that  $\mathbf{w}_i^* \xi_i = 1$ . By combining equation (3.15) and (3.18) and performing some algebraic manipulation, we arrive at the following expression:

$$\mathbf{g}(\mathbf{x}) = \mathbf{V}\Phi(\mathbf{x})^\top = \sum_{k=1}^p v_k \varphi_k \implies (\mathcal{K}\mathbf{g})(x) = \sum_{k=1}^p \mu_k v_k \varphi_k, \quad (3.19)$$

where

$$\mathbf{V} = [ \mathbf{v}_1 \ \mathbf{v}_2 \dots \mathbf{v}_p ] = (\Xi^{-1} \mathbf{B})^\top = (\mathbf{W}^* \mathbf{B})^\top \quad (3.20)$$

and  $v_i = (\mathbf{w}_i^* \mathbf{B})^\top$  is the  $i$ th Koopman mode. This is the desired formula for the Koopman modes.

### 3.0.1.3 Convergence of the EDMD Algorithm to a Galerkin Method

In this subsection, we relate EDMD to the Galerkin methods one would use to approximate the Koopman operator with complete information about the underlying dynamical system. In this context, a Galerkin method is a weighted-residual method where the residual, as defined in (3.5), is orthogonal to the span of  $\mathcal{D}$ . In particular, we show that the EDMD approximation of the Koopman operator converges to the approximation that would be obtained from a Galerkin method in the large-data limit, i.e., when  $M \rightarrow \infty$  and where the elements of  $\mathbf{X}$  are drawn independently from a distribution on  $\mathcal{M}$  with the probability density  $\rho$ , i.e.,  $x_m \sim \rho$  ( $\rho$  is one of the natural measures associated with the underlying dynamical system). The choice of  $\mathcal{G} = L^2(\mathcal{M}, \rho)$  is required so that the inner products in the Galerkin method converge, which is relevant for problems where  $\mathcal{M} = \mathbb{R}^d$ . If EDMD were a Galerkin method, then the entries of  $\mathbf{G}$  and  $\mathbf{A}$  in (3.8) would be defined as

$$\hat{\mathbf{G}}_{ij} = \int_{\mathcal{M}} \psi_i^*(\mathbf{x}) \psi_j(\mathbf{x}) \rho(\mathbf{x}) d\mathbf{x} = \langle \psi_i, \psi_j \rangle_\rho, \quad (3.21a)$$

$$\hat{\mathbf{A}}_{ij} = \int_{\mathcal{M}} \psi_i^*(\mathbf{x}) \psi_j(\mathbf{F}(\mathbf{x})) \rho(\mathbf{x}) d\mathbf{x} = \langle \psi_i, \mathcal{K}\psi_j \rangle_\rho, \quad (3.21b)$$

where

$$\langle f, h \rangle_\rho = \int_{\mathcal{M}} f^*(\mathbf{x}) h(\mathbf{x}) \rho(\mathbf{x}) d\mathbf{x} \quad (3.22)$$

is the inner product and the finite-dimensional *Galerkin approximation* of the Koopman operator would be

$$\hat{\mathbf{K}} = \hat{\mathbf{G}}^{-1} \hat{\mathbf{A}}. \quad (3.23)$$

The effectiveness of this approach is influenced by the selection of  $\psi_j$  and  $\rho$ . However, it is still considered a Galerkin method since the residual is perpendicular to  $\mathcal{G}_{\mathcal{D}}$ .

For a finite  $M$ , the  $ij$ th element of  $\mathbf{G}$  and  $\mathbf{A}$  are

$$\mathbf{G}_{ij} \triangleq \frac{1}{M} \sum_{m=1}^M \psi_i^*(\mathbf{x}_m) \psi_j(\mathbf{x}_m), \quad \mathbf{A}_{ij} \triangleq \frac{1}{M} \sum_{m=1}^M \psi_i^*(\mathbf{x}_m) \psi_j(\mathbf{y}_m). \quad (3.24a)$$

The  $ij$ th components of  $\mathbf{G}$  and  $\mathbf{A}$  consist of the sample mean of  $\psi_i(\mathbf{x})\psi_j(\mathbf{x})$  and  $\psi_i(\mathbf{x})\psi_j(\mathbf{y})$ , respectively.

When the number of data points,  $M$ , is finite, equation (3.21) is approximated by equation (3.24). However, the expected values are almost surely approached as the number of samples increases, according to the law of large numbers. The expectations for this system can be expressed as

$$\lim_{M \rightarrow \infty} \mathbf{G}_{ij} = \lim_{M \rightarrow \infty} \frac{1}{M} \sum_{m=1}^M \psi_i^*(x_m)\psi_j(x_m) = \int_{\mathcal{M}} \psi_i^*(\mathbf{x})\psi_j(\mathbf{x})\rho(\mathbf{x})d\mathbf{x} = \langle \psi_i, \psi_j \rangle_{\rho} = \hat{\mathbf{G}}_{ij},$$

$$\lim_{M \rightarrow \infty} \mathbf{A}_{ij} = \lim_{M \rightarrow \infty} \frac{1}{M} \sum_{m=1}^M \psi_i^*(x_m)\psi_j(y_m) = \int_{\mathcal{M}} \psi_i^*(\mathbf{x})\psi_j(\mathbf{F}(\mathbf{x}))\rho(\mathbf{x})d\mathbf{x} = \langle \psi_i, \mathcal{K}\psi_j \rangle_{\rho} = \hat{\mathbf{A}}_{ij},$$

The inclusion of integrals in equation (3.21) restores the entries of  $\mathbf{A}$  and  $\mathbf{G}$ , causing them to converge to their respective analytical values. As a result, the output of the EDMD method will converge to that of a Galerkin method.

It should be noted that when the number of data points,  $M$ , is small, EDMD will not be an effective Galerkin method due to the significant quadrature errors generated by the Monte Carlo integrator. Consequently, the residual may not be perpendicular to  $\mathcal{G}_{\mathcal{D}}$ .

### 3.0.1.4 EDMD with Stochastic Data

For a discrete-time Markov process,

$$x \mapsto \mathbf{F}(x; \omega), \quad (3.25)$$

the Stochastic Koopman Operator (SKO) is defined as

$$(\mathcal{K}\psi)(x) = \mathbb{E}[\psi(\mathbf{F}(x; \omega))], \quad (3.26)$$

where  $\omega \in \Omega_s$  represents an element in the probability space that is associated with the stochastic dynamics ( $\Omega_s$ ) and has a probability measure of  $P$ , and  $\mathbb{E}$  denotes the expected value over that space, while  $\psi \in \mathcal{G}$  is a scalar observable. For further information, please refer to [17]. As a result of the system's stochastic nature, there are two probability spaces involved: one related to the samples in  $\mathbf{X}$  and another for the stochastic dynamics. Since the system experiences "process" noise instead of "measurement" noise, the values of  $x_i$  are known with certainty, and therefore the interpretation of the Gram matrix,  $\mathbf{G}$ , remains the same

$$\lim_{M \rightarrow \infty} \mathbf{G}_{ij} = \int_{\mathcal{M}} \psi_i^*(\mathbf{x})\psi_j(\mathbf{x})\rho(\mathbf{x})d\mathbf{x} = \langle \psi_i, \psi_j \rangle_{\rho}, \quad (3.27)$$

Assuming that  $\omega$  and  $x$  are independent, when  $M$  is sufficiently large, the law of large numbers applies, which is the same as the deterministic case. However, the definition of  $\mathbf{A}$  will be modified.

$$\begin{aligned} \lim_{M \rightarrow \infty} \mathbf{A}_{i,j} &= \mathbb{E}[\psi_i^*(\mathcal{K}\psi_j)] = \int_{\mathcal{M} \times \Omega_s} \psi_i^*(\mathbf{x})\psi_j(\mathbf{F}(\mathbf{x}, \omega))\rho(\mathbf{x})d\mathbf{x}dP(\omega) \\ &= \int_{\mathcal{M}} \psi_i^*(\mathbf{x})\mathbb{E}[\psi_j(\mathbf{F}(\mathbf{x}, \omega))]\rho(\mathbf{x})d\mathbf{x} = \langle \psi_i, \mathcal{K}\psi_j \rangle_{\rho}. \end{aligned} \quad (3.28)$$

The equation (3.20) can be used to calculate the "stochastic Koopman modes," but they must be viewed as the weights required to reconstruct the full-state observable's expected value using the eigenfunctions of the SKO. These modes are the ones that we genuinely compute when we apply EDMD to experimental data, which inherently contains some level of noise.

### 3.0.1.5 Dynamic Mode Decomposition (DMD)

Dynamic mode decomposition (DMD) is a widely used algorithm in the fluid dynamics community to estimate the Koopman operator from data. There are various equivalent definitions of DMD that differ mathematically, but we use the exact DMD described in [14], which can be applied to states and their images or updated positions after a fixed time interval  $\Delta t$ . DMD utilizes singular value decomposition (SVD), or proper orthogonal decomposition (POD) in fluid dynamics, to achieve efficient dimensionality reduction for high-dimensional data. The algorithm approximates a linear matrix operator that advances high-dimensional measurements of a system forward in time, and therefore approximates the Koopman operator for the measurement subspace based on the state of the system. DMD can be applied to both experimental and simulated data, as it only requires measurement data and not knowledge of the governing equations.

The objective of the DMD algorithm is to find a linear matrix operator  $\mathbf{K}_D$  that best approximates the advancement of a system's state,  $\mathbf{x} \in \mathbb{R}^d$ , in time according to a linear dynamical system

$$\mathbf{x}_{k+1} = \mathbf{K}_D \mathbf{x}_k, \quad (3.29)$$

where  $\mathbf{x}_k = \mathbf{x}(k\Delta t)$ . Thus, the matrix  $\mathbf{K}_D$  is an approximation of the Koopman operator  $\mathcal{K}$  restricted to a measurement subspace spanned by direct measurements of the state  $x$ .

The Exact DMD algorithm can handle irregularly spaced data and data from multiple time series that are concatenated together. Therefore, the times  $t_k$  associated with each snapshot  $x_k$  do not have to be in sequence or evenly spaced. For each snapshot  $x_k$ , there is a corresponding snapshot  $y_k$  that is one time step  $\Delta t$  in the future, denoted as  $y_k = \mathbf{F}(x_k) = x_{k+1}$  in a set of data pairs  $\{(x_1, y_1), \dots, (x_M, y_M)\}$ . Similar to the EDMD method, these snapshots are organized into two data matrices,  $\mathbf{X}$  and  $\mathbf{Y}$ .

$$\mathbf{X} = [x_1 \ x_2, \dots, x_M], \quad \mathbf{Y} = [y_1 \ y_2, \dots, y_M]. \quad (3.30)$$

The equation (3.29) can be expressed using the data matrices as:

$$\mathbf{Y} \approx \mathbf{K}_D \mathbf{X}. \quad (3.31)$$

To put it differently, equation (3.8) of the EDMD formulation illustrates how DMD and EDMD are related. If we define the observable vector as  $\Psi(\mathbf{x}) = \mathbf{x}$ , then we have:

$$\Psi_X = X \quad \text{and} \quad \Psi_Y = Y, \quad (3.32)$$

which leads to

$$\mathbf{K} = \Psi_Y \Psi_X^\dagger = Y X^\dagger = \mathbf{K}_D, \quad (3.33)$$

meaning that the DMD matrix  $\mathbf{K}_D$  provides an approximation of the Koopman operator  $\mathcal{K}$  using only linear basis functions. Therefore, it can be said that (exact) DMD is a particular instance of EDMD.

**Remark 3.0.1.** *If there is an exact solution to  $\mathbf{K}_D \mathbf{X} = \mathbf{Y}$  (which is always the case if the vectors  $\mathbf{x}_k$  are linearly independent), then the choice (3.30) minimizes the Frebenius norm*

$$\|\mathbf{K}_D\|_F = \sqrt{\text{Tr}(\mathbf{K}_D \mathbf{K}_D^*)}. \quad (3.34)$$

*If there is no  $\mathbf{K}_D$  that exactly satisfies  $\mathbf{K}_D \mathbf{X} = \mathbf{Y}$ , then the choice (3.30) minimizes the norm*

$$\|\mathbf{K}_D \mathbf{X} - \mathbf{Y}\|_F. \quad (3.35)$$

We will now demonstrate that the Koopman modes calculated using EDMD are scalar observables of the form

$$\psi_i(\mathbf{x}) = \mathbf{e}_i^* \mathbf{x} \quad \text{for } i = 1, \dots, d, \quad (3.36)$$

meaning that the set of observables only consists of linear functions. This is the particular (but somewhat restrictive) selection of the previously mentioned dictionary. Specifically, we demonstrate that the  $i$ th Koopman mode,  $\mathbf{v}_i$ , is also an eigenvector of  $\mathbf{K}_D$ , i.e.,

$$\mathbf{V} = (\Xi^{-1})^\top = (\mathbf{W}^*)^\top, \quad (3.37)$$

and therefore a DMD mode. As the dictionary elements are the components of the full-state observable,  $\mathbf{B} = \mathbf{I}$  in (3.20). Thus, the Koopman modes are the complex conjugates of the left eigenvectors of  $\mathbf{K}$ , which implies that  $\mathbf{v}_i^\top = \mathbf{w}_i^*$ . In addition,

$$\mathbf{G}^\top = \frac{1}{M} \mathbf{X} \mathbf{X}^* \quad \text{and} \quad \mathbf{A}^\top = \frac{1}{M} \mathbf{Y} \mathbf{X}^*. \quad (3.38)$$

Then,

$$\mathbf{K}^\top = \mathbf{A}^\top \mathbf{G}^{\top\dagger} = \mathbf{Y} \mathbf{X}^* (\mathbf{X} \mathbf{X}^*)^\dagger = \mathbf{Y} \mathbf{X}^\dagger = \mathbf{K}_D, \quad (3.39)$$

which means that the DMD algorithm approximates the Koopman operator using linear functions only. Therefore,

$$\mathbf{K}_D \mathbf{v}_i = (\mathbf{v}_i^\top \mathbf{K}_D^\top)^\top = (\mathbf{w}_i^* \mathbf{K})^\top = (\mu_i \mathbf{w}_i^*)^\top = \mu_i \mathbf{v}_i, \quad (3.40)$$

and all Koopman modes computed by EDMD are eigenvectors of  $K_D$  and are therefore the DMD modes. However, the choice of dictionary is crucial, and EDMD and DMD are equivalent only for the specific dataset  $\mathcal{D}$  where the dictionary is chosen to be a set of linear monomials. In other cases, EDMD may produce different and potentially more useful results. DMD can be considered a local approximation of the Koopman eigenfunctions using linear monomials as basis functions, while EDMD extends this approximation by including additional terms determined by the elements of the dataset  $\mathcal{D}$ . The accuracy of the resulting approximation depends on the quality of  $\mathcal{G}_{\mathcal{D}}$ , which in turn depends on the choice of  $\mathcal{D}$ .

**Remark 3.0.2.** Taking another look at the map described in equation (2.66a), where the behavior is nonlinear.

$$\begin{bmatrix} x_1 \\ x_2 \end{bmatrix} \mapsto \begin{bmatrix} \lambda x_1 \\ \mu x_2 + (\lambda^2 - \mu) x_1^2 \end{bmatrix}. \quad (3.41)$$

It has been demonstrated that the Koopman operator possesses eigenvalues  $\lambda$  and  $\mu$ , along with associated eigenfunctions expressed as:

$$\varphi_\lambda = x_1 \quad \text{and} \quad \varphi_\mu(x) = x_2 - x_1^2. \quad (3.42)$$

We will apply the DMD algorithm to data using the initial states  $\mathbf{x}$ , which are given by the coordinates  $(1, 1)$ ,  $(5, 5)$ ,  $(-1, 1)$ , and  $(-5, 5)$ , with  $\lambda = 0.9$ ,  $\mu = 0.5$ . The corresponding observable  $\mathbf{g}(\mathbf{x})$  will be the full state of  $\mathbf{x}$ , i.e.,  $\mathbf{g}(\mathbf{x}) = \mathbf{x}$ . These initial states are arranged as the columns of a matrix  $\mathbf{X}$ . After applying the map in equation (3.41), the columns of a matrix  $\mathbf{Y}$  are obtained, which correspond to the mapped versions of the initial vectors. It should be noted that  $\lambda = 0.9$  and  $\mu = 0.5$  are the eigenvalues associated with the Koopman operator. So,

$$\mathbf{X} = \begin{bmatrix} 1 & 5 & -1 & -5 \\ 1 & 5 & 1 & 5 \end{bmatrix}, \quad \mathbf{Y} = \begin{bmatrix} \lambda & 5\lambda & -\lambda & -5\lambda \\ \lambda^2 & -20\mu + 25\lambda^2 & \lambda^2 & -20\mu + 25\lambda^2 \end{bmatrix}. \quad (3.43)$$

It is apparent that the eigenfunction  $\varphi_\mu$  is not contained within the span of the observables. The corresponding matrix  $\mathbf{K}_D = \mathbf{Y} \mathbf{X}^\dagger$  has eigenvalues of  $\lambda = 0.9$  and  $2.002$ . The first eigenvalue is a true Koopman eigenvalue, denoted by  $\lambda$ . However, the second eigenvalue does not correspond

to a Koopman eigenvalue, as its magnitude is greater than one. It is possible that there exists an unstable equilibrium.

The eigenvector  $\mathbf{w}$  corresponding to the eigenvalue  $\mu = 0.5$  satisfies

$$\mathbf{w}^* \mathbf{K}_D = \mathbf{w}^* \mathbf{K}. \quad (3.44)$$

This, however, is not true for the eigenvector corresponding to the eigenvalue 2.002. If it happens that the map described by equation (3.41) is a linear map, i.e.,

$$\begin{bmatrix} x_1 \\ x_2 \end{bmatrix} \mapsto \begin{bmatrix} \lambda x_1 \\ \mu x_2 \end{bmatrix}. \quad (3.45)$$

then  $\mathbf{X}$  and  $\mathbf{Y}$  are linearly consistent, and the  $2 \times 2$  matrix  $\mathbf{K}_D = \mathbf{Y}\mathbf{X}^\dagger$  is simply the diagonal matrix with entries  $\lambda$  and  $\mu$

$$\mathbf{K}_D = \begin{bmatrix} \lambda & 0 \\ 0 & \mu \end{bmatrix}, \quad (3.46)$$

where,

$$\mathbf{X}^\dagger = \frac{1}{52} \begin{bmatrix} 1 & 1 \\ 5 & 5 \\ -1 & 1 \\ -5 & 5 \end{bmatrix}, \quad \text{and} \quad \mathbf{Y} = \begin{bmatrix} \lambda & 5\lambda & -\lambda & -5\lambda \\ \mu & 5\mu & \mu & 5\mu \end{bmatrix}. \quad (3.47)$$

These eigenvalues (DMD eigenvalues) agree with the Koopman eigenvalues, and the corresponding Koopman eigenfunctions

$$\varphi_\lambda(\mathbf{x}) = x_1 \quad \text{and} \quad \varphi_\mu(\mathbf{x}) = x_2 \quad (3.48)$$

agree as well.

If we use the observable

$$\mathbf{g}(\mathbf{x}) = (x_1, x_2, x_1^2) \quad (3.49)$$

instead, then the Koopman eigenfunctions will lie in the span of the observables. In this case, with the same initial states as before, the matrices  $\mathbf{X}$  and  $\mathbf{Y}$  are linearly consistent, and the DMD eigenvalues of the  $3 \times 3$  matrix  $\mathbf{K}_D = \mathbf{Y}\mathbf{X}^\dagger$  are  $\lambda, \mu$ , and  $\lambda^2 = 0.81$ . These DMD eigenvalues agree with the Koopman eigenvalues (2.69). However, it is important to note that linear consistency alone does not guarantee that the DMD eigenvalues correspond to Koopman eigenvalues. For example, if we use the observable

$$\mathbf{g}(\mathbf{x}) = (x_1, x_2, x_2^2) \quad (3.50)$$

instead, then  $\mathbf{X}$  and  $\mathbf{Y}$  will be linearly consistent. However, the DMD eigenvalues will be  $\lambda, 0.822$ , and  $4.767$ , and the latter two eigenvalues do not correspond to Koopman eigenvalues  $\lambda, \mu$ , and  $\mu^2$ .

### 3.0.2 Numerical Examples: EDMD with Monomial Basis Functions

**Example 3.0.3. 1D Ornstein-Uhlenbeck process: EDMD with Monomials.** We revisit the one-dimensional Ornstein-Uhlenbeck process, which was introduced in Examples 2.2.9 and 2.1.1. The process is described by an Itô stochastic differential equation of the following form:

$$dX_t = -\alpha\beta^{-1}X_t dt + \sqrt{2\beta^{-1}}dW_t. \quad (3.51)$$

Koopman eigenfunctions and eigenvalues associated with this process can be computed analytically, as previously mentioned in (2.56), where

$$\lambda_\ell = \exp(-\alpha\beta^{-1}(\ell-1)t), \quad \varphi_\ell(x) = \frac{1}{\sqrt{(\ell-1)!}}H_{\ell-1}(\sqrt{\alpha}x), \quad \ell = 1, 2, \dots, \quad (3.52)$$

with the recurrence relations for the probabilist's Hermite polynomials

$$H_{\ell+1}(x) = xH_\ell(x) - \ell H_{\ell-1}(x). \quad (3.53)$$

The first four eigenfunctions that are computed analytically are as follows:

$$\begin{bmatrix} \varphi_1(x) \\ \varphi_2(x) \\ \varphi_3(x) \\ \varphi_4(x) \end{bmatrix} = \begin{bmatrix} H_0(2x) \\ H_1(2x) \\ \frac{1}{\sqrt{2}}H_2(2x) \\ \frac{1}{\sqrt{6}}H_3(2x) \end{bmatrix} = \begin{bmatrix} 1.00 \\ 2x \\ \frac{1}{\sqrt{2}}(4x^2 - 1) \\ \frac{1}{\sqrt{6}}(8x^3 - 6x) \end{bmatrix} \quad (3.54)$$

associated to the analytically computed eigenvalues

$$\begin{bmatrix} \lambda_1(t) \\ \lambda_2(t) \\ \lambda_3(t) \\ \lambda_4(t) \end{bmatrix} = \begin{bmatrix} e^0 \\ e^{-1} \\ e^{-2} \\ e^{-3} \end{bmatrix} \approx \begin{bmatrix} 1.00 \\ 0.367 \\ 0.135 \\ 0.0498 \end{bmatrix}. \quad (3.55)$$

For the numerical experiment, we chose a basis consisting of monomials of order up to and including 10, and set the parameters  $\alpha$  and  $\beta$  to be 4. We sampled  $10^5$  points uniformly in the domain  $[-2, 2]$ , and integrated them for  $10^3$  time steps with an integration step size of  $h = 10^{-3}$  using the Euler-Maruyama method to solve (3.51). The lag time was set to  $t = 1$ . Using the EDMD method, we computed the first four dominant eigenfunctions of the Koopman operator  $\mathcal{K}^t$ , which are shown in Figure 3.1. The associated eigenvalues are provided by

$$\begin{bmatrix} \lambda_1(t) \\ \lambda_2(t) \\ \lambda_3(t) \\ \lambda_4(t) \end{bmatrix} \approx \begin{bmatrix} 1.00 \\ 0.369 \\ 0.128 \\ 0.047 \end{bmatrix} \quad (3.56)$$

which are a good approximation of the analytically computed eigenvalues (4.3). We used  $10^5$  test points as the standard EDMD would typically need more than  $10^4$  test points for such an accurate approximation of the dominant eigenfunctions, see [7] for details.

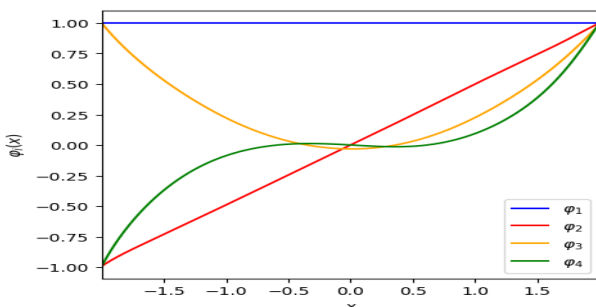


Figure 3.1: First four Koopman eigenfunctions of the Ornstein-Uhlenbeck process.

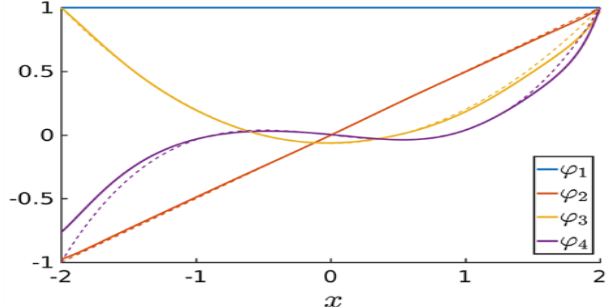


Figure 3.2: Eigenfunctions computed analytically (dotted lines). Adapted from [7]

**Example 3.0.4. 2D Double-Well Problem: EDMD with Monomials.** A two-dimensional particle living in a double-well potential landscape is subject to the stochastic differential equation

$$d\mathbf{X}_t = \nabla V(\mathbf{X}_t)dt + \sigma(t, \mathbf{X}_t)d\mathbf{W}_t \quad (3.57)$$

with  $\mathbf{W}_t$  being a Wiener process,  $\sigma = \sqrt{\frac{1}{2}} \approx 0.7$ , and the potential  $V$  shown in Figure (3.3) is given by

$$V(x_1, x_2) = (x_1^2 - 1)^2 + x_2^2 = V_1(x_1) + V(x_2), \quad \text{with} \quad \nabla V(x_1, x_2) = \begin{bmatrix} 4x_1^3 - 4x_1 \\ 2x_2 \end{bmatrix}. \quad (3.58)$$

The system exhibits metastable behavior, where the rare transitions are the jumps between the two wells. Numerically, this system can be solved using Euler-Maruyama method, which can be written as

$$x_{k+1} = x_k + \nabla V(x_k)h + \sigma(t_k, x_k)\Delta\mathbf{w}_k, \quad (3.59)$$

where  $h$  is the step size and  $\Delta\mathbf{w}_k = \mathbf{w}_{k+1} - \mathbf{w}_k \sim \mathcal{N}(0, h)$ . We will compute the leading eigenfunctions with EDMD using monomials of order up to and including 10, i.e.,

$$\mathcal{D} = \{1, x_1, x_2, x_1x_2, x_2^2, \dots, x_1^2x_2^8, x_1x_2^9, x_2^{10}\} \quad (3.60)$$

To approximate the Koopman operator, we first select  $10^5$  random points inside the domain and integrate them for  $10^4$  steps (one evaluation of the corresponding dynamical system  $\mathbf{F}$  corresponds to  $10^4$  steps, i.e., each initial condition is integrated from  $t_0 = 0$  to  $t_1 = 10$ ). That is,  $10^4$  integration steps between each evaluation under an integration step of  $h = 10^{-3}$  as we used the Euler-Maruyama method to solve (4.7), resulting in  $\Psi_X, \Psi_Y \in \mathbb{C}^{100000 \times 66}$ , where EDMD required 66 parameters to describe the eigenfunctions. EDMD exclusively selected smooth basis functions, which led to the resulting eigenfunction being smoothed automatically.

Inside the double-well potential landscape we integrate particles subject to the SDE (4.7), using Euler-Maruyama integrator and we simulate or generate (an example of) a trajectory by 20 evaluations (length of trajectory) from initial condition  $x_0 = (-1, 0)$  in the potential landscape.

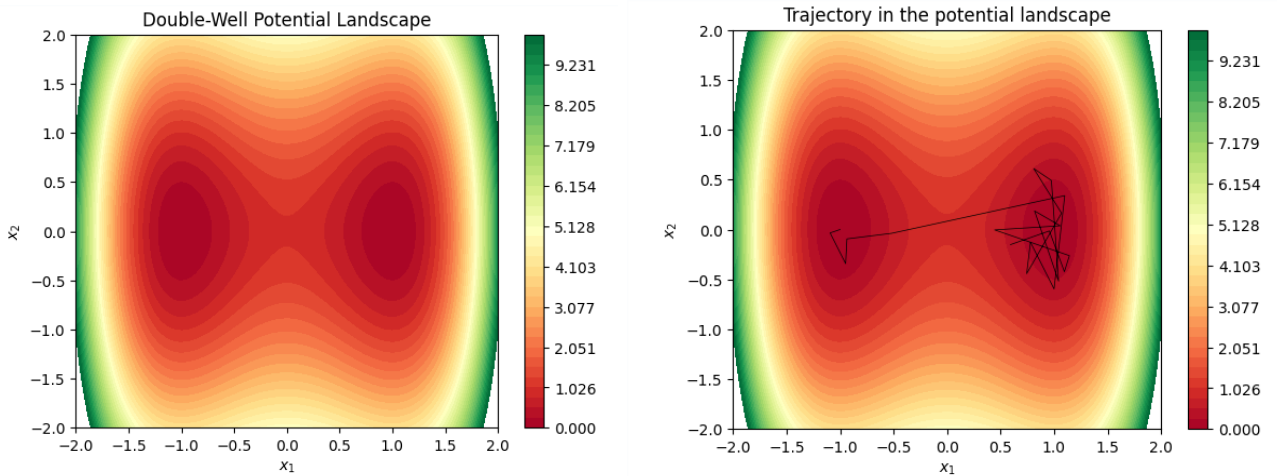


Figure 3.3: Double-well potential landscape  $V(x_1, x_2) = (x_1^2 - 1)^2 + x_2^2$  and an example of a generated trajectory from starting point  $x_0 = (-1, 0)$  in the potential landscape.

Figure (3.4) illustrates that the  $x_1$  variable tends to remain close to  $x_1 = -1$  or  $x_1 = 1$  for extended periods, and transitions between these two states are infrequent. The  $x_2$  variable, on the other hand, oscillates around the equilibrium point at  $x_2 = 0$ .

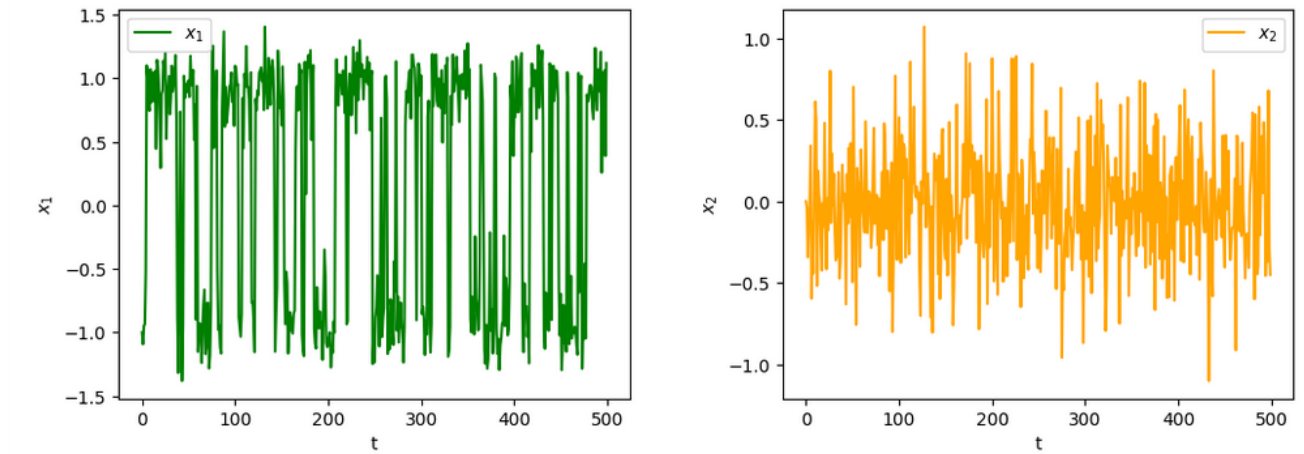


Figure 3.4: Numerical solution of the double-well SDE (4.7).

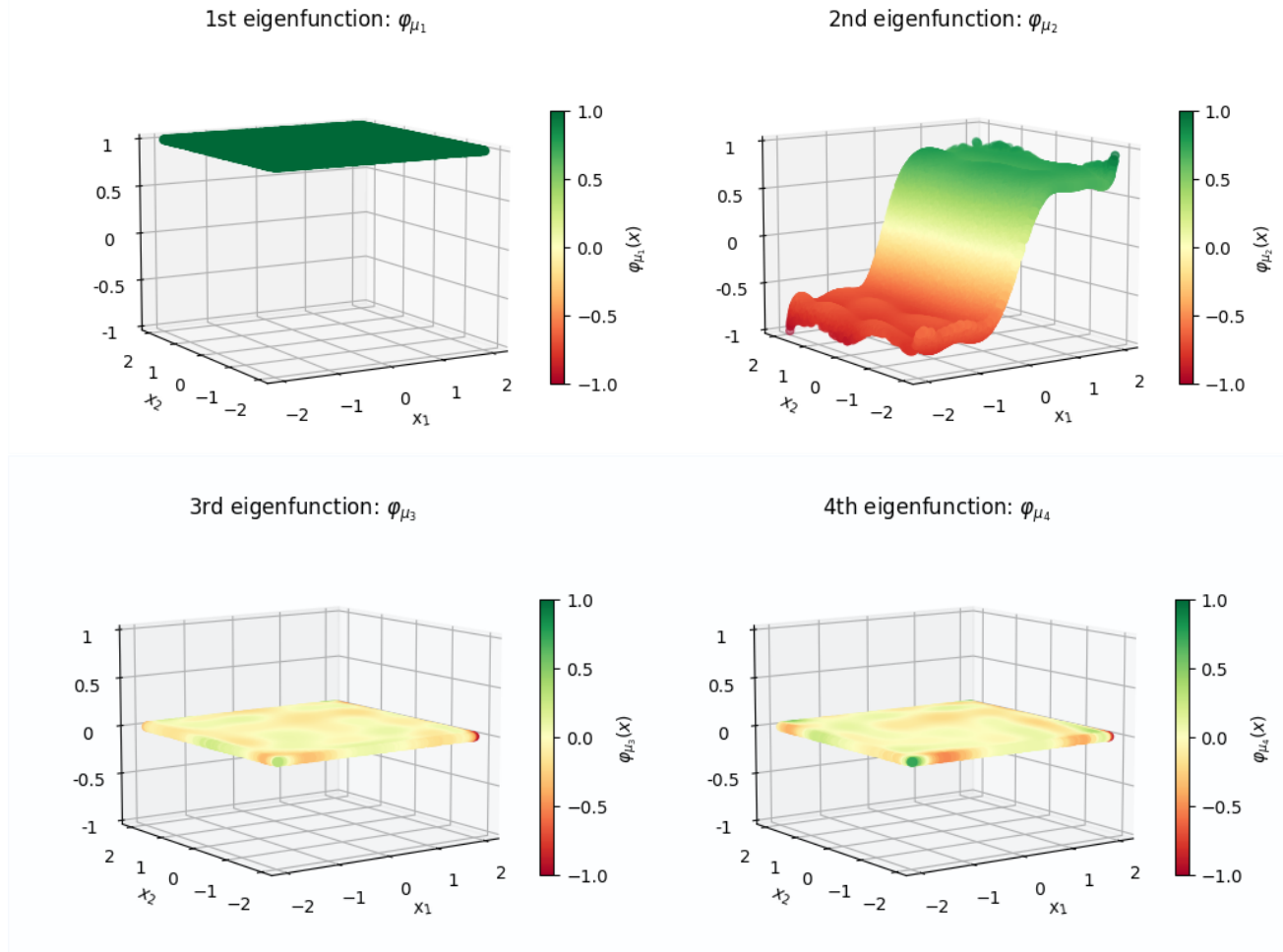


Figure 3.5: 3D plot of first four Koopman eigenfunctions. The first eigenfunction  $\varphi_{\mu_1}$  corresponds to an eigenvalue  $\mu_1 = 1.0$  of the Koopman operator, and is constant as expected. The system contains two metastable states, and the second eigenfunction  $\varphi_{\mu_2}$  associated with an eigenvalue  $\mu_2 \approx 0.75$  of the Koopman operator can be utilized to identify these states. This eigenfunction separates the two deep wells at  $(-1, 0)$  and  $(1, 0)$ , and provides information about a potential partitioning of the state space. It is almost constant in the  $x_2$ -direction, as well as in the  $x_1$ -direction, except for a sudden transition from  $-1$  to  $1$  between the two metastable sets. The remaining dominant eigenfunctions of the operator,  $\varphi_{\mu_3}$  and  $\varphi_{\mu_4}$ , associated with (numerically zero) eigenvalues  $\mu_3 = 0.016$  and  $\mu_4 = 0.0089$ , respectively, are almost zero (constants).

**Example 3.0.5. 2D Triple-Well Problem: EDMD with Monomials.** To illustrate the effectiveness of EDMD, we once again apply it to a stochastic differential equation (4.7):

$$d\mathbf{X}_t = \nabla V(\mathbf{X}_t)dt + \sigma(t, \mathbf{X}_t)d\mathbf{W}_t, \quad (3.61)$$

where  $\sigma = 1.09$ . We utilize the two-dimensional triple-well potential function, which is slightly more complex

$$V(x_1, x_2) = 3e^{-x_1^2 - (x_2 - \frac{1}{3})^2} - 3e^{-x_1^2 - (x_2 - \frac{5}{3})^2} - 5e^{-(x_1 - 1)^2 - x_2^2} - 5e^{-(x_1 + 1)^2 - x_2^2} + \frac{2}{10}x_1^4 + \frac{2}{10}\left(x_2 - \frac{1}{3}\right)^4. \quad (3.62)$$

The potential function cannot be expressed as  $V_1(x_1) + V_2(x_2)$  due to coupling between the variables  $x_1$  and  $x_2$ . The system has three metastable sets defined by the three wells, and the potential function is depicted in Figure (3.6).

To perform the EDMD, we choose a basis  $\mathcal{D}$  from Example 3.0.4 consisting of monomials of order up to and including 10. We randomly generate  $10^5$  test points within the domain  $[-2, 2] \times [-1, 2]$  and integrate each test point from  $t_0 = 0$  to  $t_1 = 0.1$  using a step size of  $h = 10^{-5}$ . This corresponds to integrating each test point for  $10^4$  steps under an integration step of  $h$ , resulting in a default lag time of  $h \times 10^4 = 0.1$ .

We obtain the first four dominant eigenfunctions of the Koopman operator, shown in Figure (3.8). The first eigenfunction  $\varphi_{\mu_1}$  is trivial with eigenvalue  $\mu_1 = 1.0$ . The remaining eigenfunctions can be utilized to identify the metastable regions.

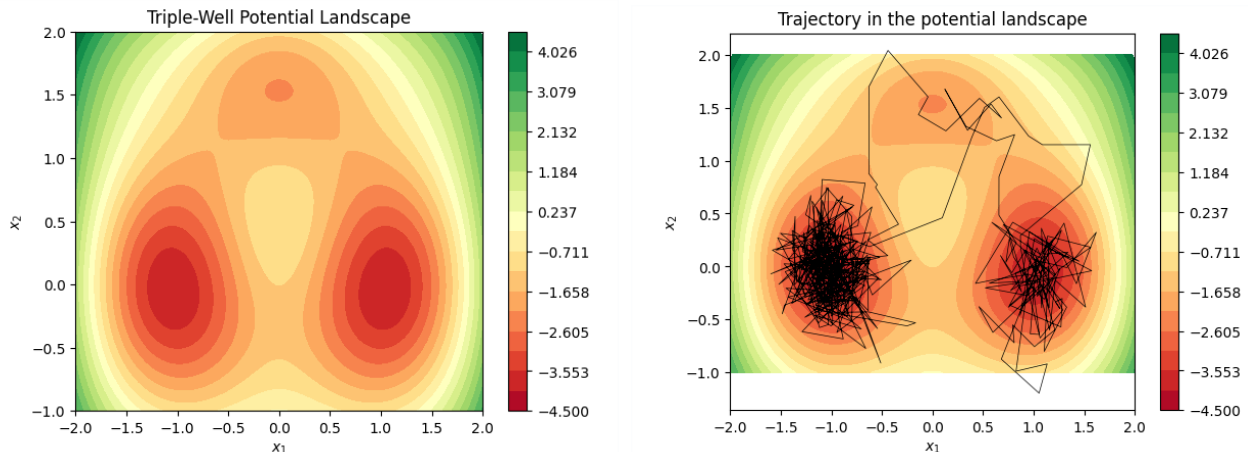


Figure 3.6: Triple-well potential landscape and an example of a generated trajectory from starting point  $(-1, 0)$ .

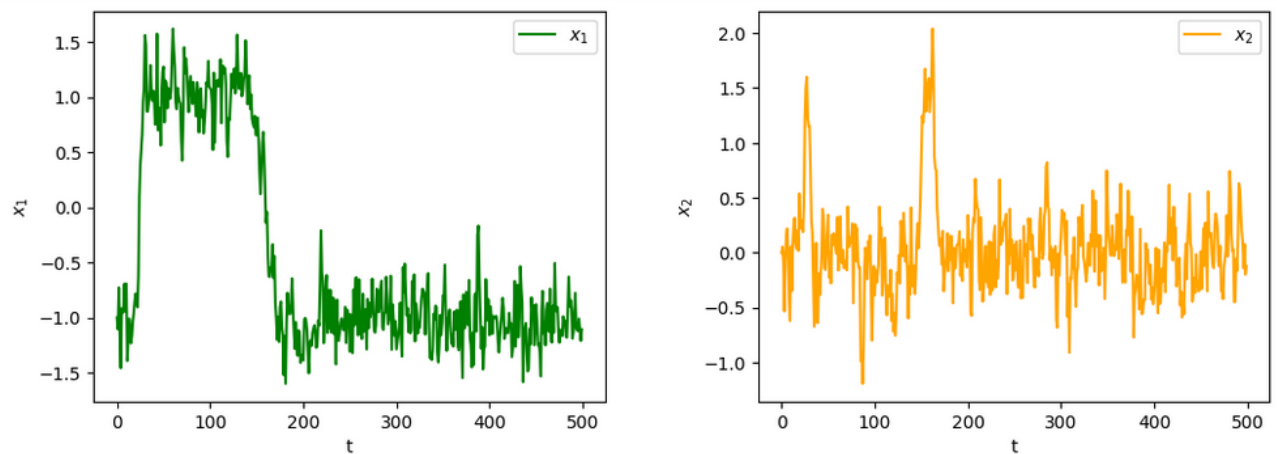


Figure 3.7: Numerical solution of the triple-well SDE (4.7).

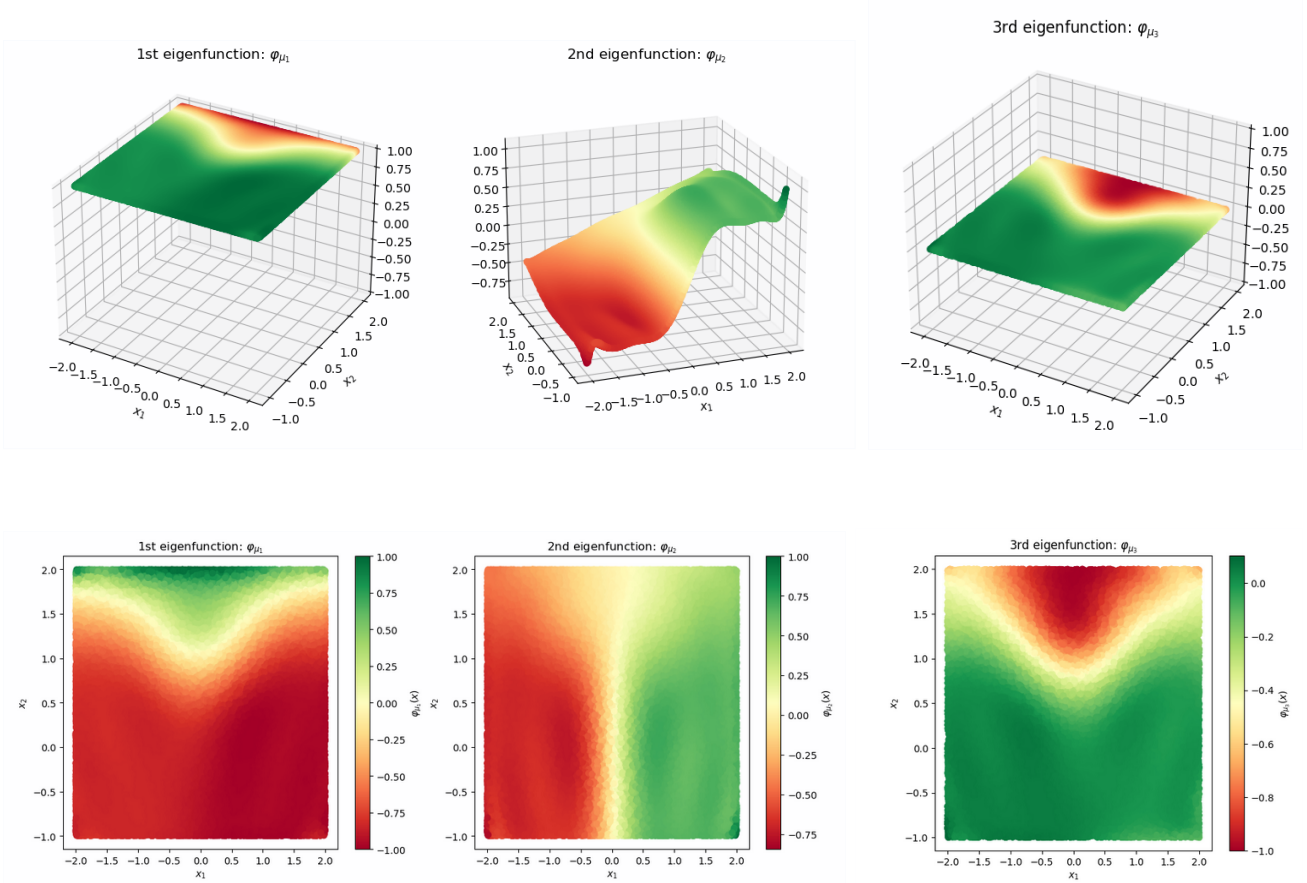


Figure 3.8: The first three dominant Koopman eigenfunctions are displayed in both 3D and 2D plots. The second eigenfunction  $\varphi_{\mu_2}$ , with eigenvalue  $\mu_2 = 0.99$ , distinguishes the two deep wells located at  $(-1, 0)$  and  $(1, 0)$ , while remaining close to zero for the well at  $(0, 1.5)$ . The third eigenfunction  $\varphi_{\mu_3}$ , with eigenvalue  $\mu_3 = 0.93$ , separates the two deep wells from the shallow well. In contrast, the fourth eigenfunction  $\varphi_{\mu_4}$ , with eigenvalue  $\mu_4 = 0.68$ , does not contribute to identifying the metastable regions, as these are already captured by the first nontrivial eigenfunctions.

**Example 3.0.6. 2D Quadruple-Well Problem: EDMD with Monomials** We consider the process  $X_t$  described by the overdamped Langevin equation, i.e., the stochastic differential equation

$$dX_t = -\nabla V(X_t)dt + \sqrt{2\beta^{-1}}dW_t \quad (3.63)$$

with the quadruple-well potential  $V$  on the domain  $\mathcal{M} = [-2, 2] \times [-2, 2]$  illustrated in Figure 3.9

$$V(x_1, x_2) = (x_1 - 1)^2 + (x_2 - 1)^2 \quad (3.64)$$

and the inverse temperature  $\beta = 4$ . We generate a long trajectory in order to observe the behavior of the system. It is common for a particle to remain in a single well for an extended period before moving to another well. As a result, there are four stable states that correspond to the four wells.

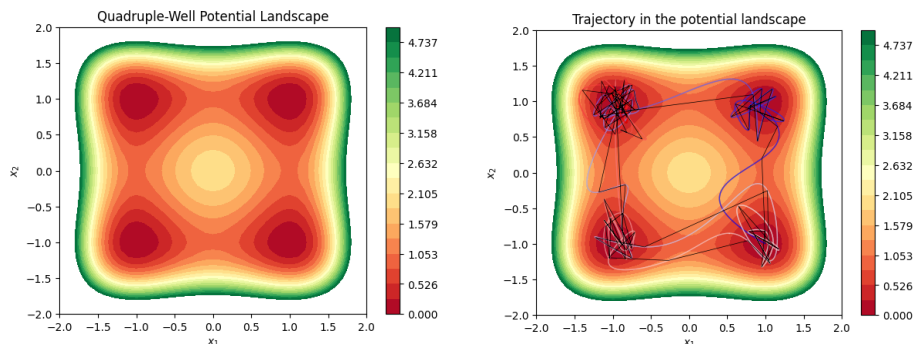


Figure 3.9: Quadruple-well potential landscape and an example of a simulated trajectory from initial condition  $(1, -1)$

The SDE is solved using the Euler-Maruyama method, where the step size is set to  $h = 10^{-3}$ . In order to approximate the Koopman operator, we employ the EDMD with 66 monomials, each up to and including 10th order. The training data is uniformly sampled from the domain  $\mathcal{M}$  and propagated forward by the dynamical system. Specifically, we select  $10^5$  training data points and integrate them for  $10^4$  steps. As a result, the lag time is  $t = \text{steps} \times h = 10$ . It is expected that there will be four eigenvalues close to one, which correspond to the dominant eigenvalues of the slow dynamics. As illustrated in Figures 4.13 and 4.14, the position of the stable states in  $\mathcal{M}$  can be determined by examining the sign structure of the dominant eigenfunctions. The ultimate objective is to create a Markov State Model (MSM), where the primary stable states serve as the states of a Markov chain. In this case, the model would consist of a  $4 \times 4$  transition rate matrix. This model is significantly simpler compared to the original two-dimensional SDE, but it still preserves the statistical properties of the long-term stable transitions.

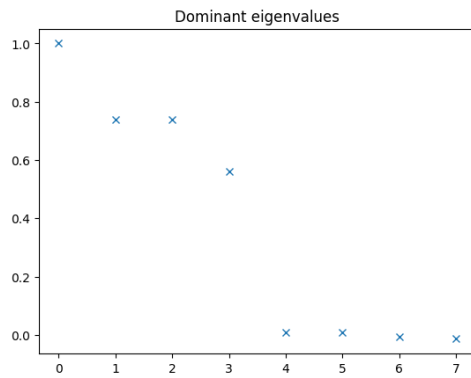


Figure 3.10: First eight dominant Koopman eigenvalues. A spectral gap after  $\mu_4$  indicates that the dominant four eigenfunctions are relevant to metastability analysis.  $\mu_1 = 1.0$ ,  $\mu_2 \approx 0.749$ ,  $\mu_3 \approx 0.738$  and  $\mu_4 \approx 0.568$

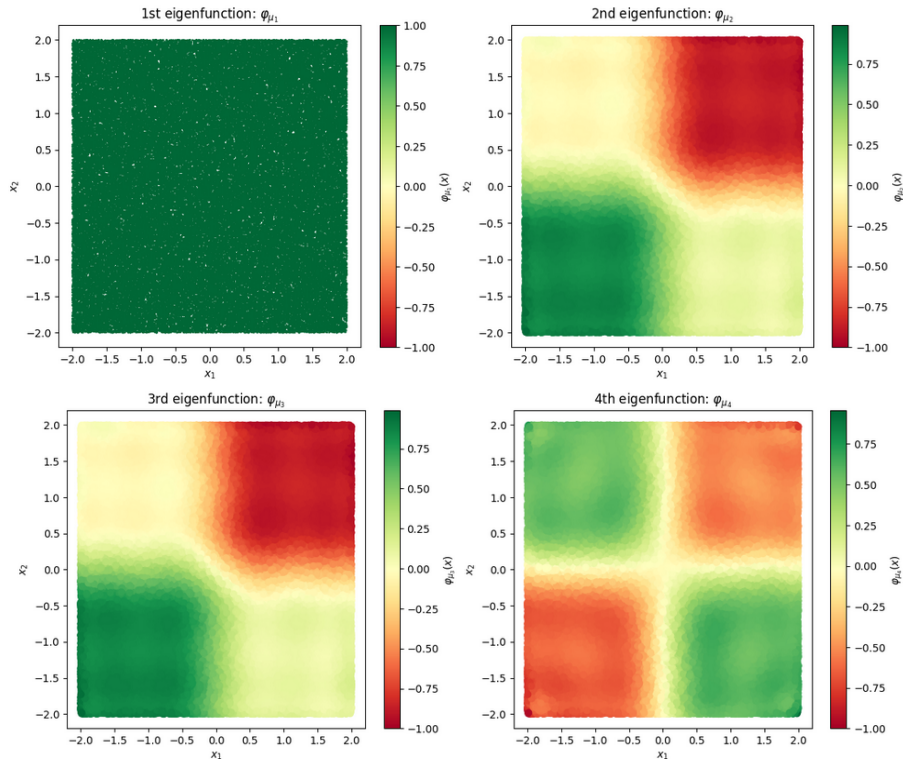


Figure 3.11: First four dominant Koopman eigenfunctions. It can be observed that the eigenfunctions are nearly constant in each of the four quadrants. This suggests that each quadrant is stable, meaning that trajectories that begin in a particular quadrant usually remain in that quadrant for an extended period of time.



# Numerical Results

This chapter showcases the numerical outcomes achieved for one and two-dimensional (linear and non-linear) problems, which were previously addressed in section 3.0.2. The primary objective is to estimate Koopman eigenfunctions using Extended Dynamical Mode Decomposition (EDMD), in conjunction with random Gaussian functions and randomly initialized neural networks (untrained) serving as the basis functions. Additionally, the chapter will present a numerical outcome obtained by training the neural network and merging it with EDMD to approximate the Koopman operator.

## Contents

---

<b>4.1 Random Dynamic Mode Decomposition (RDMD)</b> . . . . .	48
4.1.1 EDMD with Random Gaussian Functions . . . . .	48
4.1.2 EDMD with Randomized Neural Networks . . . . .	54

---

## 4.1 Random Dynamic Mode Decomposition (RDMD)

This section focuses on merging EDMD with random basis functions for one- and two-dimensional (linear and non-linear) systems, as previously mentioned in section 3.0.2. The aim is to employ random Gaussian functions and untrained randomized neural networks as basis functions to approximate the dominant Koopman eigenvalues and eigenfunctions (which are close to 1), allowing for the detection of metastable regions that indicate system stability and provide insights into the long-term behavior of the dynamic system.

### 4.1.1 EDMD with Random Gaussian Functions

Let  $\{x_1, \dots, x_M\} \sim \mathcal{U}(\mathcal{M})$  be uniformly randomly distributed points from  $\mathcal{M}$ . Let  $\rho > 0$  be a kernel bandwidth parameter. Consider the basis  $\Psi := \{\psi_1, \dots, \psi_M\}$ , where

$$\psi_i(x) = \exp\left(-\frac{\|x_i - x\|^2}{\rho^2}\right). \quad (4.1)$$

denote the random Gaussian functions with random chosen centers  $x_i$ .

**Example 4.1.1. 1D Ornstein-Uhlenbeck process: EDMD with Gaussians** Once again, we revisit the one-dimensional Ornstein-Uhlenbeck process from 3.0.3. The process is described by an Itô stochastic differential equation of the following form:

$$dX_t = -\alpha\beta^{-1}X_t dt + \sqrt{2\beta^{-1}}dW_t, \quad (4.2)$$

where  $\alpha = \beta = 4$  and  $V(x) = -\frac{\alpha}{2\beta}x^2$ . The Koopman eigenfunctions and eigenvalues associated with this process can be computed analytically, as previously mentioned in Example 3.0.3, where the first four eigenvalues that are computed analytically are as follows:

$$\begin{bmatrix} \lambda_1(t) \\ \lambda_2(t) \\ \lambda_3(t) \\ \lambda_4(t) \end{bmatrix} = \begin{bmatrix} e^0 \\ e^{-1} \\ e^{-2} \\ e^{-3} \end{bmatrix} \approx \begin{bmatrix} 1.00 \\ 0.367 \\ 0.135 \\ 0.0498 \end{bmatrix}. \quad (4.3)$$

For the numerical experiment, we chose random gaussians as a basis functions. We sampled  $25 \times 10^4$  points uniformly in the domain  $[-2, 2]$ , and integrated them for  $10^3$  time steps with an integration step size of  $h = 10^{-3}$  using the Euler-Maruyama method to solve the Ornstein-Uhlenbeck process given in (4.2). The lag time was set to  $t = 1$ . Using the EDMD method, we computed the first four dominant eigenfunctions of the Koopman operator  $\mathcal{K}^t$ , which are shown in Figures 4.1 and 4.2. The respective associated eigenvalues are provided by

$$\begin{bmatrix} \lambda_1(t) \\ \lambda_2(t) \\ \lambda_3(t) \\ \lambda_4(t) \end{bmatrix} \approx \begin{bmatrix} 1.00 \\ 0.365 \\ 0.135 \\ 0.0499 \end{bmatrix} \quad \text{and} \quad \begin{bmatrix} \lambda_1(t) \\ \lambda_2(t) \\ \lambda_3(t) \\ \lambda_4(t) \end{bmatrix} \approx \begin{bmatrix} 1.00 \\ 0.369 \\ 0.131 \\ 0.0489 \end{bmatrix} \quad (4.4)$$

which are a very good approximation of the analytically computed eigenvalues (4.3).

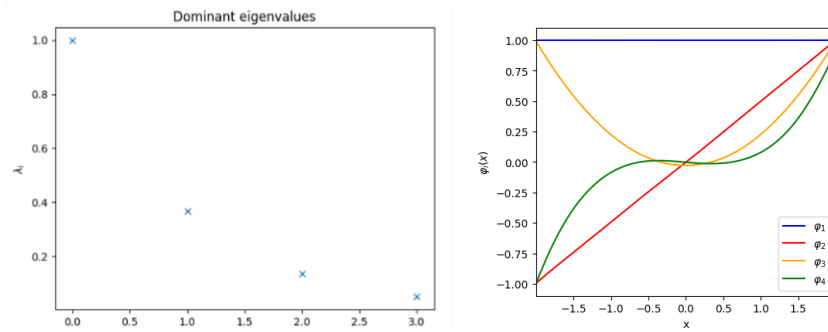


Figure 4.1: Dominant Koopman eigenvalues and eigenfunctions. Using  $M = 65$  random gaussians with  $\rho = 1.7$ .

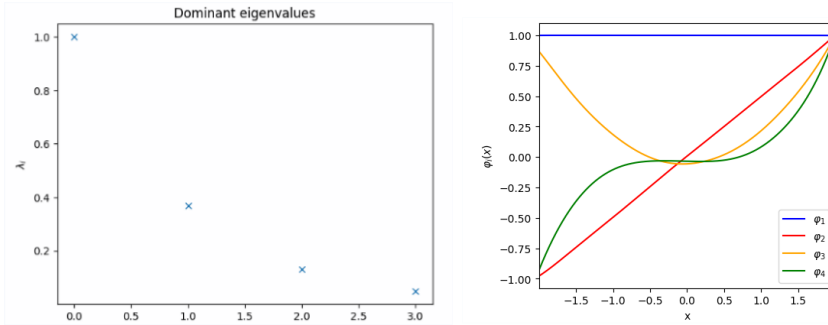


Figure 4.2: Dominant Koopman eigenvalues and eigenfunctions. Using  $M = 70$  random gaussians with  $\rho = 1.5$ .

**Example 4.1.2. 1D Triple-Well Problem: EDMD with Gaussians.** Consider the one-dimensional Stochastic Differential Equation (SDE)

$$d\mathbf{X}_t = \nabla V(\mathbf{X}_t)dt + \sigma(t, \mathbf{X}_t)d\mathbf{W}_t \quad (4.5)$$

with  $\mathbf{W}_t$  being a Wiener process,  $\sigma = \frac{3}{4}$  and the potential  $V$  shown in Figure (4.3) is given by

$$V(x) = 5 - 24.82x + 41.4251x^2 - 27.5344x^3 + 8.53128x^4 - 1.24006x^5 + 0.0684x^6. \quad (4.6)$$

The system can be interpreted as a particle in an energy landscape. The particle will typically stay for a long time in one of the wells, where the rare transitions are the jumps with a low probability between the three-wells shown in the Figure 4.3 for the triple-well potential  $V$ . To approximate the Koopman operator we generate a long trajectory that starts from  $x_0 = 0.5$  within the domain  $[0, 6]$  and we integrate each test point for  $10^4$  steps between each evaluation under an integration step of  $h = 10^{-3}$  for Euler Maruyama method, i.e., the lag time is  $t = 10$ . The system has three-metastable sets corresponding to the wells. The dominant eigenfunctions and their corresponding eigenvalues of the Koopman operator are shown in Figure 4.4.

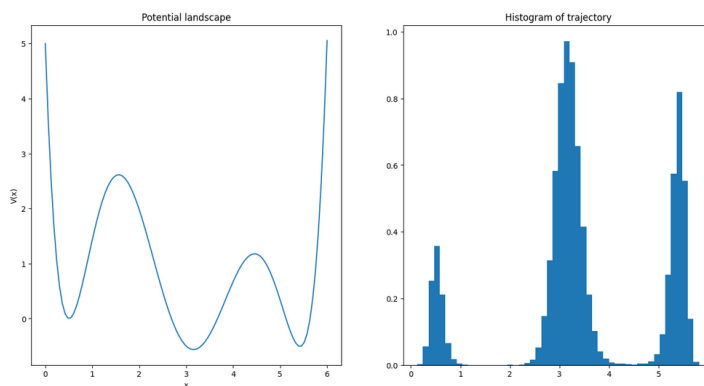


Figure 4.3: 1D Triple-well potential landscape and histogram of trajectory in the landscape (4.5).

To perform EDMD, we examine different cases where the results are as follows:

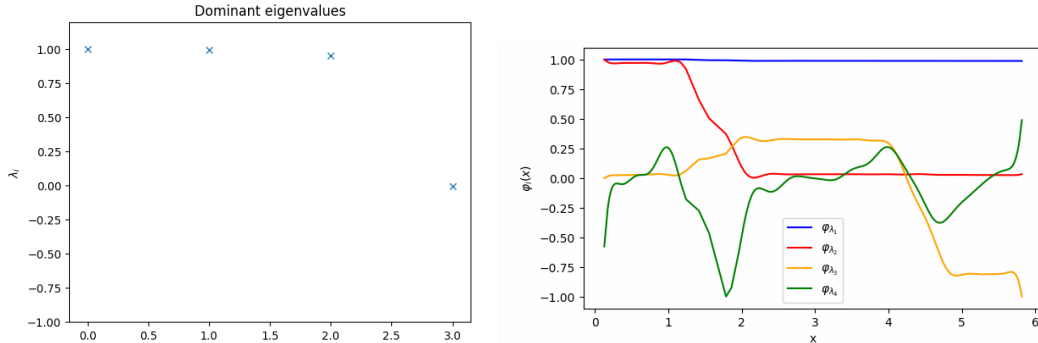


Figure 4.4: Dominant Koopman eigenvalues and eigenfunctions:  $M = 100$  gaussians,  $\rho = 0.5$  and a generated long trajectory of length  $25 \times 10^4$ . The primary and fourth Koopman eigenfunctions  $\varphi_1$  and  $\varphi_4$  with respective eigenvalues  $\lambda_1 = 1.0$  and  $\lambda_4 = -0.002$  do not provide any valuable information for identifying the metastable sets. The second eigenfunction  $\varphi_2$ , associated with eigenvalue  $\lambda_2 = 0.997$ , is almost uniform within the left well as well as within the two other wells, with a smooth transition in between, thereby identifying the maximum energy barrier. The third eigenfunction  $\varphi_3$  with eigenvalue  $\lambda_3 = 0.953$  distinguishes (separates) the middle well and the right well. A spectral gap after  $\lambda_3$  indicates that the dominant three eigenfunctions are relevant to metastability analysis.

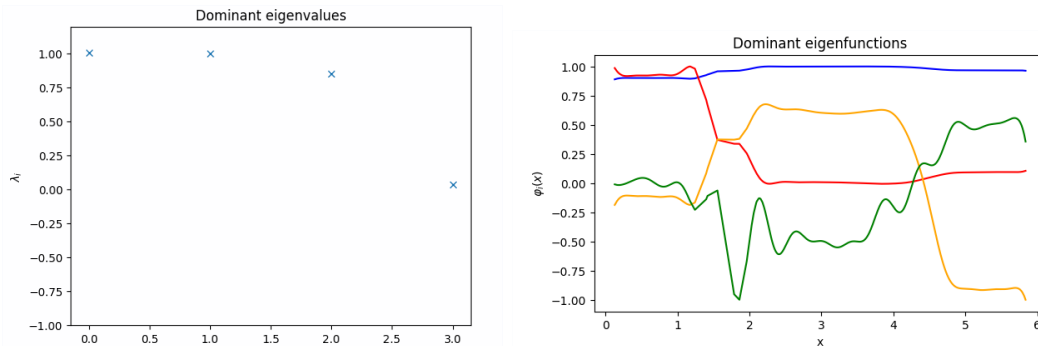


Figure 4.5:  $M = 65, \rho = 0.5$  and a long trajectory of length  $25 \times 10^4$ .  $\lambda_1 = 1.0, \lambda_2 = 0.992, \lambda_3 = 0.915$  and  $\lambda_4 = 0.041$ .

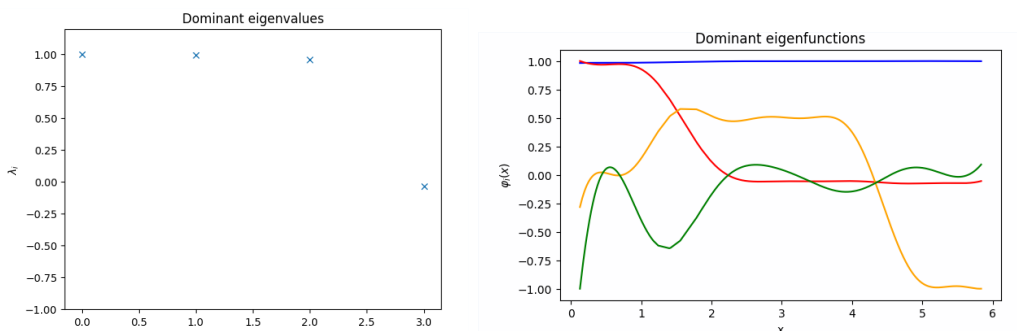


Figure 4.6:  $M = 65, \rho = 1.5$  and a long trajectory of length  $25 \times 10^4$ .  $\lambda_1 = 1.0, \lambda_2 = 0.997, \lambda_3 = 0.957$  and  $\lambda_4 = -0.0347$ .

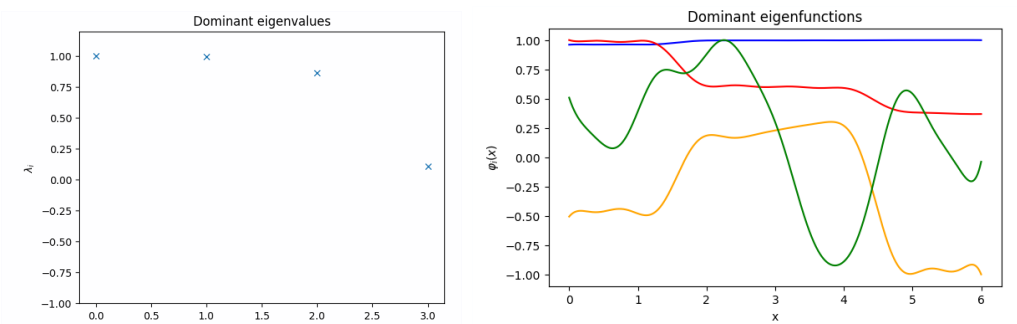


Figure 4.7: For randomly generated  $N = 5 \times 10^4$  points in the domain, with  $M = 90$  and  $\rho = 1.05$ . We obtain,  $\lambda_1 = 1.00, \lambda_2 = 0.99, \lambda_3 = 0.86$ , and  $\lambda_4 = 0.11$ .

**Example 4.1.3. 2D Double-Well Problem: EDMD with Gaussians.** We consider again, the stochastic differential equation from Example 3.0.4

$$d\mathbf{X}_t = \nabla V(\mathbf{X}_t)dt + \sigma(t, \mathbf{X}_t)d\mathbf{W}_t \quad (4.7)$$

with  $\mathbf{W}_t$  being a Wiener process,  $\sigma = \sqrt{\frac{1}{2}} \approx 0.7$ , and the potential  $V$  given by

$$V(x_1, x_2) = (x_1^2 - 1)^2 + x_2^2 = V_1(x_1) + V(x_2), \quad \text{with} \quad \nabla V(x_1, x_2) = \begin{bmatrix} 4x_1^3 - 4x_1 \\ 2x_2 \end{bmatrix}. \quad (4.8)$$

To perform the EDMD, we choose random gaussians as a basis functions with  $\rho = 1.05$  and  $M = 56$ . We randomly generate  $10^5$  test points within the domain  $[-2, 2] \times [-2, 2]$  and integrate each test point from  $t_0 = 0$  to  $t_1 = 10$  using a step size of  $h = 10^{-3}$ . This corresponds to integrating each test point for  $10^4$  steps under an integration step of  $h$ , resulting in a default lag time of  $h \times 10^4 = 10$ .

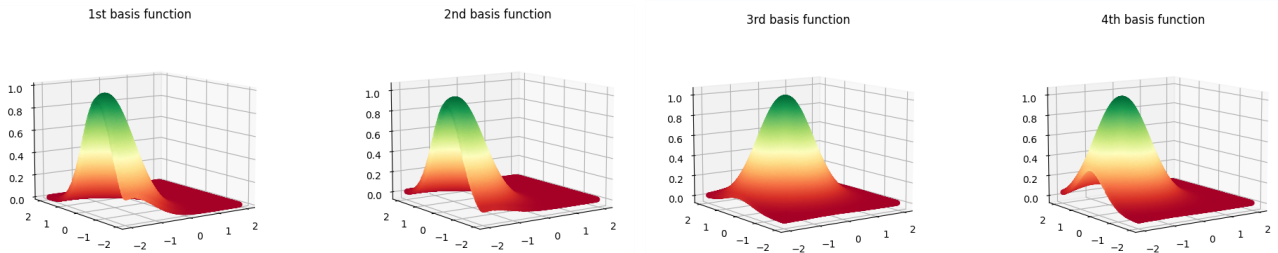


Figure 4.8: First four gaussian basis functions

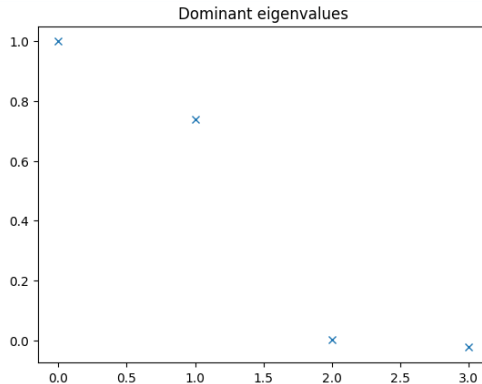


Figure 4.9: Dominant Koopman eigenvalues:  $\mu_1 \approx 1.0$ ,  $\mu_2 \approx 0.747$ ,  $\mu_3 \approx 0.0205$  and  $\mu_4 \approx -0.0184$ . A spectral gap after  $\mu_2$  indicates that the dominant two eigenfunctions are relevant to metastability analysis.

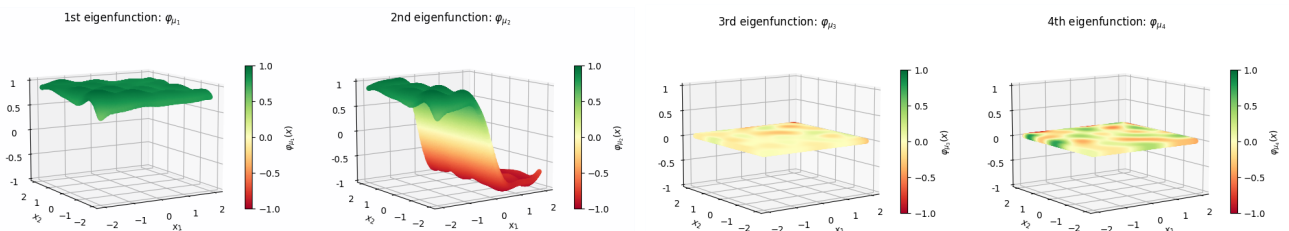


Figure 4.10: 3D plot of first four Koopman eigenfunctions using random Gaussians with  $\rho = 1.05$  and  $M = 56$ . The second eigenfunction  $\varphi_{\mu_2}$  associated with an eigenvalue  $\mu_2 \approx 0.747$  of the Koopman operator can be utilized to identify the two metastable sets of the system. This eigenfunction separates the two deep wells at  $(-1, 0)$  and  $(1, 0)$ , and provides information about a potential partitioning of the state space. It is almost constant in the  $x_2$ -direction, as well as in the  $x_1$ -direction, except for a sudden transition from  $-1$  to  $1$  between the two metastable sets. The remaining eigenfunctions do not give any information to detecting the metastable regions. The first eigenfunction  $\varphi_{\mu_1}$  corresponds  $\mu_1 \approx 1$  of the Koopman operator, is constant. The remaining dominant eigenfunctions of the operator,  $\varphi_{\mu_3}$  and  $\varphi_{\mu_4}$ , associated with eigenvalues  $\mu_3 = 0.0205$  and  $\mu_4 = -0.0184$  (numerically zero), respectively, are almost zero (constants). Only the second eigenfunction provide an information to detecting the metastable sets.

**Example 4.1.4. 2D Triple-Well Problem: EDMD with Gaussians.** We revisit again Example 3.0.5, and we apply EDMD to a stochastic differential equation:

$$d\mathbf{X}_t = \nabla V(\mathbf{X}_t)dt + \sigma(t, \mathbf{X}_t)d\mathbf{W}_t, \quad (4.9)$$

where  $\sigma = 1.09$ . We use the two-dimensional triple-well potential function,

$$V(x_1, x_2) = 3e^{-x_1^2 - (x_2 - \frac{1}{3})^2} - 3e^{-x_1^2 - (x_2 - \frac{5}{3})^2} - 5e^{-(x_1 - 1)^2 - x_2^2} - 5e^{-(x_1 + 1)^2 - x_2^2} + \frac{2}{10}x^4 + \frac{2}{10}\left(x_2 - \frac{1}{3}\right)^4. \quad (4.10)$$

To perform the EDMD, we choose random gaussians as a basis functions with  $\rho = 1.05$  and  $M = 56$ . We randomly generate  $10^5$  test points within the domain  $[-2, 2] \times [-1, 2]$  and integrate each test point for  $10^4$  steps under an integration step of  $h = 10^{-5}$ , resulting in a default lag time of  $h \times 10^4 = 0.1$ .

We obtain the first dominant eigenvalues and eigenfunctions of the Koopman operator, shown in Figures (4.11) and (4.12). The first eigenfunction  $\varphi_{\mu_1}$  is trivial with eigenvalue  $\mu_1 = 1.0$ . The 1st non-trivial eigenfunctions can be utilized to identify the metastable regions.

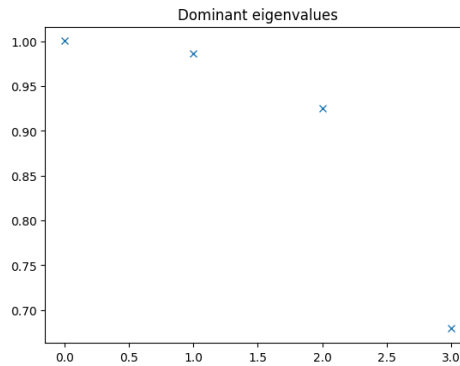


Figure 4.11: Dominant Koopman eigenvalues:  $\mu_1 \approx 1.0, \mu_2 \approx 0.986, \mu_3 \approx 0.925$  and  $\mu_4 \approx 0.679$

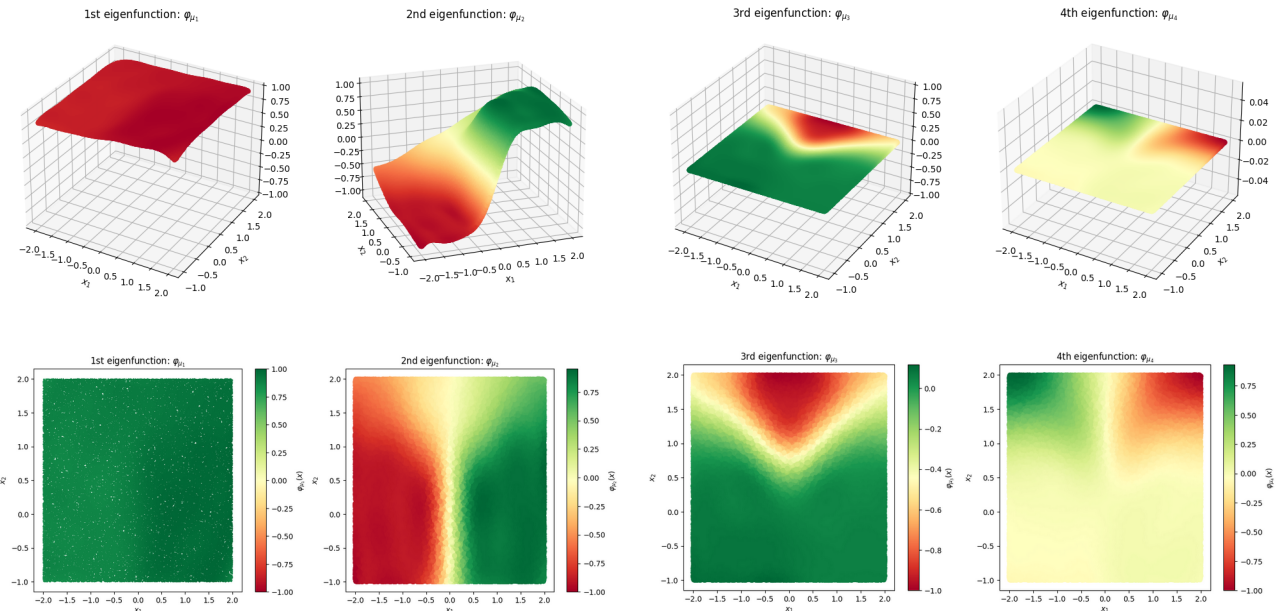


Figure 4.12: The dominant Koopman eigenfunctions are visualized in both 3D and 2D plots. The second eigenfunction  $\varphi_{\mu_2}$ , with eigenvalue  $\mu_2 = 0.986$ , separates the two deep wells located at  $(-1, 0)$  and  $(1, 0)$ , and is near zero for the well at  $(0, 1.5)$ . The third eigenfunction  $\varphi_{\mu_3}$ , with eigenvalue  $\mu_3 = 0.925$ , separates the two deep wells from the shallow well. In contrast, the first and fourth eigenfunctions  $\varphi_{\mu_1}$  and  $\varphi_{\mu_4}$ , with respective eigenvalues  $\mu_1 = 1.00$  and  $\mu_4 = 0.679$ , do not contribute to identifying the metastable sets.

**Example 4.1.5. Quadruple-Well Problem: EDMD with Gaussians.** We consider again the process  $X_t$  described by the overdamped Langevin equation, i.e., the SDE from Example 3.0.6

$$dX_t = -\nabla V(X_t)dt + \sqrt{2\beta^{-1}}dW_t \quad (4.11)$$

with the quadruple-well potential  $V$  on the domain  $\mathcal{M} = [-2, 2] \times [-2, 2]$  illustrated in Figure 3.9

$$V(x_1, x_2) = (x_1 - 1)^2 + (x_2 - 1)^2 \quad (4.12)$$

and the inverse temperature  $\beta = 4$ .

We use the Euler-Maruyama method with a step size of  $h = 10^{-3}$  to solve the SDE. In order to approximate the Koopman operator, we utilize the EDMD with  $M = 58$  Gaussian functions. The training data is uniformly sampled from the domain  $\mathcal{M}$  and propagated forward by the dynamical system. Specifically, we select  $5 \times 10^5$  training data points and integrate them for  $10^4$  steps, resulting in a lag time of  $t = \text{steps} \times h = 10$ . It is expected that there will be four eigenvalues close to one, which correspond to the dominant eigenvalues of the slow dynamics. This result would be better compared to the one in Example 3.0.6 where we used the monomials.

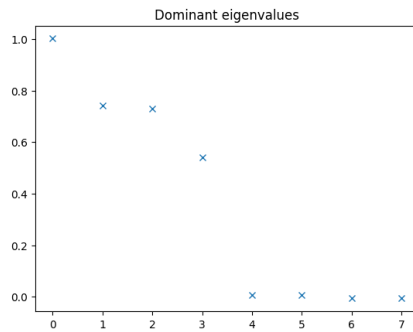


Figure 4.13: First eight dominant Koopman eigenvalues. A spectral gap after  $\mu_4$  indicates that the dominant four eigenfunctions are relevant to metastability analysis.  $\mu_1 = 1.0$ ,  $\mu_2 \approx 0.743$ ,  $\mu_3 \approx 0.730$  and  $\mu_4 \approx 0.540$

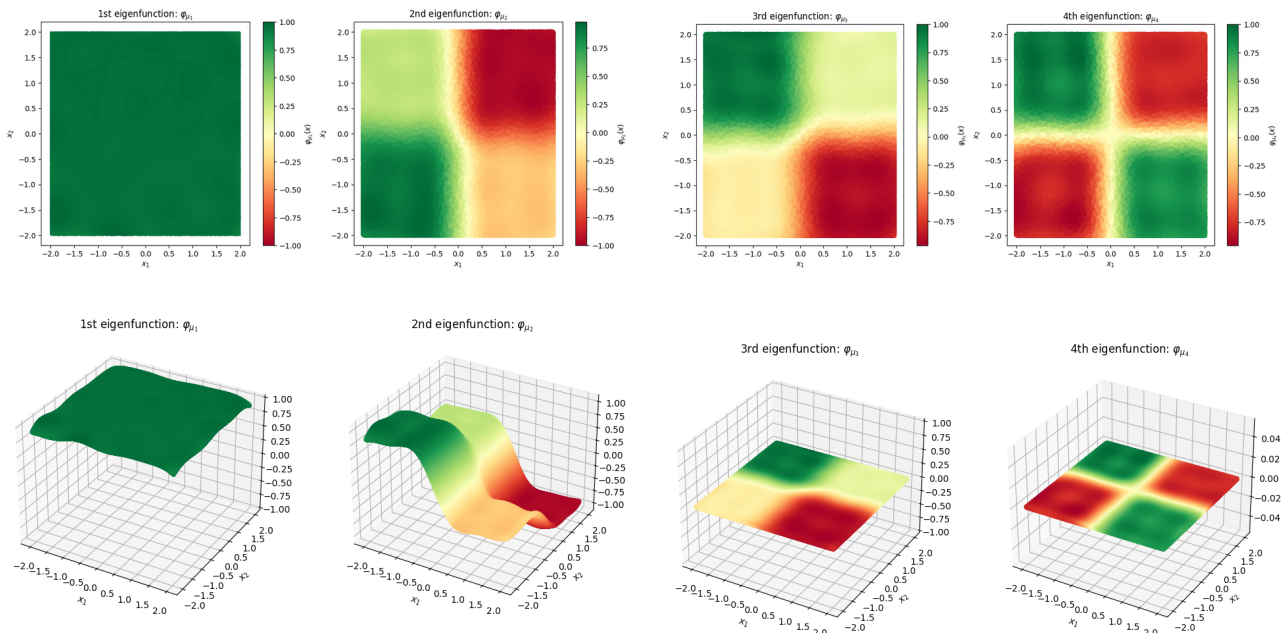


Figure 4.14: The dominant Koopman eigenfunctions are visualized in both 2D and 3D plots. We observe that the eigenfunctions are almost constant in the four quadrants. This indicates that each of the quadrants is metastable, i.e., trajectories that start in each quadrant typically stay in it for a long time.

### 4.1.2 EDMD with Randomized Neural Networks

We aim to utilize untrained Randomly Initialized Neural Networks (RINNs) as the basis functions to approximate the Koopman eigenfunctions through EDMD technique. Suppose  $\eta : \mathbb{R} \rightarrow \mathbb{R}$  represents an activation function such as the Sigmoid or Rectified Linear Unit (ReLU) function. Consider a fully-connected multi-layer neural network consisting of an input layer, hidden layers, and an output layer, which returns a single point in one dimension. For instance, a two-layer neural network with one hidden layer can be expressed as:

$$\psi_i(x) = \eta \left( \sum_{j=1}^{M_1} w_i^2(j) \eta \left( \sum_{k=1}^d w_i^1(j, k) x_k + b_i^1(j) \right) + b_i^2(1) \right). \quad (4.13)$$

$\psi_i$  is fully characterised by the hyperparameter  $h_i = (w_i^1, w_i^2, b_i^1, b_i^2)$ , where  $M_1$  is the number of neurons in the hidden layer,

$$w_i^1 \in \mathbb{R}^{M_1 \times d}, \quad w_i^2 \in \mathbb{R}^{M_1}, \quad b_i^1 \in \mathbb{R}^{M_1}, \quad b_i^2 \in \mathbb{R}, \quad i = 1, \dots, M_1. \quad (4.14)$$

We randomly select  $M$  hyperparameters  $h_1, \dots, h_M$  from a uniform distribution (or another specified distribution), to define the corresponding basis set  $\Psi := \{\psi_1, \dots, \psi_M\}$ . For instance, if the system dimension  $d = 2$  and  $M_1 = 4$ , then the neural network would consist of 2 neurons in the input layer, 4 neurons in the hidden layer, and 1 neuron in the output layer. Therefore, each neuron in the hidden layer has 2 weights for its connection to the input layer, resulting in a total of 8 weights. Additionally, each neuron in the hidden layer has 1 weight for its connection to the output layer and 1 bias term for every 4 weights in the hidden layer (4 biases), while the neuron in the output layer has 1 bias term.

To conduct the numerical experiment, we will focus on the two-dimensional triple- and double-well potential problems mentioned earlier in Examples 3.0.4 and 3.0.5. Given that the is untrained, we do not anticipate obtaining favorable results.

**Example 4.1.6. 2D Double-Well Problem: EDMD with RINNs.** We consider again, the SDE from Example 3.0.4

$$d\mathbf{X}_t = \nabla V(\mathbf{X}_t)dt + \sigma(t, \mathbf{X}_t)d\mathbf{W}_t \quad (4.15)$$

with  $\mathbf{W}_t$  being a Wiener process,  $\sigma = \sqrt{\frac{1}{2}} \approx 0.7$ , and the potential  $V$  given by

$$V(x_1, x_2) = (x_1^2 - 1)^2 + x_2^2. \quad (4.16)$$

To perform the EDMD, we choose RINNs as a basis functions with  $M = 20$ . We randomly generate  $5 \times 10^4$  test points within the domain  $[-2, 2] \times [-2, 2]$  and integrate each test point for  $10^4$  steps under an integration step of  $h = 10^{-3}$ , resulting in a default lag time of  $h \times 10^4 = 10$ .

We examine two- and three-layer neural network with specific architectural characteristics. For the two-layer neural network, the input layer consists of two neurons, as the input dimension is  $d = 2$ . The hidden layer includes eight neurons with a ReLU activation function. The output layer comprises a single neuron with a Sigmoid activation function. Thus, the network has a structure with units = [8, 1] and activations = [ReLU, Sigmoid].

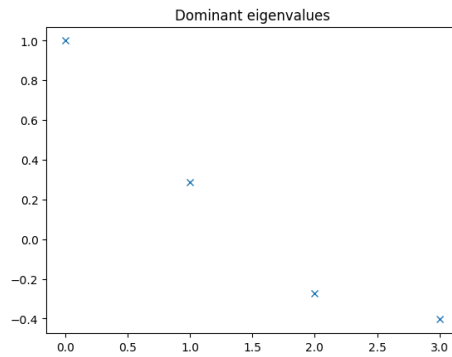


Figure 4.15: Dominant Koopman eigenvalues:  $\mu_1 \approx 1.0, \mu_2 \approx 0.28, \mu_3 \approx -0.31$  and  $\mu_4 \approx -0.42$

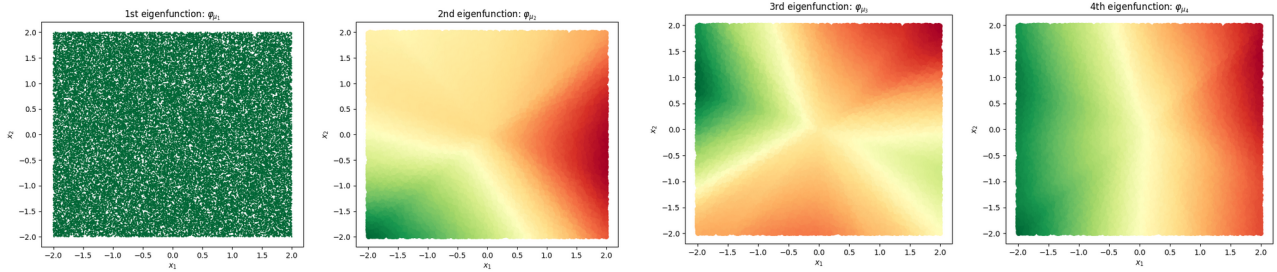


Figure 4.16: The eigenfunctions do not provide any meaningful insights for detecting the metastable regions. Consequently, we lack a reliable approximation, and the choice of basis functions is also not good enough.

For a three-layer neural network with one input layer, two hidden layers, and an output layer. The input layer consists of two neurons, the first hidden layer includes eight neurons with a ReLU activation function, while the second hidden layer comprises four neurons with a Sigmoid activation function. The output layer comprises a single neuron with a Sigmoid activation function. Thus, the network has a structure with units = [8, 4, 1] and activations = [ReLU, Sigmoid, Sigmoid].

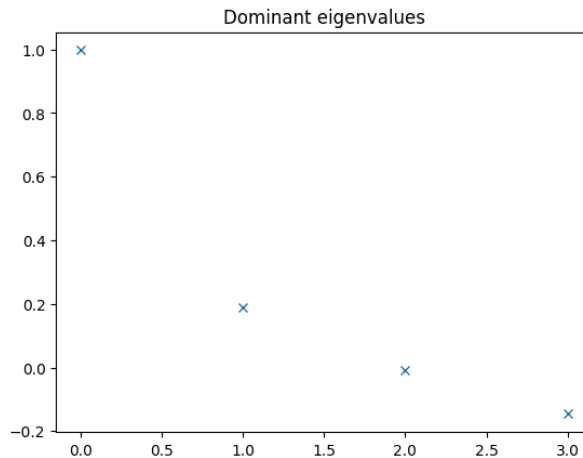


Figure 4.17: Dominant Koopman eigenvalues:  $\mu_1 \approx 1.0, \mu_2 \approx 0.19, \mu_3 \approx -0.0095$  and  $\mu_4 \approx -0.15$

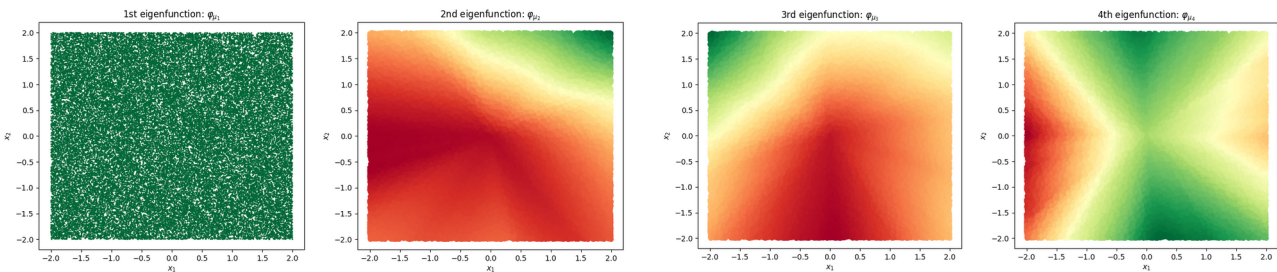


Figure 4.18: Again, we do not have a reliable approximation, and the choice of basis functions is also not satisfactory.

**Example 4.1.7. 2D Triple-Well Problem: EDMD with Randomly Initialized Neural Networks (RINNs).** We revisit again Example 3.0.5, and we apply EDMD to a SDE:

$$d\mathbf{X}_t = \nabla V(\mathbf{X}_t)dt + \sigma(t, \mathbf{X}_t)d\mathbf{W}_t, \quad (4.17)$$

where  $\sigma = 1.09$ . We use the two-dimensional triple-well potential function,

$$V(x_1, x_2) = 3e^{-x_1^2 - (x_2 - \frac{1}{3})^2} - 3e^{-x_1^2 - (x_2 - \frac{5}{3})^2} - 5e^{-(x_1 - 1)^2 - x_2^2} - 5e^{-(x_1 + 1)^2 - x_2^2} + \frac{2}{10}x^4 + \frac{2}{10}\left(x_2 - \frac{1}{3}\right)^4. \quad (4.18)$$

We examine a three-layer neural network with specific architectural characteristics. The input layer consists of two neurons, as the input dimension is  $d = 2$ . The first hidden layer includes eight neurons with a ReLU activation function, while the second hidden layer comprises eight neurons with a Sigmoid activation function. The output layer comprises a single neuron with a Sigmoid activation function. Thus, the network has a structure with units = [8, 8, 1] and activations = [ReLU, Sigmoid, Sigmoid].

To perform the EDMD, we choose RINNs as a basis functions with  $M = 22$ . We randomly generate  $5 \times 10^4$  test points within the domain  $[-2, 2] \times [-1, 2]$  and integrate each test point for  $10^4$  steps under an integration step of  $h = 10^{-5}$ , resulting in a default lag time of  $h \times 10^4 = 0.1$ .

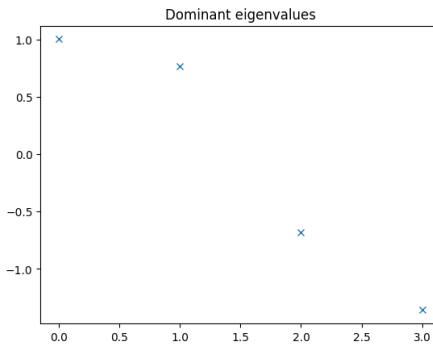


Figure 4.19: Dominant Koopman eigenvalues:  $\mu_1 \approx 1.0$ ,  $\mu_2 \approx 0.76$ ,  $\mu_3 \approx -0.68$  and  $\mu_4 \approx -1.36$

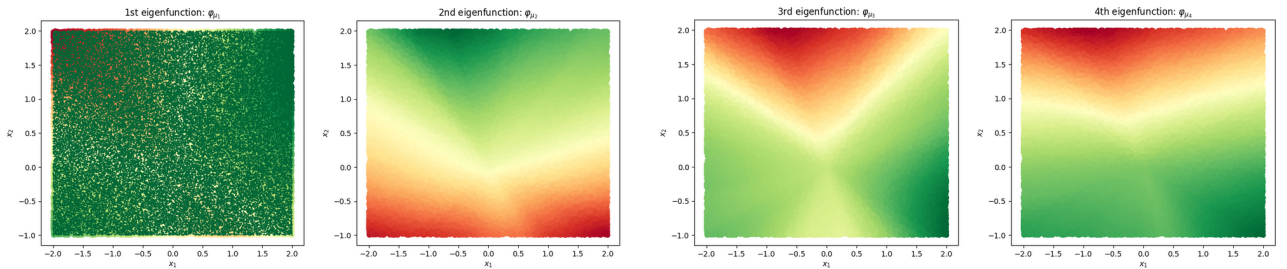


Figure 4.20: Dominant Koopman eigenfunctions. The first eigenfunction is almost constant. The remaining nontrivial eigenfunctions do not offer any valuable insights for identifying the metastable sets. Thus, we have a bad approximation and also not a good choice of basis functions.

**Remark 4.1.8.** After training our neural network and combining it with EDMD on 4.1.6 and 4.1.7, we unfortunately obtained unsatisfactory results. As a result, we are now seeking to improve the network's performance by optimizing its parameters and architecture. However, the process of manual optimization would be too time-consuming, so we require an automated solution. Optuna is a software framework that can automate the search for the best combination of parameters, including the number of layers and units per layer in a neural network model. While we will not be covering this topic in our master's thesis, it would be an interesting area for further investigation in the future.

Chapter **5**

# Conclusion and Outlook

The final chapter of this thesis provides a comprehensive conclusion and outlook on the nonlinearity of dynamical systems. It includes a summary of research findings, a discussion of their implications, an overview of study contributions, and suggestions for future research directions and questions to be addressed. Furthermore, we offer a perspective on the importance of further investigation in this field, while also providing information on the availability of the data used in our study.

## Contents

---

<b>5.1</b>	<b>Summary</b>	<b>58</b>
<b>5.2</b>	<b>Discussion</b>	<b>58</b>
<b>5.3</b>	<b>Contributions</b>	<b>58</b>
<b>5.4</b>	<b>Perspectives</b>	<b>59</b>
<b>5.5</b>	<b>Data Availability</b>	<b>60</b>

---

## 5.1 Summary

The nonlinearity of dynamical systems is a captivating aspect that should be highlighted. With the abundance of data available for modern systems, it makes sense to use data-driven methods to better understand how they behave in the long term. To answer future questions, it's important to understand how the different parts of these systems change over time. This thesis focuses on the pursuit of new coordinates that exhibit linear behavior, determining the optimal basis functions for improved approximation and identification of metastable sets via EDMD, and gaining insights into the long-term behavior of the dynamic system

## 5.2 Discussion

The use of Koopman operator theory has been investigated as a way to describe and estimate nonlinear dynamical systems in a linear framework. The Koopman operator determines the evolution of observables defined on the state space of a dynamical system, and by carefully selecting how we observe the system, we can create linear models that are valid for all or most of the state space rather than just a small area around a fixed point. This can enable linear algorithms to be used even in nonlinear settings. However, while Koopman theory provides linear but infinite dimensional dynamics, it also presents its own challenges as computing the tuples of eigenvalues, eigenfunctions, and modes is not an easy task.

The Koopman eigenfunctions are used to create a systematic linear embedding of nonlinear dynamics, which produces an intrinsic coordinate system that can be closed using the Koopman operator. These eigenfunctions can also be used for prediction and control, and they do not require dictionary selection as they are optimization-based. On the other hand, DMD is a common method used to approximate high-dimensional systems, but its basis functions are simple, leading to rough approximations. EDMD is a more general data-driven method that can provide more accurate approximations of the tuples without knowledge of the underlying dynamics or geometry, but it requires multiple basis functions in all coordinates and their combinations, making it impractical for high-dimensional systems and leading to overfitting when estimating the eigenfunctions of the Koopman operator from a finite data set.

## 5.3 Contributions

In this thesis, we focus on the analysis of nonlinear dynamical systems using operator-based approaches, specifically the theory of Koopman operators. The thesis explores Koopman analysis by investigating the Koopman Mode Decomposition and Koopman-invariant subspaces, which enable the identification of key features and patterns in the system's behavior. The thesis also provides examples of Koopman Embedding and its applications in model reduction, system identification, and data-driven methods. The extended dynamic mode decomposition (EDMD) is a projection-based numerical method that computes approximations of the Koopman eigenvalues, eigenfunctions, and modes from a set of snapshot pairs. The EDMD is shown to be effective in approximating the eigenfunctions of the Koopman operator associated with high-dimensional systems from time-series data.

The thesis demonstrates the effectiveness and accuracy of the EDMD method using several examples that deal with stochastic data generated by Markov processes. The examples include applying EDMD to a one-dimensional Ornstein-Uhlenbeck process, data taken from an SDE with

a double-well potential, and data generated by Markov processes with triple- and quadruple-well potentials. The thesis shows that combining EDMD with random Gaussians is a better choice of basis functions for approximating the Koopman operator compared to the choice of Monomials. The thesis also reveals that using untrained and trained randomly initialized neural networks as basis functions for problems with double-, triple-, and quadruple-well potentials is not an effective approach, and further investigation is required to determine the best architecture and parameters.

In summary, this thesis provides a comprehensive analysis of nonlinear dynamical systems using operator-based approaches, focusing on the theory of Koopman operators and its applications in model reduction, system identification, and data-driven methods. The thesis demonstrates the effectiveness and accuracy of the EDMD method using examples that deal with stochastic data generated by Markov processes. The thesis also reveals the importance of choosing appropriate basis functions for approximating the Koopman operator and highlights the limitations of using untrained and trained randomly initialized neural networks for certain problems.

## 5.4 Perspectives

The Koopman operator framework is becoming increasingly popular in the control world, however, there are still several outstanding questions and issues that need to be addressed. One of the primary challenges lies in dealing with the infinite-dimensional nature of the operator, as well as the inherent approximations of numerical techniques used to develop linear methods for nonlinear systems. Despite these challenges, there are still many unanswered questions and future perspectives that need to be explored.

One promising area of interest is the use of neural network representations of dynamical systems, particularly Koopman embeddings. The combination of the representational power of deep learning with the simplicity and elegance of Koopman embeddings has the potential to revolutionize the analysis and control of complex systems. However, questions remain as to whether neural networks are a suitable choice for basis functions, and if so, what architecture and choice of parameters will lead to a good representation of the eigenfunctions.

Open questions also include the convergence of EDMD when the number of basis functions and data points tend to infinity, and the extension of EDMD to non-autonomous systems. Another important issue is the optimal choice of basis functions to avoid over- and underfitting.

While there has been progress in defining a Koopman-invariant subspace that includes the original state variables as observable functions, a complete classification of nonlinear systems that admit such a subspace remains an open and interesting problem. For systems with multiple fixed points, it is clear that no finite-dimensional Koopman-invariant subspace can contain state variables explicitly as observables. In this case, the challenge is how to choose observable coordinates for a finite-rank truncation of the linear Koopman dynamics that yields useful results, not just for reconstruction of existing data, but for future state prediction and control.

In conclusion, the Koopman operator framework has the potential to transform the analysis and control of complex systems, but there are still many challenges that need to be addressed. Future research should focus on finding optimal basis functions, addressing convergence issues, and developing Koopman-invariant subspaces that include state variables explicitly as observables. Despite the difficulties, the promise of obtaining finite-dimensional linear expressions for nonlinear dynamics has spurred much interest in Koopman analysis, DMD, and EDMD.

## 5.5 Data Availability

The presented methods were implemented in Python.

- The code for DMD, EDMD, and some of the examples discussed in Chapter 3 and 4 are available at <https://github.com/sklus/d3s>.
- The Random Gaussian and Randomly Initilaized Neural Networks (RINN) codes used for the simulations in this work can be found at <https://github.com/AtwiMusa/RDMD>.

Several open source software libraries are being developed to ease this burden, including

- Data-driven dynamical systems toolbox <https://github.com/sklus/d3s>
- deeptime <https://github.com/deeptime-ml/deeptime>.

---

# List of Figures

2.1	Relation between the Koopman operator and the underlying dynamical system. <i>Adapted from [17].</i>	19
2.2	Visualization of 3D linear Koopman system from equation (2.61c) along with projection of dynamics onto the $x_1 - x_2$ plane, with $\psi \equiv y$ . The attracting slow manifold is depicted in red, the constraint $\psi_3 = \psi_1^2$ is shown in blue, and the slow unstable subspace of (2.61c) is visualized in green. The black trajectories of the linear Koopman system in $\psi$ project onto trajectories of the full nonlinear system in $x$ in the $\psi_1 - \psi_2$ plane. Here, $\mu = -0.05$ and $\lambda = 1$ . <i>Reproduced from [4].</i>	23
3.1	First four Koopman eigenfunctions of the Ornstein–Uhlenbeck process.	40
3.2	Eigenfunctions computed analytically (dotted lines). Adapted from [7]	40
3.3	Double-well potential landscape $V(x_1, x_2) = (x_1^2 - 1)^2 + x_2^2$ and an example of a generated trajectory from starting point $x_0 = (-1, 0)$ in the potential landscape.	41
3.4	Numerical solution of the double-well SDE (4.7).	42
3.5	3D plot of first four Koopman eigenfunctions. The first eigenfunction $\varphi_{\mu_1}$ corresponds to an eigenvalue $\mu_1 = 1.0$ of the Koopman operator, and is constant as expected. The system contains two metastable states, and the second eigenfunction $\varphi_{\mu_2}$ associated with an eigenvalue $\mu_2 \approx 0.75$ of the Koopman operator can be utilized to identify these states. This eigenfunction separates the two deep wells at $(-1, 0)$ and $(1, 0)$ , and provides information about a potential partitioning of the state space. It is almost constant in the $x_2$ -direction, as well as in the $x_1$ -direction, except for a sudden transition from $-1$ to $1$ between the two metastable sets. The remaining dominant eigenfunctions of the operator, $\varphi_{\mu_3}$ and $\varphi_{\mu_4}$ , associated with (numerically zero) eigenvalues $\mu_3 = 0.016$ and $\mu_4 = 0.0089$ , respectively, are almost zero (constants).	42
3.6	Triple-well potential landscape and an example of a generated trajectory from starting point $(-1, 0)$ .	43
3.7	Numerical solution of the triple-well SDE (4.7).	43
3.8	The first three dominant Koopman eigenfunctions are displayed in both 3D and 2D plots. The second eigenfunction $\varphi_{\mu_2}$ , with eigenvalue $\mu_2 = 0.99$ , distinguishes the two deep wells located at $(-1, 0)$ and $(1, 0)$ , while remaining close to zero for the well at $(0, 1.5)$ . The third eigenfunction $\varphi_{\mu_3}$ , with eigenvalue $\mu_3 = 0.93$ , separates the two deep wells from the shallow well. In contrast, the fourth eigenfunction $\varphi_{\mu_4}$ , with eigenvalue $\mu_4 = 0.68$ , does not contribute to identifying the metastable regions, as these are already captured by the first nontrivial eigenfunctions.	44
3.9	Quadruple-well potential landscape and an example of a simulated trajectory from initial condition $(1, -1)$	44
3.10	First eight dominant Koopman eigenvalues. A spectral gap after $\mu_4$ indicates that the dominant four eigenfunctions are relevant to metastability analysis. $\mu_1 = 1.0$ , $\mu_2 \approx 0.749$ , $\mu_3 \approx 0.738$ and $\mu_4 \approx 0.568$	45

3.11	First four dominant Koopman eigenfunctions. It can be observed that the eigenfunctions are nearly constant in each of the four quadrants. This suggests that each quadrant is stable, meaning that trajectories that begin in a particular quadrant usually remain in that quadrant for an extended period of time. . . . .	45
4.1	Dominant Koopman eigenvalues and eigenfunctions. Using $M = 65$ random gaussians with $\rho = 1.7$ . . . . .	49
4.2	Dominant Koopman eigenvalues and eigenfunctions. Using $M = 70$ random gaussians with $\rho = 1.5$ . . . . .	49
4.3	1D Triple-well potential landscape and histogram of trajectory in the landscape (4.5). . . . .	49
4.4	Dominant Koopman eigenvalues and eigenfunctions: $M = 100$ gaussians, $\rho = 0.5$ and a generated long trajectory of length $25 \times 10^4$ . The primary and fourth Koopman eigenfunctions $\varphi_1$ and $\varphi_4$ with respective eigenvalues $\lambda_1 = 1.0$ and $\lambda_4 = -0.002$ do not provide any valuable information for identifying the metastable sets. The second eigenfunction $\varphi_2$ , associated with eigenvalue $\lambda_2 = 0.997$ , is almost uniform within the left well as well as within the two other wells, with a smooth transition in between, thereby identifying the maximum energy barrier. The third eigenfunction $\varphi_3$ with eigenvalue $\lambda_3 = 0.953$ distinguishes (separates) the middle well and the right well. A spectral gap after $\lambda_3$ indicates that the dominant three eigenfunctions are relevant to metastability analysis.	50
4.5	$M = 65, \rho = 0.5$ and a long trajectory of length $25 \times 10^4$ . $\lambda_1 = 1.0, \lambda_2 = 0.992, \lambda_3 = 0.915$ and $\lambda_4 = 0.041$ . . .	50
4.6	$M = 65, \rho = 1.5$ and a long trajectory of length $25 \times 10^4$ . $\lambda_1 = 1.0, \lambda_2 = 0.997, \lambda_3 = 0.957$ and $\lambda_4 = -0.0347$ . .	50
4.7	For randomly generated $N = 5 \times 10^4$ points in the domain, with $M = 90$ and $\rho = 1.05$ . We obtain, $\lambda_1 = 1.00, \lambda_2 = 0.99, \lambda_3 = 0.86$ , and $\lambda_4 = 0.11$ . . . . .	50
4.8	First four gaussian basis functions . . . . .	51
4.9	Dominant Koopman eigenvalues: $\mu_1 \approx 1.0, \mu_2 \approx 0.747, \mu_3 \approx 0.0205$ and $\mu_4 \approx -0.0184$ . A spectral gap after $\mu_2$ indicates that the dominant two eigenfunctions are relevant to metastability analysis. . . . .	51
4.10	3D plot of first four Koopman eigenfunctions using random Gaussians with $\rho = 1.05$ and $M = 56$ . The second eigenfunction $\varphi_{\mu_2}$ associated with an eigenvalue $\mu_2 \approx 0.747$ of the Koopman operator can be utilized to identify the two metastable sets of the system. This eigenfunction separates the two deep wells at $(-1, 0)$ and $(1, 0)$ , and provides information about a potential partitioning of the state space. It is almost constant in the $x_2$ -direction, as well as in the $x_1$ -direction, except for a sudden transition from $-1$ to $1$ between the two metastable sets. The remaining eigenfunctions do not give any information to detecting the metastable regions. The first eigenfunction $\varphi_{\mu_1}$ corresponds $\mu_1 \approx 1$ of the Koopman operator, is constant. The remaining dominant eigenfunctions of the operator, $\varphi_{\mu_3}$ and $\varphi_{\mu_4}$ , associated with eigenvalues $\mu_3 = 0.0205$ and $\mu_4 = -0.0184$ (numerically zero), respectively, are almost zero (constants). Only the second eigenfunction provide an information to detecting the metstable sets.	51
4.11	Dominant Koopman eigenvalues: $\mu_1 \approx 1.0, \mu_2 \approx 0.986, \mu_3 \approx 0.925$ and $\mu_4 \approx 0.679$ . . . . .	52
4.12	The dominant Koopman eigenfunctions are visualized in both 3D and 2D plots. The second eigenfunction $\varphi_{\mu_2}$ , with eigenvalue $\mu_2 = 0.986$ , separates the two deep wells located at $(-1, 0)$ and $(1, 0)$ , and is near zero for the well at $(0, 1.5)$ . The third eigenfunction $\varphi_{\mu_3}$ , with eigenvalue $\mu_3 = 0.925$ , separates the two deep wells from the shallow well. In contrast, the first and fourth eigenfunctions $\varphi_{\mu_1}$ and $\varphi_{\mu_4}$ , with respective eigenvalues $\mu_1 = 1.00$ and $\mu_4 = 0.679$ , do not contribute to identifying the metastable sets. . . . .	52
4.13	First eight dominant Koopman eigenvalues. A spectral gap after $\mu_4$ indicates that the dominant four eigenfunctions are relevant to metastability analysis. $\mu_1 = 1.0, \mu_2 \approx 0.743, \mu_3 \approx 0.730$ and $\mu_4 \approx 0.540$ . . . . .	53
4.14	The dominant Koopman eigenfunctions are visualized in both 2D and 3D plots. We observe that the eigenfunctions are almost constant in the four quadrants. This indicates that each of the quadrants is metastable, i.e., trajectories that start in each quadrant typically stay in it for a long time. . . . .	53

4.15 Dominant Koopman eigenvalues: $\mu_1 \approx 1.0, \mu_2 \approx 0.28, \mu_3 \approx -0.31$ and $\mu_4 \approx -0.42$	55
4.16 The eigenfunctions do not provide any meaningful insights for detecting the metastable regions. Consequently, we lack a reliable approximation, and the choice of basis functions is also not good enough.	55
4.17 Dominant Koopman eigenvalues: $\mu_1 \approx 1.0, \mu_2 \approx 0.19, \mu_3 \approx -0.0095$ and $\mu_4 \approx -0.15$	55
4.18 Again, we do not have a reliable approximation, and the choice of basis functions is also not satisfactory.	55
4.19 Dominant Koopman eigenvalues: $\mu_1 \approx 1.0, \mu_2 \approx 0.76, \mu_3 \approx -0.68$ and $\mu_4 \approx -1.36$	56
4.20 Dominant Koopman eigenfunctions. The first eigenfunction is almost constant. The remaining nontrivial eigenfunctions do not offer any valuable insights for identifying the metastable sets. Thus, we have a bad approximation and also not a good choice of basis functions.	56



---

# Bibliography

- [1] Laurence A. Baxter. Chaos, fractals, and noise: Stochastic aspects of dynamics, second edition, 1994, by andrzej lasota and michael c. mackey, applied mathematical sciences, vol. 97 (new york: Springer-verlag), xiv 472 pp. *Probability in the Engineering and Informational Sciences*, 10(2):311–313, 1996. doi: 10.1017/S0269964800004368. URL <https://doi.org/10.1017/S0269964800004368>.
  - [2] B.O.Koopman. *Hamiltonian Systems and Transformation in Hilbert Space*. Proceedings of the National Academy of Sciences, 1931. doi: 10.1073/pnas.17.5.315. URL <https://doi.org/10.1073/pnas.17.5.315>.
  - [3] Steven L. Brunton and J. Nathan Kutz. *Data-Driven Science and Engineering: Machine Learning, Dynamical Systems, and Control*. Cambridge University Press, 2019. doi: 10.1017/9781108380690. URL <https://doi.org/10.1017/9781108380690>.
  - [4] Steven L. Brunton, Bingni W. Brunton, Joshua L. Proctor, and J. Nathan Kutz. Koopman invariant subspaces and finite linear representations of nonlinear dynamical systems for control. *PLOS ONE*, 11(2):1–19, 02 2016. doi: 10.1371/journal.pone.0150171. URL <https://doi.org/10.1371/journal.pone.0150171>.
  - [5] Steven L. Brunton, Marko Budivsić, Eurika Kaiser, and J. Nathan Kutz. Modern koopman theory for dynamical systems, 2021. URL <https://arxiv.org/abs/2102.12086>.
  - [6] Marko Budivsić, Ryan Mohr, and Igor Mezić. Applied koopmanism. *Chaos: An Interdisciplinary Journal of Nonlinear Science*, 22(4):047510, dec 2012. doi: 10.1063/1.4772195. URL <https://doi.org/10.1063%2F1.4772195>.
  - [7] Stefan Klus, Feliks Nüske, Péter Koltai, Hao Wu, Ioannis Kevrekidis, Christof Schütte, and Frank Noé. Data-driven model reduction and transfer operator approximation. *Journal of Nonlinear Science*, 28(3):985–1010, jan 2018. doi: 10.1007/s00332-017-9437-7. URL <https://doi.org/10.1007%2Fs00332-017-9437-7>.
  - [8] Stefan Klus, Feliks Nüske, Sebastian Peitz, Jan-Hendrik Niemann, Cecilia Clementi, and Christof Schütte. Data-driven approximation of the koopman generator: Model reduction, system identification, and control. *Physica D: Nonlinear Phenomena*, 406:132416, may 2020. doi: 10.1016/j.physd.2020.132416. URL <https://doi.org/10.1016%2Fj.physd.2020.132416>.
  - [9] Yueheng Lan and Igor Mezić. Linearization in the large of nonlinear systems and koopman operator spectrum. *Physica D: Nonlinear Phenomena*, 242:42–53, 2013.
-

- [10] Benedict Leimkuhler, Christophe Chipot, Ron Elber, Aatto Laaksonen, Alan Mark, Tamar Schlick, Christof Schütte, and Robert Skeel. *New Algorithms for Macromolecular Simulation*. Lecture Notes in Computational Science and Engineering. 2006. ISBN 9783540255420.
- [11] Igor Mezić. Spectral properties of dynamical systems, model reduction and decompositions. *Nonlinear Dynamics*, 2005. doi: 10.1007/s11071-005-2824-x. URL <https://doi.org/10.1007/s11071-005-2824-x>.
- [12] Grigorios A. Pavliotis. *Stochastic Processes and Applications. Diffusion Processes, the Fokker-Planck and Langevin Equations*. Springer New York, NY, 2014. URL <https://doi.org/10.1007/978-1-4939-1323-7>.
- [13] Christof Schütte, Pé ter Koltai, and Stefan Klus. On the numerical approximation of the perron-frobenius and koopman operator. *Journal of Computational Dynamics*, 3(1):1–12, sep 2016. doi: 10.3934/jcd.2016003. URL <https://doi.org/10.3934%2Fjcd.2016003>.
- [14] Jonathan H. Tu, Clarence W. Rowley, Dirk M. Luchtenburg, Steven L. Brunton, and J. Nathan Kutz. On dynamic mode decomposition: Theory and applications. *Journal of Computational Dynamics*, 1(2):391–421, 2014. ISSN 2158-2491. doi: 10.3934/jcd.2014.1.391. URL <https://doi.org/10.3934/jcd.2014.1.391>.
- [15] Nelida vCernjarić vZic, Senka MaćevSić, and Igor Mezić. Koopman operator spectrum for random dynamical systems, 2017. URL <https://arxiv.org/abs/1711.03146>.
- [16] Matthew O. Williams, Clarence W. Rowley, Igor Mezić, and Ioannis G. Kevrekidis. Data fusion via intrinsic dynamic variables: An application of data-driven koopman spectral analysis. *Europhysics Letters*, 109, 2014.
- [17] Matthew O. Williams, Ioannis G. Kevrekidis, and Clarence W. Rowley. A data–driven approximation of the koopman operator: Extending dynamic mode decomposition. *Journal of Nonlinear Science*, 25(6):1307–1346, jun 2015. doi: 10.1007/s00332-015-9258-5. URL <https://doi.org/10.1007%2Fs00332-015-9258-5>.